Radiative corrections and accuracy tests of Monte Carlo generators used at meson factories

Ph.D. Thesis

Michał Gunia

Supervisor: prof. dr hab. Henryk Czyż

Department of Field Theory and Particle Physics
University of Silesia - Institute of Physics Katowice, Poland

Katowice, 2013

Acknowledgements

I would like to thank my supervisor prof. dr hab. Henryk Czyż for his suggestions and advice during the course of this work. A Ph.D. thesis would have been impossible to produce without help of many people. Special thanks to Bartosz Dziewit, prof. dr hab. Janusz Gluza, Wojciech Gunia and dr Sebastian Zając. M. Gunia was supported by Świder PhD program

Contents

Chapter 1

Introduction

The amazing progress of research in the field of elementary particles in the second half of the twentieth century led to the formulation of the theory known as the Standard Model (SM). With this theory it was possible to connect in one model three of the four known fundamental interactions [1]. At the same time, technological developments had allowed experimental methods to be improved. The accelerators used in experiments reached ever higher energies of accelerated particles while increasing the precision of the detectors. On the other hand, significant progress was made in the field of theoretical research and calculations. The predictions of the SM were confirmed by experiments, but the SM cannot be treated as a full theory of particle physics. First of all, the SM treats particle masses as parameters - they cannot be obtained by theoretical predictions. Furthermore, the SM does not describe particle physics phenomena such as dark matter or matter antimatter asymmetry, etc. This means that the SM should be considered as an effective theory. This is one of the reasons that suggest the need for searching for so called new physics or physics beyond the SM. Research conducted at high energies in the large hadron collider (LHC) could answer some of this question. However, there is a possibility of a parallel search for evidences of new physics. It is possible to test known parameters of the SM like for example the anomalous magnetic moment.

This kind of test requires the comparison between the experimental measurement and the theoretical prediction done with extremely high precision. Thus, this advance of theoretical calculation and experimental methods has resulted in today's tests of the SM requiring an inclusion of higher order effects. In an era of high energy measurements at the TeV level in the LHC, calculations and experiments conducted for low energy particle physics could play a crucial role in searching for traces of physics beyond the SM [2].

The hadronic contribution to the anomalous magnetic moment of the

muon a_μ^{had} is an example of a quantity that depends strongly on low energy data. The low energy hadronic contributions are not calculable in the quantum chromodynamics (QCD) perturbation theory and the calculations require use of phenomenological models and the precise experimental data studies.

The hadronic contribution to the anomalous magnetic moment of the muon a_μ^{had} is divided into three parts: the leading-order (LO) $a_\mu^{had,LO}$ and higher-order (HO) $a_\mu^{had,HO}$ vacuum polarisation contributions, and the light-by-light scattering contribution $a_\mu^{had,lbl}$. The leading order contribution can be obtained from the data for the processes $e^+e^- \to hadrons$ and using the dispersion integral it can be presented in the following form [3]:

$$a_\mu^{had,LO} = \frac{1}{4\pi^3} \int_{m_\pi^2}^{\infty} dsK(s)\sigma_{had}(s) \tag{1.1}$$

where $\sigma_{had}(s)$ is the total hadronic cross section (without the vacuum polarisation corrections). The $K(s)$ function is called kernel function and is calculated within quantum electrodynamics (QED). The behaviour of this function shows that it decreases monotonically with increasing value of s. Therefore the $a_\mu^{had,LO}$ integrand is dominated by the hadron production below a few GeV. The hadron part of the anomalous magnetic moment of the muon obtained from e^+e^- data is [4]:

$$a_\mu^{had} = (6955 \pm 49) \cdot 10^{-11} \tag{1.2}$$

Where:

$$a_\mu^{had,LO} = (6949.1 \pm 42.7) \cdot 10^{-11} \tag{1.3}$$

$$a_\mu^{had,HO} = (-98.4 \pm 0.7) \cdot 10^{-11} \tag{1.4}$$

$$a_\mu^{had,lbl} = (105 \pm 26) \cdot 10^{-11} \tag{1.5}$$

The error for the leading order contribution is the biggest one.

The sum of all contributions to the value of the anomalous magnetic moment of the muon obtained for the SM prediction is equal to:

$$a_\mu^{SM} = 116591828(50) \cdot 10^{-11} \tag{1.6}$$

The errors were added in quadrature. This value also contains a_μ^{had}.

The value taken from the experiment gives:

$$a_\mu^{exp} = 116592089(63) \cdot 10^{-11} \tag{1.7}$$

A careful comparison of these two values gives the difference equal to 3.3 standard deviation:

$$\Delta a_\mu = a_\mu^{exp} - a_\mu^{SM} = 261(80) \cdot 10^{-11} \tag{1.8}$$

This discrepancy could suggest the existence of some unknown effects, so it is very important to improve the accuracy of the experimental and theoretical value of a_μ to check if it is true. The uncertainty of theoretical calculations depends strongly on the hadronic contribution at low energies. The error of a_μ^{SM} is equal to $50 \cdot 10^{-11}$, while the error of $a_\mu^{had,LO}$ is equal to $42.7 \cdot 10^{-11}$. So the biggest contribution to the error of a_μ^{SM} comes from the prediction of the leading-order hadronic contribution $a_\mu^{had,LO}$. The biggest contribution to the value of $a_\mu^{had,LO}$ comes from the region between 0.32 and 1.43 GeV and is equal to $(6065 \pm 34) \cdot 10^{-11}$ [4]. The second in order is the region between 2 and 11.09 GeV where the contribution is equal to $(411.9 \pm 8.2) \cdot 10^{-11}$. Here, for the region between 2.6 and 3.73 GeV for some channels, perturbative QCD (pQCD) was used. The contribution for energies above 11.09 GeV (obtained with pQCD) is equal to $0.211 \cdot 10^{-11}$ and gives the error below 10^{-14}. So the error of $a_\mu^{had,LO}$ is dominated by the low energy hadron production. This example shows the importance of results obtained for low energies where the use of perturbation methods for hadrons is not possible.

A similar influence of low-energy data occurs for the hadronic part of the fine structure constant $\Delta\alpha^{had}(M_z)$. The dispersion relation gives the following form of this magnitude [5]:

$$\Delta\alpha^{had}(M_z) = -\frac{\alpha M_z^2}{3\pi} \mathrm{Re} \int_{m_\pi^2}^{\infty} ds \frac{R(s)}{s(s - M_z^2 - i\epsilon)} \tag{1.9}$$

Here the *R(s)* function depends on the total cross section σ_{had} of the process $e^+e^- \to hadrons(muons) + \gamma$:

$$R(s) = \frac{3s\sigma_{had}}{4\pi\alpha^2} \tag{1.10}$$

The error of $\Delta\alpha^{had}(M_z)$, at the level of about one percent, comes mainly from the process at the scale of about a few GeV [4]. The precise determination of the value of $\Delta\alpha^{had}(M_z)$ is, for example, necessary for the better determination of the Higgs mass .

To increase accuracy of the theoretical value of a_μ^{had} or $\Delta\alpha^{had}(M_z)$, it is necessary to improve the determination of the hadronic cross section. It is connected with the accuracy of the Monte Carlo (MC) generators used for the analysis of the experimental data. Generators like BabaYaga@NLO, MCGPJ and PHOKHARA are examples of generators that include NLO

Part I

Studies on the accuracy of the contributions from NNLO hadronic and leptonic corrections to Bhabha scattering in BabaYaga@NLO MC generator

Chapter 2

Missing NNLO corrections in the BabaYaga@NLO MC generator

2.1 Aim

The comparison between SM predictions and precise experimental data is an invaluable tool to test the theory at the quantum level. The advancements in theoretical calculation and experimental methods have resulted in precision tests of the SM requiring an inclusion of higher order effects. Every collider experiment in particle physics - both for high and low energy - needs a high accuracy of the luminosity value for the reference process, which includes theoretical and experimental parts - Eq. 1.11. The process of Bhabha scattering: $e^+e^- \to e^+e^-$ is mostly used as a reference [2].

To obtain the results with the high accuracy, a proper tool is necessary. For luminosity measurement at meson factories, the BabaYaga@NLO Monte Carlo generator is used. An estimated accuracy of this generator is 0.1% [10],[11]. It contains the corrections to the Bhabha process up to next-to-next-to-leading order. However, this generator does not include a full set of NNLO corrections and some of the ones implemented in BabaYaga@NLO are approximated and/or were not independently tested.

The aim of this part of the work is to calculate independently the untested and missing NNLO corrections and to compare the complete calculations with the approximate ones realised in the MC generator BabaYaga@NLO. It was very important to prepare the numerical results for energies and cuts as close as possible to the experimental ones used at the meson factories (Φ factory Daphne, at the B factories PEP-II and at KEK and at the charm/τ

factory BEPC II, Beijing).

The second task was to confirm the stability of the accuracy in respect to change of the event selection by adding further accolinearities and angular cuts close the experimental ones. Besides the BabaYaga@NLO MC generator, the following software was used: package BHA_NNLO_HF [25], Monte Carlo generators: EKHARA [26], BHAGHEN–1PH (with additional vacuum polarisation part) [27], [28] and HELAC-PHEGAS [29].

In this chapter, the theoretical part of this work is presented. In the next sections, all considered NNLO contributions are described [6].

2.2 The NNLO corrections

The NNLO corrections to the Bhabha process considered in this work can be divided into three parts, each reflecting different types of the corrections:

$$\frac{d\sigma^{\mathrm{NNLO}}_{N_f}}{d\Omega} = \frac{d\sigma^{\mathrm{NNLO}\,1}_{virt}}{d\Omega} + \frac{d\sigma^{\mathrm{NLO}\,2}_{\gamma}}{d\Omega} + \frac{d\sigma^{\mathrm{LO}\quad 3}_{realpairs}}{d\Omega} \tag{2.1}$$

Upper index points the software that was used for the calculations of the studied corrections:

1 - BHA_NNLO_HF

2 - BHAGHEN–1PH+VAC, BHA_NNLO_HF

3 - HELAC–PHEGAS, EKHARA

Here $\frac{d\sigma^{\mathrm{NNLO}}_{virt}}{d\Omega}$ denotes the virtual part of corrections. $\frac{d\sigma^{\mathrm{NLO}}_{\gamma}}{d\Omega}$ is a part with emission of one real photon, both hard and soft. $\frac{d\sigma^{\mathrm{LO}}_{realpairs}}{d\Omega}$ is a part with production of the real lepton and hadron pairs. The presented contribution could be introduced in the following form:

- the $\sigma^{\mathrm{NNLO}}_{virt}$ consists of virtual *two-loop corrections* $\sigma^{\mathrm{NNLO}}_{2L}$ shown in Fig. 2.1 and $\sigma^{\mathrm{NNLO}}_{1L1L}$ corrections shown in Fig. 2.2:

$$\sigma^{\mathrm{NNLO}}_{virt} = \sigma^{\mathrm{NNLO}}_{2L} + \sigma^{\mathrm{NNLO}}_{1L1L} \tag{2.2}$$

- contributions with *real photon emission*, shown in Fig. 2.3:

$$\sigma^{\mathrm{NLO}}_{\gamma} = \sigma^{\mathrm{NLO}}_{\gamma,soft}(\omega) + \sigma^{\mathrm{NLO}}_{\gamma,hard}(\omega) \tag{2.3}$$

- contributions with *real pair or hadron emission* Figs. 2.4-2.6:

$$\sigma^{\mathrm{LO}}_{real} = \sigma^{\mathrm{LO}}_{e^+e^-(e^+e^-)} + \sigma^{\mathrm{LO}}_{e^+e^-(\mu^+\mu^-)} + \sigma^{\mathrm{LO}}_{e^+e^-(\tau^+\tau^-)} + \sigma^{\mathrm{LO}}_{e^+e^-(hadrons)} \tag{2.4}$$

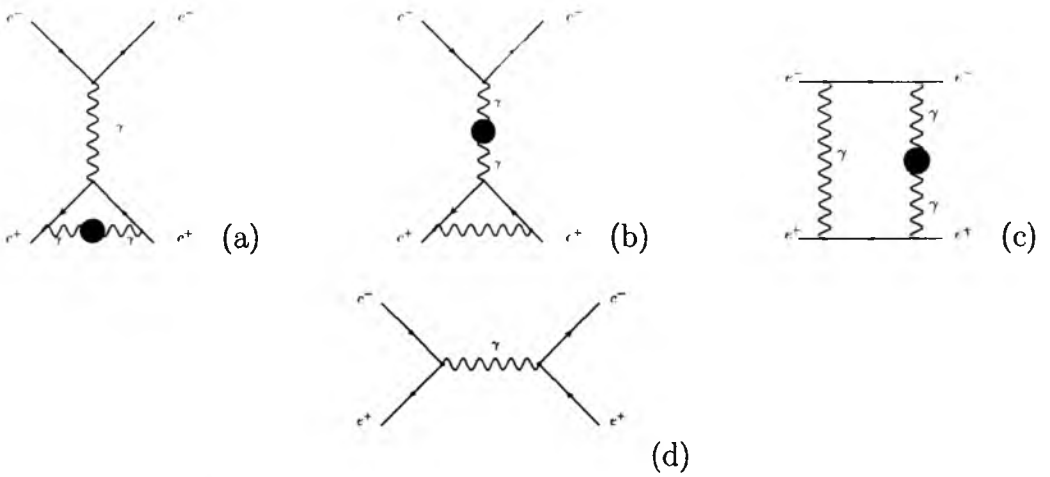

Figure 2.1: (a)–(c) Samples of two-loop diagrams. The considered NNLO corrections consist of their interference with (d).

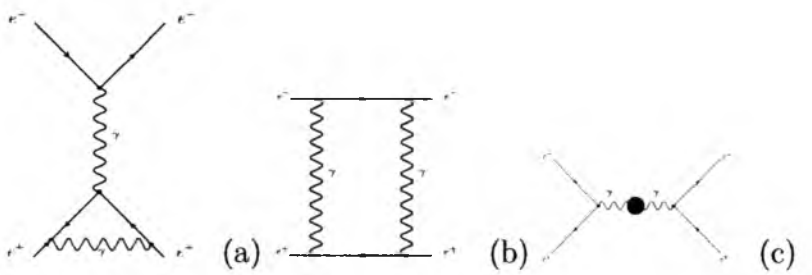

Figure 2.2: (a)–(b) Samples of the loop-by-loop corrections. The considered NNLO corrections consist of their interference with(c).

Various software was used to present calculations in this work. The virtual and soft corrections were calculated together:

$$\sigma_{v+s}^{\mathrm{NNLO}} = \sigma_{virt}^{\mathrm{NNLO}} + \sigma_{\gamma,soft}^{\mathrm{NLO}}(\omega), \tag{2.5}$$

The BHA_NNLO_HF package was used for these calculations [25]. The contribution with the emission of real and hard photon was calculated separately by BHAGHEN–1PH+VAC generator:

$$\sigma_{h}^{\mathrm{NNLO}} = \sigma_{\gamma,hard}^{\mathrm{NLO}}(\omega). \tag{2.6}$$

For the real pair emission (Eq. 2.4) two routines were used. The HELAC–PHEGAS was used for leptons and EKHARA for hadrons (pions).

2.2.1 Hard photonic corrections $\sigma_h^{\rm NNLO}$

The correction $\sigma_h^{\rm NNLO}$ with emission of one real hard photon $e^+(p_+) + e^-(p_-) \to e^+(q_+) + e^-(q_-) + \gamma(k)$, with the vacuum polarisation insertion is not missing correction in the BabaYaga@NLO generator, however correctness of this contribution was not tested independently.

The classes of diagrams representing these corrections are shown in Fig. 2.3. The emission of real hard photon depends on the soft photon cut-off $\omega = E^{\rm min}_{\gamma,hard}/E_{beam} = E^{\rm max}_{\gamma,soft}/E_{beam}$, with the sum of hard and soft part $\sigma^{\rm NNLO}_{v+s+h}$ being cut independently ($E^{\rm min}_{\gamma,hard}$ is a minimum energy of hard photon, $E^{\rm max}_{\gamma,soft}$ is a maximum energy of soft photon, $E_{beam} = \sqrt{s}/2$ - in the centre of mass frame).

All numerical calculations of $\sigma_h^{\rm NNLO}$ are based on an extended version of the BHAGHEN-1PH+VAC [27] Monte Carlo generator. The notation follows the one presented in [28]. The considered process is $e^+(p_+) + e^-(p_-) \to e^+(q_+) + e^-(q_-) + \gamma(k)$. We denote:

$$\begin{aligned} &s = (p_+ + p_-)^2\,, \quad t = (p_+ - q_+)^2\,, \quad u = (p_+ - q_-)^2\,, \quad s_1 = (q_+ + q_-)^2, \\ &t_1 = (p_- - q_-)^2\,, \quad u_1 = (p_- - q_+)^2\,, \quad k_\pm = p_\pm.k\,, \quad h_\pm = q_\pm.k\,. \end{aligned} \tag{2.7}$$

The differential cross section can be written as a sum of three parts X, Y, and Z, describing s, t and u channels:

$$d\sigma_h^{\rm NNLO} = \frac{\alpha^3}{2\pi^2 s}(X + Y + Z)\frac{d^3q_+}{E_+}\frac{d^3q_-}{E_-}\frac{d^3k}{E_\gamma}\delta^4(p_+ + p_- - q_+ - q_- - k)\,, \tag{2.8}$$

where E_+, E_-, E_γ are the energies of the final positron, electron and photon, X is the part of the cross section for Bhabha scattering that includes electron -positron annihilation, Y describes the Coulomb part, and Z is the interference part of the s and t channel. The same structure of the contributions is preserved inside the generator. Using introduced notation, it can be written

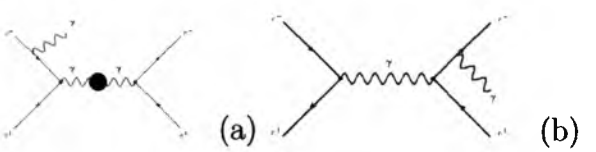

Figure 2.3: Interference of (a) and (b) is a sample of the considered hard contribution.

in the following form:

$$
\begin{aligned}
\bar{Z} \;=\; & \frac{u^2+u_1^2}{4}\Bigg[\frac{\Pi(t)+\mathrm{Re}(\Pi(s))}{st} \\
& \left(\frac{u}{k_-h_+}+\frac{s}{h_+h_-}-\frac{t}{k_-h_-}\right) \\
& +\frac{\Pi(t_1)+\mathrm{Re}(\Pi(s))}{st_1}\left(\frac{u_1}{k_+h_-}+\frac{s}{h_+h_-}-\frac{t_1}{k_+h_+}\right) \\
& +\frac{\Pi(t)+\mathrm{Re}(\Pi(s_1))}{s_1t}\left(\frac{u_1}{k_+h_-}+\frac{s_1}{k_+k_-}-\frac{t}{k_-h_-}\right) \\
& +\frac{\Pi(t_1)+\mathrm{Re}(\Pi(s_1))}{s_1t_1}\left(\frac{u}{k_-h_+}+\frac{s_1}{k_+k_-}-\frac{t_1}{k_+h_+}\right)\Bigg] \\
& -\frac{m_e^2}{st_1}\left(\Pi(t_1)+\mathrm{Re}(\Pi(s))\right)\frac{u^2}{(h_+)^2} \\
& -\frac{m_e^2}{s_1t_1}\left(\Pi(t_1)+\mathrm{Re}(\Pi(s_1))\right)\frac{u_1^2}{(k_+)^2} \\
& -\frac{m_e^2}{st}\left(\Pi(t)+\mathrm{Re}(\Pi(s))\right)\frac{u_1^2}{(h_-)^2} \\
& -\frac{m_e^2}{s_1t}\left(\Pi(t)+\mathrm{Re}(\Pi(s_1))\right)\frac{u^2}{(k_-)^2}
\end{aligned}
\tag{2.9}
$$

$$
\begin{aligned}
Y \;=\; & \left[(\Pi(t)+\Pi(t_1))(s^2+s_1^2+u^2+u_1^2)\right]\frac{1}{4tt_1} \\
& \left[\frac{u}{k_+h_-}+\frac{u_1}{k_-h_+}+\frac{s}{k_+k_-}+\frac{s_1}{h_+h_-}\right] \\
& -2\Pi(t)(s^2+s_1^2+u^2+u_1^2)\frac{1}{4tk_-h_-} \\
& -2\Pi(t_1)(s^2+s_1^2+u^2+u_1^2)\frac{1}{4t_1k_+h_+} \\
& -2\Pi(t_1)\frac{m_e^2}{2t_1^2}\left[\frac{s^2}{(h_+)^2}+\frac{s_1^2}{(k_+)^2}+\frac{u^2}{(h_+)^2}+\frac{u_1^2}{(k_+)^2}\right] \\
& -2\Pi(t)\frac{m_e^2}{2t^2}\left[\frac{s^2}{(h_-)^2}+\frac{s_1^2}{(k_-)^2}+\frac{u_1^2}{(h_-)^2}+\frac{u^2}{(k_-)^2}\right]
\end{aligned}
\tag{2.10}
$$

$$
\begin{aligned}
X &= (\mathrm{Re}(\Pi(s)+\Pi(s_1)))(t^2+t_1^2+u^2+u_1^2)\frac{1}{4ss_1} \\
&\left[\frac{u}{k_+h_-}+\frac{u_1}{k_-h_+}-\frac{t}{k_+h_+}-\frac{t_1}{k_-h_-}\right] \\
&+ 2\mathrm{Re}(\Pi(s_1))((t^2+t_1^2+u^2+u_1^2)\frac{1}{4s_1k_+k_-} \\
&+ 2\mathrm{Re}(\Pi(s))((t^2+t_1^2+u^2+u_1^2)\frac{1}{4sh_+h_-} \\
&- 2\mathrm{Re}(\Pi(s))\frac{m_e^2}{2s^2}\left[\frac{t_1^2}{(h_+)^2}+\frac{t^2}{(h_-)^2}+\frac{u^2}{(h_+)^2}+\frac{u_1^2}{(h_-)^2}\right] \\
&- 2\mathrm{Re}(\Pi(s_1))\frac{m_e^2}{2s_1^2}\left[\frac{t_1^2}{(k_+)^2}+\frac{t^2}{(k_-)^2}+\frac{u_1^2}{(k_+)^2}+\frac{u^2}{(k_-)^2}\right] \qquad (2.11)
\end{aligned}
$$

Here Π denotes the renormalized vacuum polarisation, which has the following form [2]:

$$\Pi(q^2)=\frac{\alpha q^2}{3\pi}\int_{4m^2}^{\infty}\frac{dz}{z}\frac{R(z)}{q^2-z+i\epsilon} \qquad (2.12)$$

The form of the formula for the real part of the vacuum polarisation for leptons is presented below.

BHAGHEN-1Ph+VAC

As it was mentioned, the numerical calculations were done with use of extended version of the BHAGHEN-1Ph [28] MC generator called BHAGHEN-1Ph+VAC[27]. This code is written in FORTRAN77. Few changes were introduced to this program. The original version does not calculate vacuum polarisation contribution Π, so this correction was added to the code. For the purpose of this work, five types of contributions to the vacuum polarisation were prepared for the calculations: with electrons, muons, taus, pions, and hadrons. The part used for the calculation of the electroweak corrections was removed and only the QED part was retained - the original formulas for the cross section contained the weak Z boson contributions. For energies used in this work, the Z contribution is negligible. The generation of the phase space was not changed. For the calculations of the vacuum polarisation with hadrons, the VPHLMNT code [30] was used inside BHAGHEN-1Ph+VAC. For leptons and pions, an additional routine for calculations of the vacuum polarisation was prepared.

The problem with the pole $q^2 = z - i\epsilon$ (Eq. 2.12) is solved by addition and subtraction $R(q^2)$ in the integrand for s - channel ($q^2 > 0$). Together with the change of variables: $q^2 = \frac{4m^2}{y}$ it gives the following expressions:

$$\Pi(t) = \frac{\alpha q^2}{3\pi} \int_0^1 dy \frac{t}{yt - 4m^2} R(4m^2/y) \tag{2.13}$$

$$\Pi(s) = \frac{\alpha q^2}{3\pi} \left[\log\left(1 - \frac{s}{4m^2 - i\epsilon}\right) R(s) \right] \tag{2.14}$$
$$+ \frac{\alpha q^2}{3\pi} \left[\int_0^1 \frac{dys}{ys - 4m^2} \left(R\left(\frac{4m^2}{y}\right) - R(s) \right) \right]$$

For lepton with the mass m at leading order, $R(q^2)$ has the following form:

$$R(q^2) = (1 + \frac{2m^2}{q^2})\sqrt{1 - \frac{4m^2}{q^2}} \tag{2.15}$$

In this case, presented integrands were solved analytically and coded inside BHAGHEN-1PH+VAC. The formulas for the hard contribution σ_h^{NNLO} - Eq. 2.9, 2.10, 2.11 contain only the real part of the Π (for t channel solution is real, for s channel it contains also an imaginary part), so the formulas presented below do not contain the imaginary part of the solution. For $q^2 \in (0, 4m^2)$ the formula can be presented in the following form:

$$\Pi(q^2) = \frac{\alpha}{2\pi} \frac{\arctan\left(1/\sqrt{4m^2/q^2 - 1}\right)}{\sqrt{4m^2/q^2 - 1}} \left(\frac{16m^4}{q^4} + \frac{4m^2}{q^2} - 2 \right) \tag{2.16}$$
$$+ \frac{\alpha}{2\pi} \left(-\frac{5}{3} - \frac{4m^2}{q^2} \right)$$

For the other values of q^2 it takes the following form:

$$\Pi(q^2) = -\frac{\alpha q^2}{2\pi m^2} \left[C_1 + C_2 \log\left(\frac{|1 - x_1|}{|x_1|}\right) + C_3 \log\left(\frac{1 - x_2}{|x_2|}\right) \right] \tag{2.17}$$

$$C_1 = \frac{5x_1^3 + 22x_1^2 + 5x_1}{3(x_1 + 1)^4} \tag{2.18}$$
$$C_2 = \frac{x_1^4 + 3x_1^3 - 3x_1^2 - x_1}{(x_1 + 1)^5}$$
$$C_3 = \frac{x_2^4 + 3x_2^3 - 3x_2^2 - x_2}{(x_2 + 1)^5}$$

Where x_1 and x_2 have the form:

$$x_1 = \frac{q^2 - 2m^2 + \sqrt{q^2(q^2-4m^2)}}{2m^2} \qquad (2.19)$$
$$x_2 = \frac{q^2 - 2m^2 - \sqrt{q^2(q^2-4m^2)}}{2m^2}$$

For pions with mass m_π:

$$R(q^2) = \frac{\beta_\pi^3}{4}|F_\pi(q^2)|^2 \qquad (2.20)$$

Where $F_\pi(q^2)$ is a form factor constructed phenomenologically.

$$\beta_\pi = \sqrt{1 - \frac{4m_\pi^2}{q^2}} \qquad (2.21)$$

In the presented calculations, the form factor used in the PHOKHARA7.0 [14] MC generator was used inside BHAGHEN-1PH+VAC. For this case, the vacuum polarisation contribution was calculated numerically with use of an eight point Gaussian quadrature for numerical integration.

2.2.2 The virtual plus soft photon corrections $\sigma_{v+s}^{\mathrm{NNLO}}$

The classes of virtual corrections used for the purposes of this study are presented in Figs. 2.1 and 2.2. There are three types of corrections that interfere with the Born diagram (Figs. 2.1d, 2.2c). Two of these corrections, the factorizable vertex and the box corrections in Fig. 2.1(b) and Fig. 2.2(a,b) and the irreducible box corrections in Fig. 2.1(c), are not infrared finite. Only the part of the corrections in Fig. 2.1(a), the irreducible vertex correction, is infrared finite. As it was mentioned, the calculations of the virtual corrections were done together with the soft part of the contribution. The infrared divergence is compensated by the soft corrections.

$$\frac{d\sigma_{v+s}^{\mathrm{NNLO}}}{d\Omega} = \frac{d\sigma_{virt,e^+e^-}^{\mathrm{NNLO}}}{d\Omega} + \sum_{f=\mu,\tau} \frac{d\sigma_{virt,f^+f^-}^{\mathrm{NNLO}}}{d\Omega} \qquad (2.22)$$
$$+ \frac{d\sigma_{virt,had}^{\mathrm{NNLO}}}{d\Omega} + \frac{d\sigma_{virt}^{\mathrm{NLO}}}{d\Omega} \times F_{\gamma,soft}(\omega)$$

The last term $\sigma_{virt}^{\mathrm{NLO}} \times F_{\gamma,soft}(\omega)$ describes the interference of the (soft) single-photon bremsstrahlung diagrams, where one of the diagrams has a self-energy

insertion and depends on the infrared cut-off:

$$\omega \;=\; E^{\max}_{\gamma,soft}/E_{beam} \;=\; E^{\min}_{\gamma,hard}/E_{beam} \tag{2.23}$$

The factor $F_{\gamma,soft}(\omega)$ was used in the calculations in the limit of the small electron mass m_e as compared with $\sqrt{s}$:

$$\begin{aligned} F_{\gamma,soft}(\omega) \;=\; \frac{\alpha}{\pi}\Bigg\{ & \left[\frac{F_\epsilon}{\epsilon} - \ln\left(s/m_e^2\right) - 2\ln\left(\frac{2\omega}{\sqrt{s}}\right)\right] \\ & \left[-2\ln\left(s/m_e^2\right) + 2 - 2\ln\left(\frac{t}{u}\right)\right] \\ & - \ln\left(s/m_e^2\right)^2 - 4\zeta_2 + 2\ln\left(s/m_e^2\right) \\ & + 2\mathrm{Li}_2\left(-\frac{t}{u}\right) - 2\mathrm{Li}_2\left(-\frac{u}{t}\right)\Bigg\}. \end{aligned} \tag{2.24}$$

The cut-off dependence disappears for the sum of the soft and hard photon contribution. The virtual plus soft photon cross section can be presented in the following form:

$$\begin{aligned} \sigma^{\mathrm{NNLO}}_{v+s} \;&=\; \sigma^{\mathrm{NNLO}}_{virt} + \sigma^{\mathrm{NLO}}_{\gamma,soft}(\omega) \\ &=\; \sigma^{\mathrm{NNLO}}_{fact} + \sigma^{\mathrm{NNLO}}_{vert} + \sigma^{\mathrm{NNLO}}_{box} + \sigma^{\mathrm{NLO}}_{virt} \times F_{\gamma,soft}(\omega). \end{aligned} \tag{2.25}$$

The virtual corrections with the sum over M $= m_\mu, m_\tau, m_\pi$ are :

$$\begin{aligned} \sigma^{\mathrm{NLO}}_{virt} \;\sim\; & \left(\frac{\alpha}{\pi}\right)^3 \Bigg\{ \sigma^{\mathrm{NLO}}_{virt,e^+e^-} + \mathrm{Re}\sum_M \int_{M_0^2}^{\infty} \frac{dz\ R(z)}{z} [C_s^{\mathrm{NLO}}\ K_{SE}(s,z) \\ & + C_t^{\mathrm{NLO}} K_{SE}(t,z)] \Bigg\} \end{aligned}$$

$$\begin{aligned} \sigma^{\mathrm{NNLO}}_{fact} \;\sim\; & \left(\frac{\alpha}{\pi}\right)^4 \Bigg\{ \sigma^{\mathrm{NNLO}}_{fact,e^+e^-} + \mathrm{Re}\sum_M \int_{M_0^2}^{\infty} \frac{dz\ R(z)}{z} [C^{\mathrm{NNLO}}_{fact,s}\ K_{SE}(s,z) \\ & + C^{\mathrm{NNLO}}_{fact,t} K_{SE}(t,z)] \Bigg\} \end{aligned}$$

$$\sigma_{vert}^{\rm NNLO} \sim \left(\frac{\alpha}{\pi}\right)^4 \left\{ \sigma_{vert,e^+e^-}^{\rm NNLO} + {\rm Re} \sum_M \int_{M_0^2}^{\infty} \frac{dz\ R(z)}{z} [C_{vert,s}^{\rm NNLO}\ K_{vert}(s,z) + C_{vert,t}^{\rm NNLO}\ K_{vert}(t,z)] \right\}$$

$$\begin{aligned}\sigma_{box}^{\rm NNLO} \sim \left(\frac{\alpha}{\pi}\right)^4 \Bigg\{ & \sigma_{box,e^+e^-}^{\rm NNLO} + {\rm Re} \sum_M \int_{M_0^2}^{\infty} \frac{dz\ R(z)}{z} \Big\{ C_{box,s}^{\rm NNLO} \big[K_{box,A}(s,t,z) \\ & + K_{box,B}(t,s,z) + K_{box,C}(u,t,z) - K_{box,B}(u,s,z) \big] \\ & + C_{box,t}^{\rm NNLO} \big[K_{box,B}(s,t,z) + K_{box,A}(t,s,z) \\ & - K_{box,B}(u,t,z) + K_{box,C}(u,s,z) \big] \Big\} \Bigg\}. \end{aligned} \tag{2.26}$$

The integration limit is equal $M_0^2 = 4m^2$ for leptons and $M_0^2 = m_{\pi^0}^2$ for hadrons. The limit for the hadrons corresponds to the lightest state $\pi^0\gamma$. The photon propagator has the form:

$$K_{SE}(q^2,z) = \frac{1}{q^2 - z + i\delta}. \tag{2.27}$$

For heavy leptons with mass m_M the R function is given by Eq. 2.15. For hadrons it is:

$$R_{had}(z) = \frac{\sigma_{had}(z)}{(4\pi\alpha^2)/(3z)}, \tag{2.28}$$

where $\sigma_{had}(z) \equiv \sigma(e^+e^- \to \gamma^* \to \text{hadrons}; z)$. The formulas for the box kernel functions: $K_{box,i}$ (i = A,B,C) are presented in [23].

The calculations for the presented contributions were done with the use of the available software, so the formulas for $\sigma_{v+s}^{\rm NNLO}$ are presented selectively to show their structure. However, there is one important detail related to the irreducible vertex corrections from the fermion pair, which should be mentioned. The contribution to the cross section for this correction contains terms with $\ln^3(s/m^2)$. The contribution for electrons is particularly important, because of the significant size due to a small value of electron mass comparing to $\sqrt{s}$. This term is cancelled, if the contributions with the real pair emission are taken into account and if the integrals are done over the full phase space. This is the reason of studies on the size of their contribution for a specific experimental event selection.

The virtual plus soft contributions were calculated with an updated version BHA_NNLO_HF of the Fortran package BHBHNNLOHF and the Mathematica program CROSSSECTION.M [25].

2.2.3 Real pair contributions $\sigma^{\rm LO}_{real}$

The third type of the tested contribution consists of the corrections with emission of the additional real pair of leptons or hadrons (pions). The influence of these corrections allows the cancellations of the terms with $\ln^3(s/m^2)$, also present in the virtual plus soft part. The most important contributions are present for the emission of electron pair: $\sigma^{\rm LO}_{e^+e^-(e^+e^-)}$. The types of diagrams involved in this process are presented in Fig. 2.4.

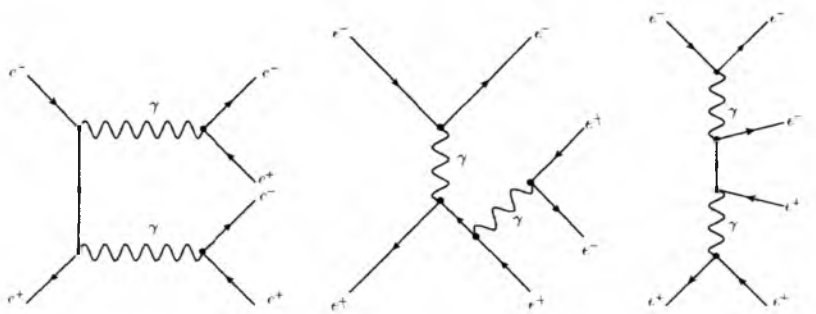

Figure 2.4: Classes of diagrams for the contribution $e^+e^- \to e^+e^-e^+e^-$.

The cancellations with the virtual irreducible vertex corrections are related to the production of the two electron pairs in the final state (Fig. 2.4(a)). This contribution in the limit of the soft electron pairs was presented in [31]. The limit of small m_e and the small cut-off parameter D of the unresolved e^+e^- pair can be approximated as follows :

$$\sigma^{\rm LO}_{e^+e^-(e^+e^-)} \sim \sigma^{\rm LO}_{e^+e^-} \left(\frac{\alpha}{\pi}\right)^2 \delta^e_{soft}, \tag{2.29}$$

with:

$$\delta^e_{soft} = \frac{1}{3}\left[\frac{1}{3}L_s^3 + L_s^2\left(2\ln(D) - \frac{5}{3}\right) + L_s\left(4\ln^2(D) - \frac{20}{3}\ln(D) + A_s\right)\right. \\ + \frac{1}{3}L_t^3 + L_t^2\left(2\ln(D) - \frac{5}{3}\right) + L_t\left(4\ln^2(D) - \frac{20}{3}\ln(D) + A_t\right) \\ \left. - \frac{1}{3}L_u^3 - L_u^2\left(2\ln(D) - \frac{5}{3}\right) - L_u\left(4\ln^2(D) - \frac{20}{3}\ln(D) + A_u\right)\right], \tag{2.30}$$

where

$$L_s = \ln\left(\frac{s}{m_e^2}\right), \tag{2.31}$$

$$L_v = \ln\left(-\frac{v}{m_e^2}\right), \quad v = t, u, \tag{2.32}$$

$$A_s = \frac{56}{9} - 4\zeta_2, \tag{2.33}$$

$$A_v = A_s + 2\mathrm{Li}_2\left(\frac{1 \pm \cos\theta}{2}\right), \quad v = t, u. \tag{2.34}$$

There are the following conditions for parameter D:

$$2m_e << DE_{\mathrm{bcam}} << E_{\mathrm{bcam}}. \tag{2.35}$$

The expression 2.30 explicitly shows the existence of the contributions with $\ln^3(s/m^2)$.

The production of muon and tau pair to Bhabha scattering gives another twelve diagrams for each process of types presented in Fig. 2.5. In case of heavy lepton pairs and energies of meson factories, the assumption of masses much smaller than $\sqrt{s}$ is not right and the formulas used for the electron pair emission is not right - Eq. 2.29. The contributions require the full lowest order calculations.

All the results of calculations for lepton pair production presented in the next chapter were done using HELAC-PHEGAS[29] MC program and PHEGAS [32] for the phase space integration.

The last considered type of corrections with the real pair production is the production of the pion pair $\pi^+\pi^-$ - the lightest hadronic final states. The sample diagrams describing the pion pair corrections are presented in Fig. 2.6. All the calculations were conducted with the Monte Carlo generator EKHARA [26]. Here the pion-photon is described by the vector dominance

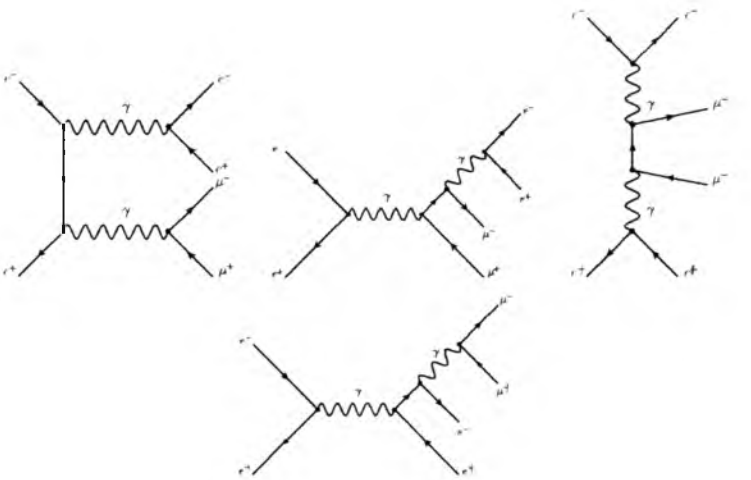

Figure 2.5: Samples of diagrams for muon pair production $e^+e^- \to e^+e^-\mu^+\mu^-$. A similar set of diagrams describes $e^+e^- \to e^+e^-\tau^+\tau^-$.

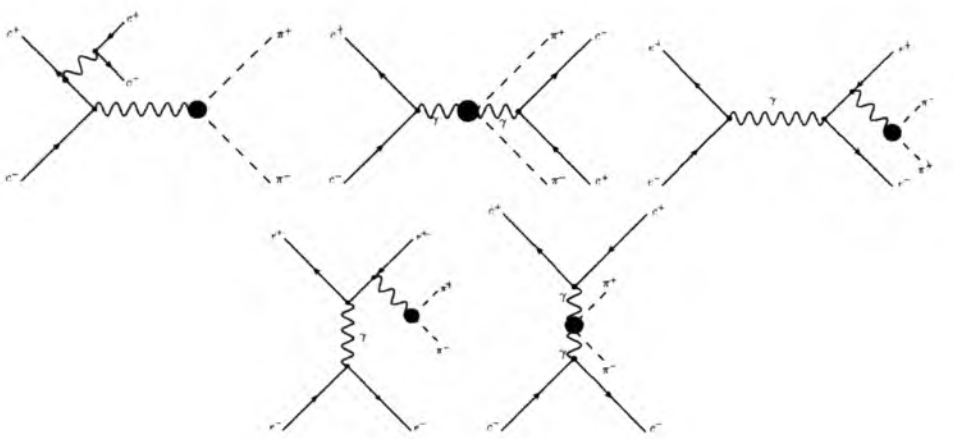

Figure 2.6: Sample diagrams with real pion pair emission.

model . The pion form factor is from [33]. The contributions for the process $e^+e^- \to e^+e^-$ with the emission of the other real hadrons were not added to the final results of this analysis. There does not exist a MC generator that contains this kind of corrections. Due to the fact that the pions are the lightest produced hadrons and that the highest energy of the meson factories is about 10 GeV, they should dominate the cross section.

2.2.4 NNLO corrections in BabaYaga@NLO MC generator

BabaYaga@NLO [10] is a Monte Carlo event generator used as a tool for luminosity studies. It simulates the following processes $e^+e^- \to e^+e^-$, $\mu^+\mu^-$, $\gamma\gamma$. All the processes include the QED corrections. The generator has been already used in all four experiments, whose energies and cuts were included and presented in this work's studies: KLOE, BaBar, BES-III and Belle.

The estimated accuracy of the generator for the process of Bhabha scattering is equal to 0.1% and comes partly from the NNLO part of the contributions presented in this work. Moreover, some parts of the NNLO corrections are not coded inside the generator and their size is only estimated. The hard part of corrections presented in Fig. 2.3 has been taken into account inside BabaYaga@NLO, while for the virtual plus soft part only the class of diagrams presented in Fig. 2.1b and Fig. 2.2 can be found in the generator. The rest of the presented contributions, including the real pair productions, are not included in the BabaYaga@NLO generator.

Chapter 3

Numerical studies

In this chapter, numerical tests and studies of the size of the NNLO corrections to the Bhabha process are presented.

In Section 3.1 the comparison between hard contribution obtained using the BHAGHEN-1PH+VAC [27] generator with the corresponding contributions from BabaYaga@NLO [10] is presented.

In Section 3.2 the results of the hard-soft cut independence test are presented.

In Section 3.3 information about the pion and hadron contributions to the vacuum polarisation is presented.

In Section 3.4 the numerical results for the exact NNLO calculations and approximate ones from the BabaYaga@NLO generator are presented. The event selection close to the experimental conditions for KLOE, BaBar, Belle and BESS III is used with an additional check for changes of the event selection.

3.1 Test of hard emission

As mentioned in the previous chapter that both BabYaga@NLO and exact NNLO calculations done with BHAGHEN-1PH+VAC contain the contribution with the real hard photon emission presented in Fig. 2.3. The hard photonic correction σ_h^{NNLO} present in the BabaYaga@NLO generator was not independently tested, so the tests were performed during our calculations. The comparison between the results can also be treated as a test of the vacuum polarisation contribution in BHAGHEN-1PH+VAC. The relative difference between results for BabaYaga@NLO and BHAGHEN-1PH+VAC was calculated, according to Eq. 7.1:

$$\Delta = \frac{\sigma_h - \sigma_h^{BY}}{\sigma_h} \tag{3.1}$$

Here, σ_h is the hard part of the NNLO calculations that comes from BHAGHEN-1PH+VAC and σ_h^{BY} is the corresponding contribution obtained with BabaYaga@NLO generator. This test was done for all event selections (Appendix 7.0.3) independently for all particles: electrons, muons, tau and hadron production. The analysis of the results of this test shows that there is full agreement between the generators. The example of the relative differ-

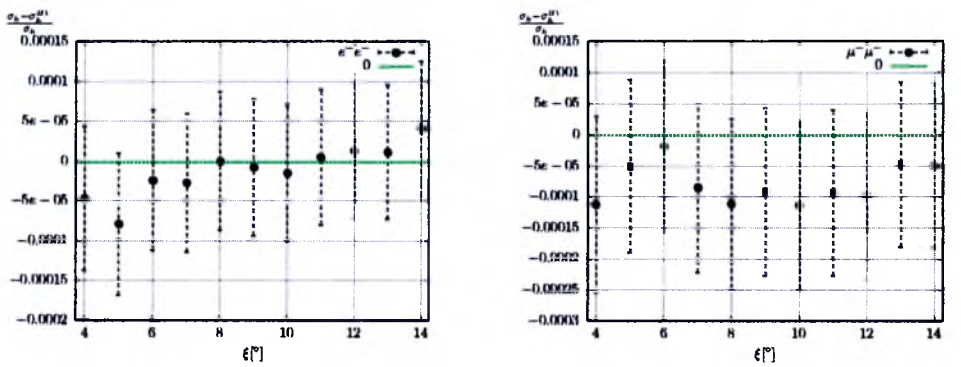

Figure 3.1: $\Delta = \frac{\sigma_h - \sigma_{hBY}}{\sigma_h}$ - comparison between the hard parts, an example for KLOE for electrons and muons.

ence for the KLOE cuts are presented in Fig. 3.1. The precision for all other investigated experiments and event selection was similar; the agreement was checked up to 10^{-4}.

3.2 Hard-soft cut independence

To check if the behaviour of the soft part of the calculations is correct, the sum of the hard and soft contributions was calculated for different values of the cut $\omega = E^{max}_{\gamma,soft}/E_{beam}$. The typical values of ω in the simulations chosen for tests are between 10^{-6} and 10^{-3}. In this case, two values were used: $\omega = 10^{-5}$ and $\omega = 10^{-4}$.

Because of the structure of the BHA_NNLO_PH package, it was possible to check the sum of the hard, soft, and virtual parts. The virtual and soft part is calculated together inside this code.

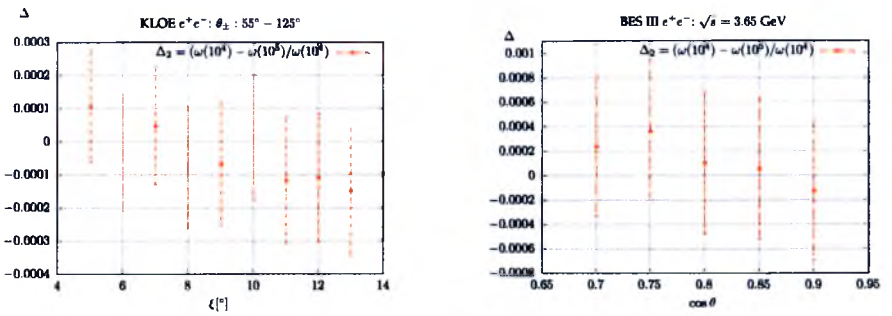

Figure 3.2: Examples of the cut independence, between the hard, soft and virtual part of the corrections for the electron case and KLOE, BES-III cuts.

All points for the presented in Appendix 7.0.3 experiments and the event selections were checked for the electron, muon, tau and hadron production. Sample results for the electron production for KLOE and BES-III experiments are presented in Fig. 3.2. To compare the results for both values of the ω cut, relative difference was calculated with $\omega = 10^{-4}$ in denominator. For all of the investigated points, the results show that all sums are cut independent.

3.3 Pion vs. hadron influence on the vacuum polarisation

Although for the hadron part of the real emission only the contribution of the pair of charged pions was calculated, it is possible to include the other hadronic states in case of the vacuum polarisation's contribution. The $R(s)$ function describes the influence of the virtual particles in the vacuum polarisation's contribution (Eq. 2.12). It is possible to compare the difference between the results obtained for the pion production and for the hadrons. Fig. 3.3 shows the behaviour of $R(s)$ for two cases, inclusion of pions and inclusion of hadrons. For the hadron case the VPHLMNT code was used [30]. For pions, the form factor present in Eq. 2.20 came from PHOKHARA7.0 [14]. The difference visible for low energies comes from the contribution of three pions and of kaon pairs that are produced for ω and ϕ resonances. For higher energies $R_{\pi\pi}$ goes to 0, while R_{had} obtains the value of few units .

Tab. 3.1 presents the comparison of contributions that include the vacuum polarisation for four experimental energies and cuts: KLOE, BaBar, BES-III, Belle for pions and hadrons. σ_{S+V} means the contribution to the cross

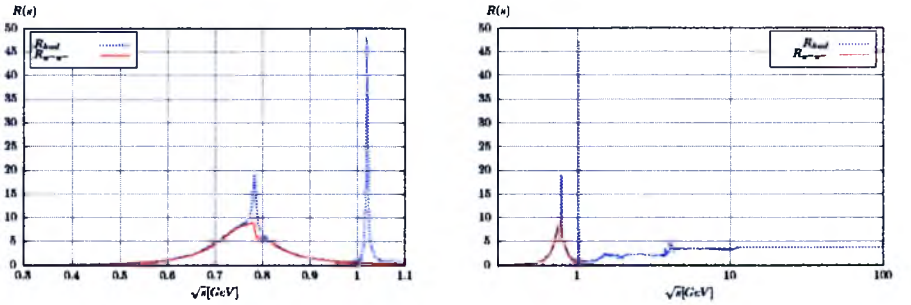

Figure 3.3: The R_{had} vs. $R_{\pi^+\pi^-}$. Narrow resonances are not included.

	σ_{S+V} [nb]	σ_{S+V+H} [nb]
pions $R_{\pi\pi}$		
KLOE	-1.35988(2)	-0.18586(8)
BaBar	-0.053328(3)	-0.002291(4)
BES	-0.81806(3)	-0.04469(3)
Belle	-0.0612(1)	-0.0067(1)
hadrons R_{had}		
KLOE	-1.062(8)	0.438(8)
BaBar	-1.888(4)	-0.0088(4)
BES	-1.81(1)	-0.15(1)
Belle	-0.2124(5)	-0.0227(5)

Table 3.1: Comparison of the corrections with the vacuum polarisation modelled by $R_{\pi^+\pi^-}$ and R_{had}

section from virtual plus soft correction, while σ_{S+V+H} is completed with hard part. The difference between the corresponding results is significant in all investigated cases. It shows that the pion contribution is not sufficient for full analysis. At present, it is not possible to include the real hadron emission to calculations except pion pairs. The example of the influence of the hadron corrections on the vacuum polarisation also shows, that in case of the real hadron emission, it is necessary to wait for progress in the Monte Carlo generator's area or develop the existing Monte Carlo generators.

3.4 The numerical studies of NNLO corrections to Bhabha scattering

In this section, the numerical results for the exact NNLO corrections σ^{NNLO} obtained with BHA_NNLO_PH, EKHARA , BHAGHEN–1PH+VP and HELAC–PHEGAS and the approximate ones σ_{BY}^{NNLO} calculated with the BabaYaga@NLO generator are analysed. For all calculations, event selections are based on real experimental ones from KLOE, BaBar, Belle and BES-III. All used cuts are presented in Appendix 7.0.3.

Tables 3.2, 3.3, 3.4, and 3.5 contain the results for these four experiments. Every table is organised as follows: in columns there are the results for hard contributions σ_h, virtual plus soft contributions σ_{s+v}, real pair emission σ_{pairs} and the sum of all of them. In every table the complete cross section σ_{BY} (without vacuum polarisation) for experimental cuts is presented. The σ_{BY} cross section was calculated with use of the BabaYaga@NLO MC generator. Every table is divided into a part containing exact NNLO calculations σ^{NNLO} and a part that contains approximated calculations σ_{BY}^{NNLO}. The rows contain the lepton and hadron NNLO contributions. At the end of every table, the relative difference is presented for the lepton and hadron NNLO corrections:

$$\Delta = \frac{|\sigma^{NNLO} - \sigma_{BY}^{NNLO}|}{\sigma_{BY}} \tag{3.2}$$

For every type of the experimental cuts, the stability of the obtained results against changes of the event selection is tested. The outcome of this analysis is presented in the form of plots for every experiment. The plots show the values of the relative difference between the exact NNLO corrections and the approximate ones for the hadronic and leptonic contributions and their sums.

KLOE

In Tab. 3.2 an analysis of the results of the NNLO calculations is presented for the KLOE event selection. The energy for the KLOE experiment is $\sqrt{s} = 1.02$ GeV. This is the smallest energy among examined experiments.

For the lepton part, both for the exact NNLO calculations and approximated ones, electrons provide the main contribution. Also, pair production for the exact NNLO calculations is dominated by the electron pairs. The value of σ_{pairs} for muons is very small and does not affect the result. For tau and hadrons (pions) there is no pair production. For tau it is caused by low energy of the experiment. For hadrons (pions) it is caused by the KLOE cuts.

KLOE σ_{BY} = 455.71(5) nb				
particles	σ_h [nb]	σ_{v+s} [nb]	σ_{pairs} [nb]	sum [nb]
EXACT NNLO				
electron	9.5021(2)	-11.5666	0.2712(15)	-1.793(2)
muon	1.49406(3)	-1.7356(2)	0.246(7)*10^{-7}	-0.2415(2)
tau	0.0201637(4)	-0.023412(2)	0	-0.003248(2)
leptons sum: σ^{NNLO}_{lep}				**-2.038(2)**
hadrons	1.5248(6)	-1.062(8)	0	0.463(8)
BabaYaga NNLO				
electron	9.5022(8)	-11.0721(4)	-	-1.5699(9)
muon	1.4942(2)	-1.7441(2)	-	-0.2499(3)
tau	0.020166(3)	-0.023704(2)	-	-0.003538(4)
leptons sum: σ^{NNLO}_{BYlep}				**-1.823(1)**
hadrons	1.5247(5)	-1.126(2)	-	0.399(2)
leptons relative difference: $\lvert\sigma^{NNLO}_{lep} - \sigma^{NNLO}_{BYlep}\rvert/\sigma_{BY}$				**0.471(4)‰**
hadrons relative difference: $\lvert\sigma^{NNLO} - \sigma^{NNLO}_{BY}\rvert/\sigma_{BY}$				**0.14(2)‰**

Table 3.2: Comparison between exact NNLO results and the approximate ones from BabaYaga@NLO for KLOE experiment cuts at $\sqrt{s}$=1.02 GeV

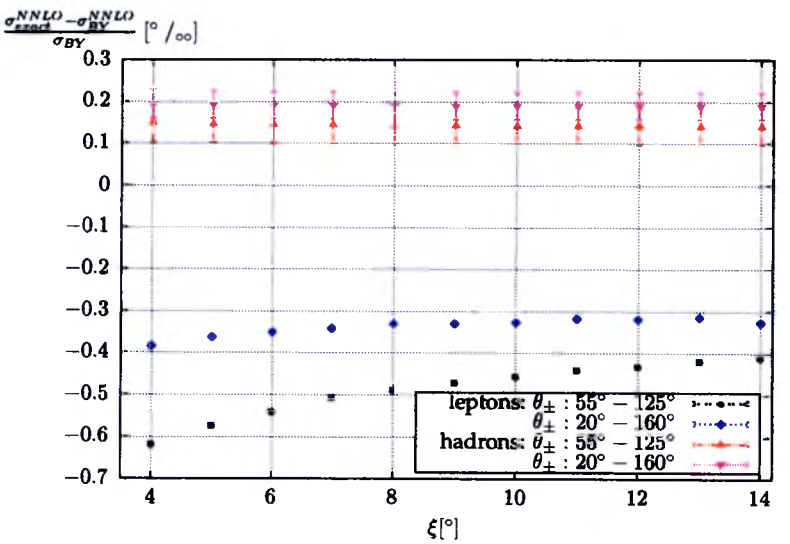

Figure 3.4: The relative difference of NNLO massive corrections, as a function of 2d acollinearity for KLOE for leptons and hadrons.

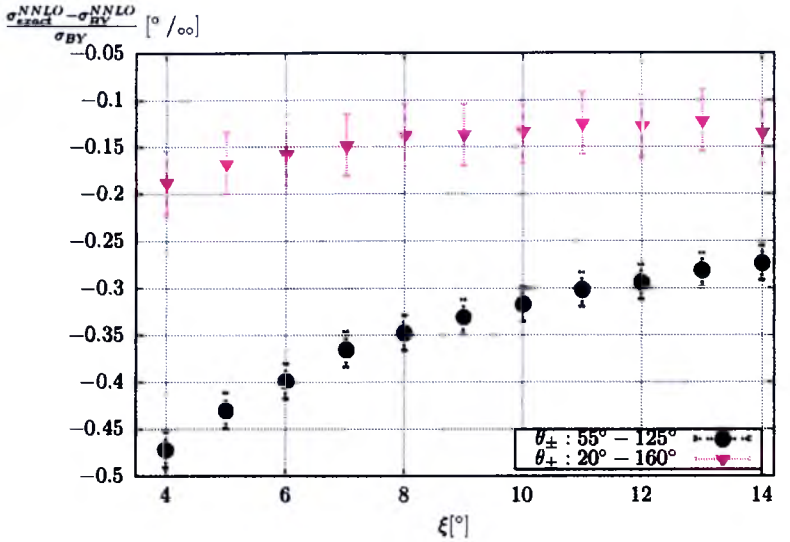

Figure 3.5: The relative difference of NNLO massive corrections, as a function of 2d acollinearity for KLOE. The sum of the lepton and hadron contribution.

The relative difference for leptons is equal to 0.471(4)‰. For hadrons it is equal to 0.14(2)‰. The contributions for hadrons and leptons have opposite signs, so the total error is equal to 0.33(4)‰. It is less than 1‰ estimated for the BabaYaga@NLO MC generator.

For the KLOE event selection the additional comparison for various values of 2d acollinearity (Eq. 7.6) was done for two angular cuts. The results are presented in Figs. 3.4 and 3.5.

Fig. 3.4 shows that for all values of the acollinearity and the angular cuts, the lepton and hadron corrections have opposite signs. The results are stable - they do not change rapidly as a function of acollinearity, both for the wider and narrower angular cuts. For all of the checked points the sum of the lepton and hadron contribution is negative; the lepton corrections dominate the total result. The biggest value of the relative difference is less than 0.5 ‰ for the narrower angular cuts and less than 0.22‰ for the wider angular cuts, even if the maximum value of the error is taken (Fig. 3.5).

BaBar

The BaBar experiment operates at energy $\sqrt{s} = 10.56$ GeV. The results collected in Tab. 3.3 show that for the lepton NNLO corrections, electrons give the biggest contribution. The ratio between them and the second in

order muon corrections is smaller than for KLOE. The real lepton pair production is dominated by electrons. The results given by tau real pairs are negligible.

BaBar σ_{BY} = 5.195(2) nb				
particles	σ_h [nb]	σ_{v+s} [nb]	σ_{pairs} [nb]	sum [nb]
EXACT NNLO				
electron	0.202439(7)	-0.223667	0.01355(8)	-0.00768(8)
muon	0.075789(2)	-0.079231(2)	0.000451(2)	-0.002991(3)
tau	0.0138398(4)	-0.0144654(2)	0.120(3)*10^{-8}	-0.0006257(5)
leptons sum: σ^{NNLO}_{lep}				**-0.01130(8)**
hadrons	0.17995(2)	-0.1888(4)	0.000029(3)	-0.0088(4)
BabaYaga NNLO				
electron	0.20244(2)	-0.20971(5)	-	-0.00727(5)
muon	0.07580(1)	-0.07872(2)	-	-0.00292(2)
tau	0.013847(4)	-0.014541(4)	-	-0.000694(6)
leptons sum: σ^{NNLO}_{BY}				**-0.01088(5)**
hadrons	0.17984(2)	-0.18760(4)	-	-0.00776(5)
leptons relative difference: $\lvert\sigma^{NNLO}_{lep} - \sigma^{NNLO}_{BY\,lep}\rvert/\sigma_{BY}$				**0.08(2)‰**
hadrons relative difference: $\lvert\sigma^{NNLO} - \sigma^{NNLO}_{BY}\rvert/\sigma_{BY}$				**0.23(8)‰**

Table 3.3: Comparison between exact NNLO results and the approximate ones from BabaYaga@NLO for BaBar experiment cuts at $\sqrt{s}$=10.56 GeV

For the BaBar event selection, the relative difference for the hadron contributions is equal to 0.23(8)‰ and is about three times bigger than the lepton contribution (which is equal to 0.08(2) ‰). The signs of the lepton and hadron contributions are both negative. The sum of the relative differences is equal to 0.31(8) ‰. It means that the estimation of the generator accuracy for the BaBar conditions is also right.

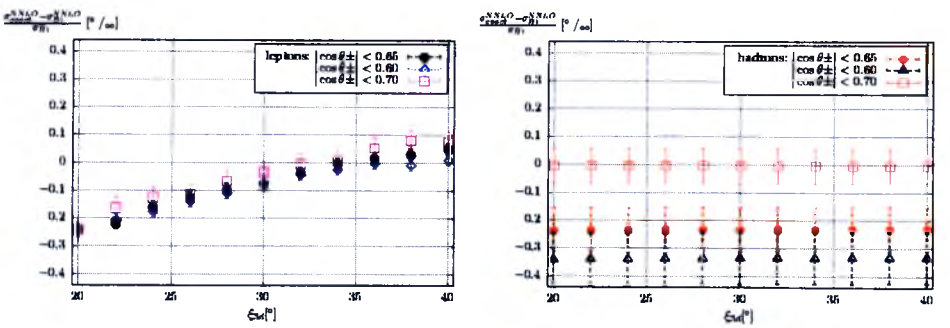

Figure 3.6: The relative difference of NNLO massive corrections, as a function of 3d acolinearity for BaBar for leptons(left) and hadrons (right).

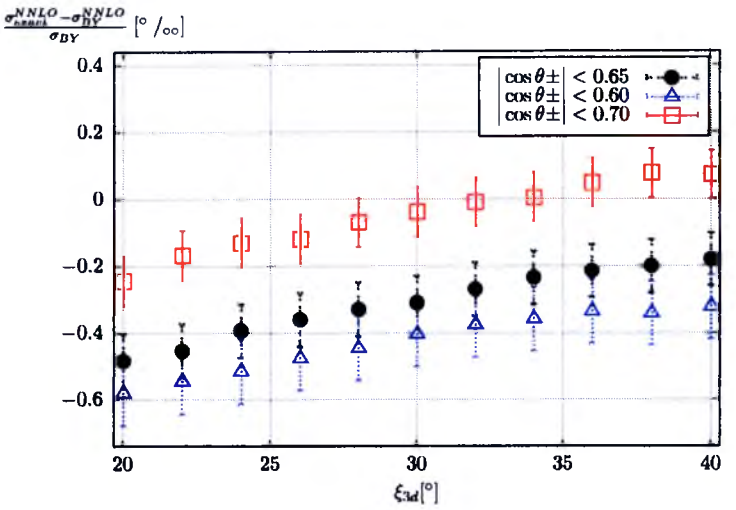

Figure 3.7: The relative difference of NNLO massive corrections, as a function of 3d acolinearity for BaBar. The sum of the lepton and hadron contribution.

For the additional analysis, three different sets of the angular cuts were chosen. Figures 3.6 and 3.7 present the relative difference as a function of 3d acollinearity (Eq. 7.7). All obtained results are stable. The estimated accuracy of the BabaYaga@NLO MC generator is smaller than 1 ‰. The worst value of the relative difference for the sum of the lepton and hadron corrections for all various cuts is about 0.6 ‰.

Belle

The energy for the Belle experiment is close to BaBar - $\sqrt{s}$=10.58 GeV. It is the experiment with the biggest energy of the incoming particles among the examined. The results of the calculated NNLO corrections are presented in Tab. 3.4.

The leptonic part of the Bhabha corrections is dominated by electrons. The second in order muons gives three times smaller contribution. Tau production is small compared with the rest of the corrections. The hadron and lepton contributions have the same sign. Their relative differences are added together. The sum is equal to 0.74(9) ‰. This value is still smaller than the estimated accuracy of BabaYaga@NLO, but it will combine with other uncertainties.

For Belle, an additional scan over various values of 2d acollinearity for three sets of the angular cuts was done (Fig. 3.8 and 3.9). The values close

BELLE σ_{BY} = 5.501(5) nb				
particles	σ_h [nb]	σ_{v+s} [nb]	σ_{pairs} [nb]	sum [nb]
NNLO				
electron	0.21572(7)	-0.25596	0.01310(5)	-0.02714(9)
muon	0.080377(8)	-0.09009(1)	0.000759(1)	-0.00895(2)
tau	0.014428(4)	-0.01602(1)	0.0000321(1)	-0.00156(1)
leptons sum: σ^{NNLO}_{lep}				**-0.03765(9)**
hadrons	0.18969(1)	-0.2124(5)	0.00015(1)	-0.0226(5)
BabaYaga NNLO				
electron	0.21563(2)	-0.23994(2)	-	-0.02431(3)
muon	0.080376(6)	-0.08948(2)	-	-0.009104(2)
tau	0.014423(1)	-0.016091(7)	-	-0.001668(7)
leptons sum: σ^{NNLO}_{BYlep}				**-0.03508(3)**
hadrons	0.18964(3)	-0.21089(5)	-	-0.02125(6)
leptons relative difference: $\|\sigma^{NNLO}_{lep} - \sigma^{NNLO}_{BYlep}\|/\sigma_{BY}$				**0.47(2)‰**
hadrons relative difference: $\|\sigma^{NNLO} - \sigma^{NNLO}_{BY}\|/\sigma_{BY}$				**0.27(9)‰**

Table 3.4: Comparison between exact NNLO results and the approximate ones from BabaYaga@NLO for BELLE experiment cuts at $\sqrt{s}$=10.58 GeV

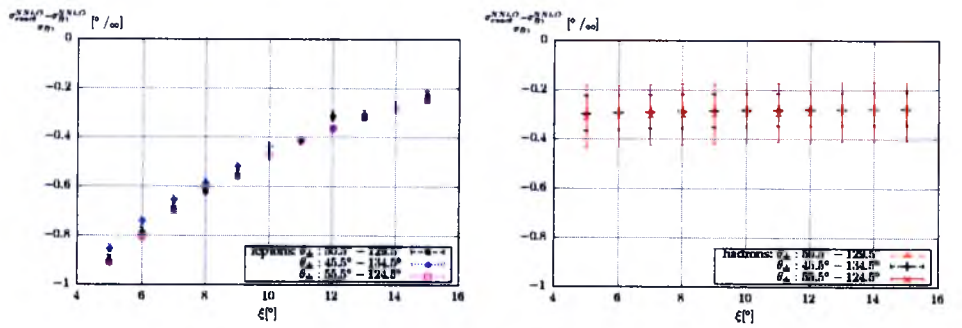

Figure 3.8: The relative difference of NNLO massive corrections, as a function of 2d acollinearity for Belle for leptons(left) and hadrons (right).

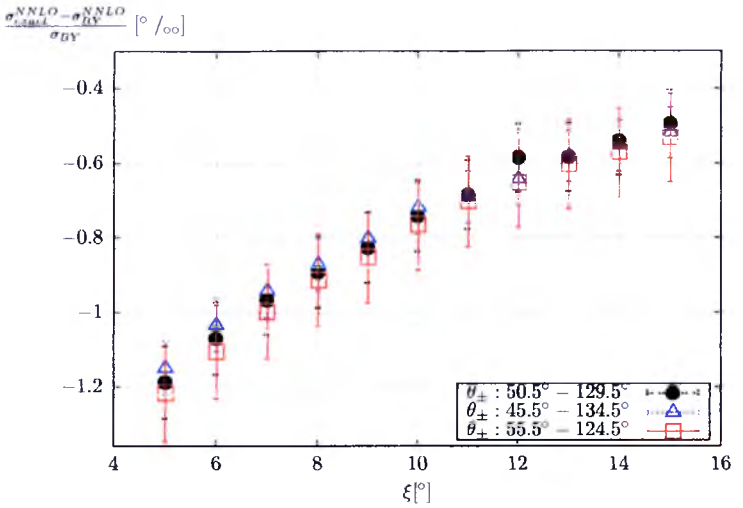

Figure 3.9: The relative difference of NNLO massive corrections, as a function of 2d acollinearity for Belle. The sum of the lepton and hadron contribution.

to the central point ($\xi = 10°$) do not exceed the estimated 1 ‰ accuracy. For the smallest values of acollinearity the relative differences can be bigger than 1 ‰. However, this difference is not significant.

Although the BaBar and Belle experiments run at almost the same energy and the complete cross sections σ_{BY} for them have similar values, the different event selection causes NNLO corrections to behave in a different way. It shows that generally we cannot predict the accuracy of a generator without direct studies of experimental setups.

BES-III

The BES-III experiment works at energy between $\sqrt{s} = 2.5$ and $\sqrt{s} = 5$ GeV. The event selection is different from the one for the previous presented experiments. BES-III event selection does not contain cuts for acollinearity. The energy chosen for BES-III is equal to $\sqrt{s} = 3.65$ GeV and the results of the calculations are presented in Tab. 3.5. For leptons, the electron contributions are dominant. The total contribution from electrons is about four times bigger than the contribution with muons, and about thirty five times bigger than the one for tau production. For tau there is no real pair contribution.

The relative differences are as follows: 0.057 ‰ for leptons and 0.21 ‰for hadrons. The contributions have opposite signs. The sum of the lepton and hadron contributions gives 0.15(9) ‰. It is below the 1 ‰ accuracy declared

BES III σ_{BY} = 116.41(2) nb				
particles	σ_h [nb]	σ_{v+s} [nb]	σ_{pairs} [nb]	sum [nb]
NNLO				
electron	3.19544(9)	-3.55544	0.188856(997)	-0.171(1)
muon	0.83245(2)	-0.88149(1)	0.002003(6)	-0.04704(1)
tau	0.058674(2)	-0.0633(1)	0	-0.0046(1)
leptons sum: σ_{lep}^{NNLO}				**-0.223(1)**
hadrons	1.66065(8)	-1.81(1)	0.000539(7)	-0.15(1)
BabaYaga NNLO				
electron	3.1960(3)	-3.3730(2)	-	-0.1770(4)
muon	0.83252(7)	-0.88041(9)	-	-0.0479(1)
tau	0.058679(7)	-0.06323(2)	-	-0.00455(2)
leptons sum: σ_{BY}^{NNLO}				**-0.2295(4)**
hadrons	1.6613(3)	-1.7860(2)	-	-0.1247(4)
leptons relative difference: $\lvert\sigma_{lep}^{NNLO} - \sigma_{BYlep}^{NNLO}\rvert/\sigma_{BY}$				**0.057(9)‰**
hadrons relative difference: $\lvert\sigma^{NNLO} - \sigma_{BY}^{NNLO}\rvert/\sigma_{BY}$				**0.21(9)‰**

Table 3.5: Comparison between exact NNLO results and the approximate ones from BabaYaga@NLO for BES III experiment cuts at $\sqrt{s}$=3.65 GeV

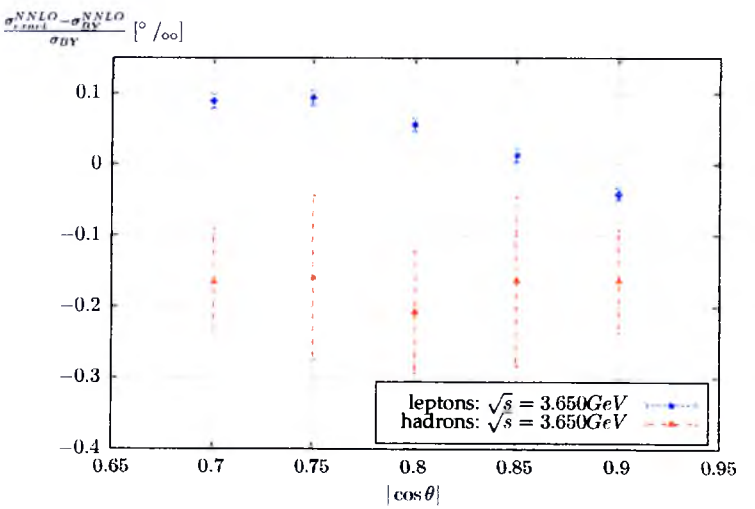

Figure 3.10: The relative difference of NNLO massive corrections, as a function of $\cos\theta$ for BES III for leptons and hadrons.

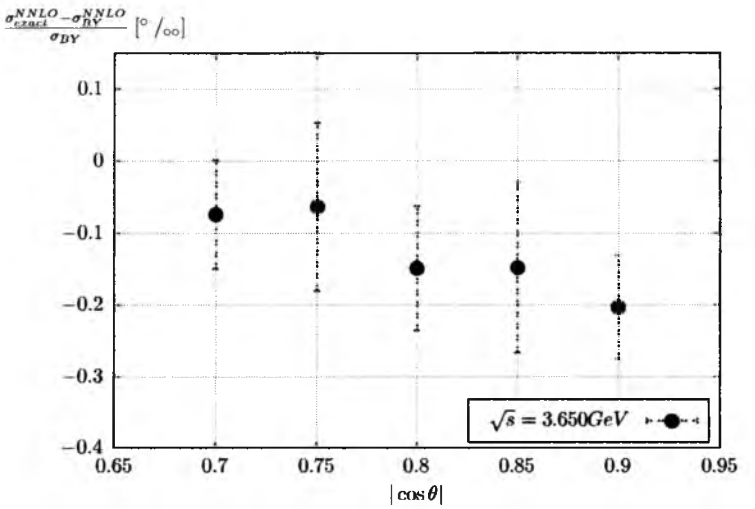

Figure 3.11: The relative difference of NNLO massive corrections, as a function of $\cos\theta$ for BES III. The sum of the lepton and hadron contribution.

by BabaYaga@NLO.

An additional scan over values of $\cos\theta$ was done to check the stability of the results (Figs. 3.10, 3.11). The obtained values of the accuracy are less than 0.3 ‰. The results are stable, and there are no unexpected changes of accuracy.

3.5 Conclusions

Exact calculations of the NNLO massive corrections to Bhabha scattering are presented and compared with approximate results of the BabaYaga@NLO Monte Carlo generator, for four sets of cuts as close to the experimental ones as possible: KLOE, BaBar, BES-III, Belle. The theoretical accuracy of the generator BabaYaga@NLO was tested. For realistic event selections, the maximum observed difference is at the level of 0.07%. When cuts are changed, the sum of the missing pieces can reach 0.1%. This situation occurs for very tight acollinearity cuts for Belle.

Stability of the results for the additional event selections was examined, and there are no dramatic changes of accuracy. The calculations prove correctness of the estimated accuracy of the BabaYaga@NLO generator. The approximation done for missing virtual corrections and real pair emissions is right for precision luminosity measurements with 10^{-3} accuracy.

For lepton part of the contributions, the electron-positron influence is dominant. The tau part is negligible. Except for KLOE, where the pair emission was excluded by the event selection, there is still an open question about contribution from real hadron emissions (different than $\pi^+\pi^-$).

Part II

NNLO ISR corrections to $e^+e^- \to hadrons(muons)$ in the PHOKHARA generator

Chapter 4

0 photon contribution in the PHOKHARA MC generator

The aim of this work is to prepare a new, extended version of the PHOKHARA Monte Carlo generator [13]. The contributions without real and hard photon emissions were added for all available final states: $\mu^+\mu^-$, $\pi^+\pi^-$, $2\pi_0\pi^+\pi^-$, $2\pi^+2\pi^-$, $\bar{p}p$, $\bar{n}n$, K^+K^-, $\bar{K}^0K^0$, $\pi^+\pi^-\pi^0$, $\Lambda(\to \pi^-p)\bar{\Lambda}(\to \pi^+\bar{p})$, $\eta\pi^+\pi^-$. The virtual and soft part of the new corrections were added to the e^+e^- vertex. These contributions will be called zero photon contribution. The zero photon option in present version of the PHOKHARA8.0 generator is limited to initial state emission (ISR). Together with already existing ISR corrections, the new part allows for calculations of full NNLO ISR contribution. The $\Lambda(\to \pi^-p)\bar{\Lambda}(\to \pi^+\bar{p})$ mode is an exception, since only the NLO contributions are available for this case. All new contributions are based on those existing in the following publication [35]. The formulas presented in this publication and used in PHOKHARA8.0 do not contain narrow resonances. The contributions with narrow resonances are presented in [36]. Inclusion of these contributions requires further work.

4.1 The NNLO ISR corrections

The set of NNLO ISR corrections in the PHOKHARA8.0 Monte Carlo generator consists of three parts:

$$\begin{aligned} d\sigma(e^+e^- \to \text{hadrons(muons)} + \text{photons}) = \\ d\sigma(e^+e^- \to \text{hadrons(muons)}) \\ + d\sigma(e^+e^- \to \text{hadrons(muons)} + \text{one hard photon}) \\ + d\sigma(e^+e^- \to \text{hadrons(muons)} + \text{two hard photons}) \end{aligned} \tag{4.1}$$

The first component $d\sigma(e^+e^- \to \text{hadrons(muons)})$ is a new part in the generator's code and describes the zero photon emission. This part can be written as a contraction between a leptonic $L^0_{\mu\nu}$ and a hadronic (muonic) $H^{\mu\nu}$ tensor:

$$d\sigma(e^+e^- \to \text{hadrons}) = \frac{1}{2s} L^0_{\mu\nu} H^{\mu\nu} d\Phi_n(p_1 + p_2; q_1, \cdot, q_n) \tag{4.2}$$

$d\Phi_n(p_1 + p_2; q_1, \cdot, q_n)$ is a Lorentz invariant phase space element, p_1 is a positron four-momenta, p_2 is an electron four-momenta, q_i $(i = 1, ..., n)$ denote the outgoing particles four-momenta and $s = (p_1 + p_2)^2$. The separation between the initial leptons described by $L^0_{\mu\nu}$ and the final hadrons or muons described by $H^{\mu\nu}$ allows the addition of the zero photon mode without interference in the part of the code that describes final states. The corrections were added only to the leptonic tensor, which is the same for all final states. The form of the $H^{\mu\nu}$ tensor depends strongly on the hadron state and phenomenological model used in calculations. The leptonic tensor $L^0_{\mu\nu}$ contains the LO, NLO and NNLO contributions to the zero photon corrections for the electron-positron vertex:

$$L^0_{\mu\nu} = 16\pi\alpha(p_{1\mu}p_{2\nu} - g_{\mu\nu}\frac{s}{2} + p_{1\mu}p_{2\nu})|\frac{1}{1 - \Delta_{VP}(s)}|^2(1 + \Delta)$$

The expression $16\pi\alpha(p_{1\mu}p_{2\nu} - g_{\mu\nu}\frac{s}{2} + p_{1\mu}p_{2\nu})$ denotes Born contribution (LO) (Fig. 4.1). The other zero photon corrections are described by Δ. $\Delta_{VP}(s)$ is the vacuum polarisation.

$$\Delta = \Delta_{virt,1ph} + \Delta_{soft,1ph} + \Delta_{virt,2ph} + \Delta_{soft,2ph} + \Delta_{virt,soft,1ph} \tag{4.3}$$

$$\Delta_{soft,1ph} = \frac{\alpha}{\pi}(\frac{1}{2}\log^2(s/m_e^2) + 2\log(2w)(\log(s/m_e^2) - 1) - 2\zeta_2) \tag{4.4}$$

where $s = (p_1 + p_2)^2$, m_e - electron mass, $\zeta_2 = 1/6\pi^2$ - zeta Riemann function, and ω denotes the cut between hard and soft photon emissions and is defined with the use of minimal energy of hard photon (E_γ^{min}) as:

$$\omega = \frac{E_\gamma^{min}}{\sqrt{s}} \tag{4.5}$$

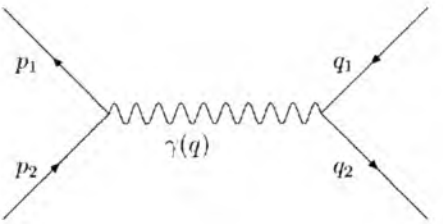

Figure 4.1: Born contribution to the process $e^+e^- \to hadrons(muons)$

The sum of all contributions with hard and soft photon emissions is cut independent.

$$\Delta_{virt,1ph} = 2\mathrm{Re}(F_1) = \frac{2\alpha}{\pi}(-\log^2(s/m_e^2)/4 + 3\log(s/m_e^2) - 1 + 2\zeta_2) \quad (4.6)$$

$$\mathrm{Im(F_1)} = \alpha(\log^2(s/m_e^2)/2 - \frac{3}{4}) \quad (4.7)$$

The form of the function F_1 is given in the limit of $s >> m_e^2$.

$$\Delta_{soft,2ph} = \frac{\Delta^2_{soft,1ph}}{2} \quad (4.8)$$

$$\Delta_{virt,soft,1ph} = \Delta_{soft,1ph}\Delta_{virt,1ph} \quad (4.9)$$

$$\Delta_{virt,2ph} = |F_1|^2 + 2\mathrm{Re}(F_2) \quad (4.10)$$

where:

$$\mathrm{Re}(F_2) = (\frac{\alpha}{\pi})^2(\log^4(s/m_e^2) - 3\frac{\log^3(s/m_e^2)}{16} + \log^2(s/m_e^2)(\frac{17}{32} - \frac{5\zeta_2}{4}) \quad (4.11)$$
$$+ \log(s/m_e^2)(-\frac{21}{32} + 3\zeta_2 + \frac{3\zeta_3}{2}) - 3\zeta_2\log(2) - \frac{\zeta_2}{2} + \frac{405}{216})$$

The $\Delta_{soft,1ph}$ comes from the corrections with one soft ISR photon presented in Fig. 4.2. The NLO virtual contribution $\Delta_{virt,1ph}$ comes from the corrections presented in Fig. 4.3. Both contributions, virtual $\Delta_{virt,1ph}$ and soft $\Delta_{soft,1ph}$, are infra-red divergent. In both cases, the photon mass λ was introduced to regulate these divergences and generate the terms $\log(\lambda^2/m_e^2)$ with the opposite signs. In formulas Eq. 4.4 and 4.6 these terms are subtracted.

The NNLO part of the zero photon corrections consists of three parts:

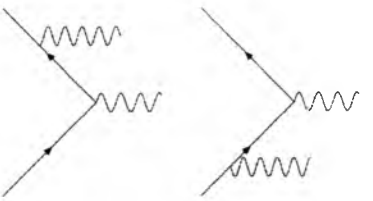

Figure 4.2: The NLO soft corrections to the process $e^+e^- \to hadrons(muons)$

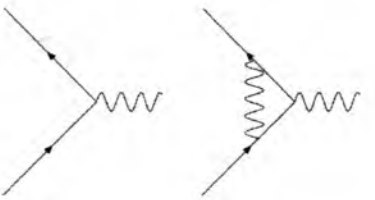

Figure 4.3: Samples of the NLO virtual corrections to the process $e^+e^- \to hadrons(muons)$

- contributions with two virtual photons $\Delta_{virt,2ph}$ presented in Fig. 4.4;
- contributions with one soft and one virtual photon $\Delta_{virt,soft,1ph}$ presented in Fig. 4.5;
- contributions with two soft photons $\Delta_{soft,2ph}$ presented in Fig. 4.6.

The $\Delta_{virt,2ph}$ and $\Delta_{soft,2ph}$ contributions contain $\log(\lambda^2/m_e^2)$ terms with the opposite signs (similarly to the NLO corrections, photon mass is used). In the presented formulas these terms are subtracted. The formula Eq. 4.8

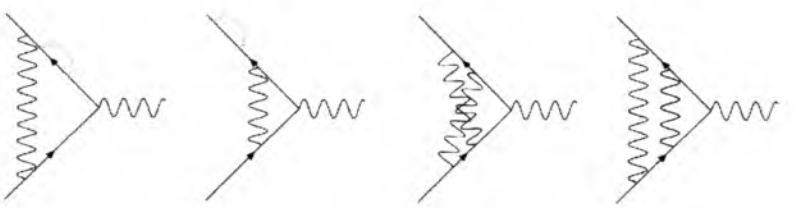

Figure 4.4: Samples of the NNLO virtual corrections to the process $e^+e^- \to hadrons(muons)$

that describes $\Delta_{soft,2ph}$ differs from the one presented in [35] by the factor

$\frac{\alpha^2}{\pi^2}[-2\zeta_2(\log(s/m_e^2)+1)^2]$. It is caused by different division of the two photon phase space in the PHOKHARA8.0 generator presented in Fig. 4.7. In his work [35], Berends does not use the division of the phase space as used here and showed in Fig. 4.7. The boundary for the contribution with two soft photons is defined in this case by the sum of the energies of photons:

$$E_1 + E_2 < E^{\gamma}_{min} \tag{4.12}$$

E_i (i=1,2) denotes photon energy, E^{γ}_{min} is the energy cut-off. In the division used in PHOKARA8.0, the conditions for the contribution with the two photon emission is: $E_1 < E^{\gamma}_{min}$ and $E_2 < E^{\gamma}_{min}$. These different conditions lead to the different limits for photon energies in the two soft photon integrand. Hence, this is an additional factor in Berend's formula [35]. In case of PHOKHARA8.0, this factor is included in the contributions with the real photon emission.

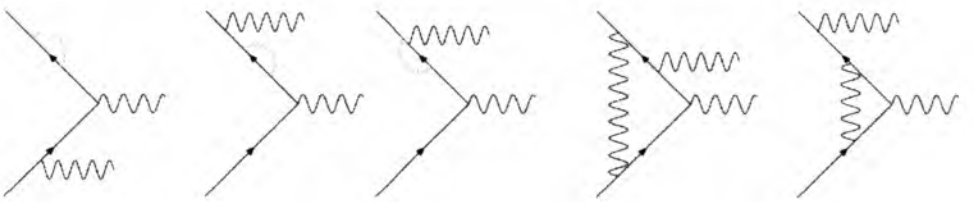

Figure 4.5: Samples of the NNLO corrections to the process $e^+e^- \to$ *hadrons(muons)* with one virtual and one soft photon

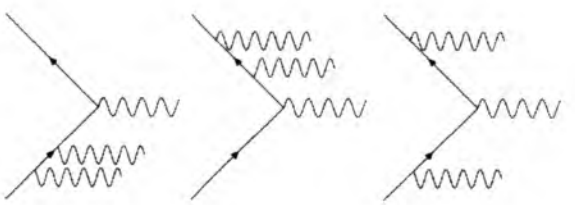

Figure 4.6: Samples of the NNLO soft corrections to the process $e^+e^- \to$ *hadrons(muons)*

The contributions $d\sigma(e^+e^- \to$ hadrons(muons) + one hard photon) and $d\sigma(e^+e^- \to$ hadrons(muons) + two hard photons) denote, respectively, the part with one [37] and two real hard photon emissions [37]. In both cases the vacuum polarisation is also included.

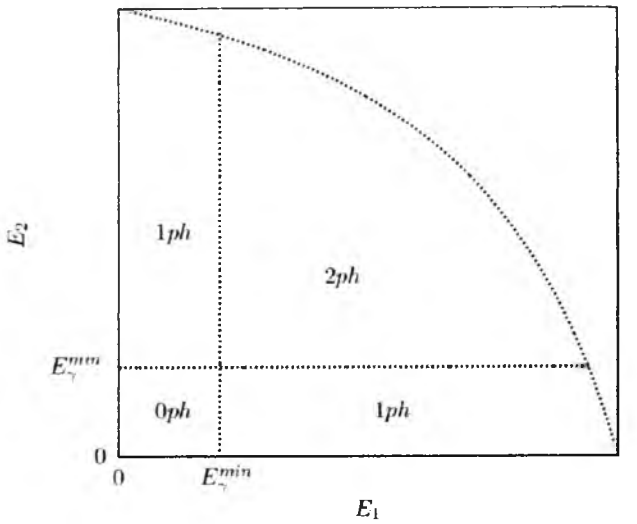

Figure 4.7: Division of the phase space. 0ph is described by $d\sigma(e^+e^- \to$ hadrons(muons)), 1ph by $d\sigma(e^+e^- \to$ hadrons(muons) + one hard photon) and 2ph by $d\sigma(e^+e^- \to$ hadrons(muons) + two hard photons)

4.2 The generator and numerical results

Cut independence

The structure of the hadronic tensor was not changed during implementation of the zero photon part. The new part of routine that includes $L^0_{\mu\nu}$ and generates the phase space for the particles for the process $e^+e^- \to$ hadrons(muons) was added to the generator. The leptonic tensor $L^0_{\mu\nu}$ is common to all final states. The main test of the new routine checks the ω cut independence of the total cross section $\sigma(e^+e^- \to$ hadrons(muons) + photons). Two values of ω were used for this purpose: 10^{-4} and 10^{-5}. The first value is recommended for generator. For $\omega = 10^{-5}$, some negative weights are observed. To check, if the results of the calculations are correct in the presence of negative weights, Monte Carlo integrand (Eq. 7.4, 7.5) was used. The results for $\omega = 10^{-5}$ obtained by the simulation were compared with results obtained with Monte Carlo integrand. The relative difference was used for the comparison between two values of the ω cut (Eq. 7.1) with the cross section obtained for $\omega = 10^{-4}$ in denominator. The results of the test are presented in Fig. 4.8 for two values of energies: $\sqrt{s} = 1.02$ GeV and $\sqrt{s}$=3.65

GeV. On X-axis there is a number of the mode: 0 ($\mu^+\mu^-$), 1 ($\pi^+\pi^-$), 2 ($2\pi^0\pi^+\pi^-$), 3 ($2\pi^+2\pi^-$), 4 ($p\bar{p}$), 5 ($n\bar{n}$), 6 (K^+K^-), 7 ($K^0\bar{K}^0$), 8 ($\pi^0\pi^+\pi^-$), 9 ($\Lambda(\to \pi^-p)\bar{\Lambda}(\to \pi^+\bar{p})$), 10 ($\eta\pi^+\pi^-$). For the smaller energies, some modes are absent because the energy is too small to generate these final states. For

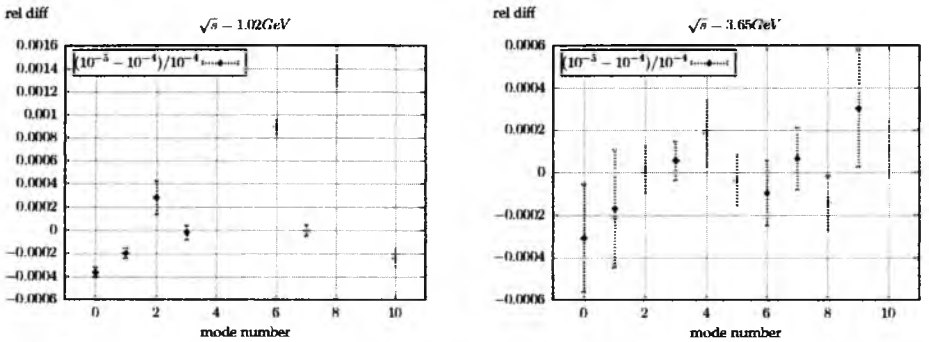

Figure 4.8: Test of the cut independence for two sample energies: $\sqrt{s}$ =1.02 and 3 GeV

the energy $\sqrt{s}$=3.65 GeV there is full agreement between results for both ω cuts. The same agreement was observed for other tested energies (2-5 GeV). However, there is a small discrepancy for some modes for $\sqrt{s}$ = 1.02 GeV. It is caused by the fact that this is energy of narrow resonance ϕ. As was mentioned before, the new contributions used in PHOKHARA8.0 do not contain the contributions with narrow resonances. The test for $\sqrt{s}$ = 1.02 GeV is an example of the behaviour of the results near the resonance. So for narrow resonances, the generator should be used carefully. For energies outside the close vicinity of the narrow resonance regions, the cut independence is confirmed.

Comparisons between KKMC4.13 and PHOKHARA8.0 for $\mu^+\mu^-$ final state

There was the possibility to make another test for the mode $\sigma(e^+e^- \to$ muons + photons). The test is based on the comparison between KKMC and PHOKHARA7.0 presented in [38]. The integrated cross section σ_I for muon production is calculated as a function of q^2_{min} according to:

$$\sigma_I(q^2_{min}) = \int_{q^2_{min}}^{s} \frac{d\sigma}{dq^2} dq^2 \tag{4.13}$$

The comparison between the results obtained with KKMC4.13 and PHOKHARA8.0 is presented in Fig. 4.9. The ratio between results is used to

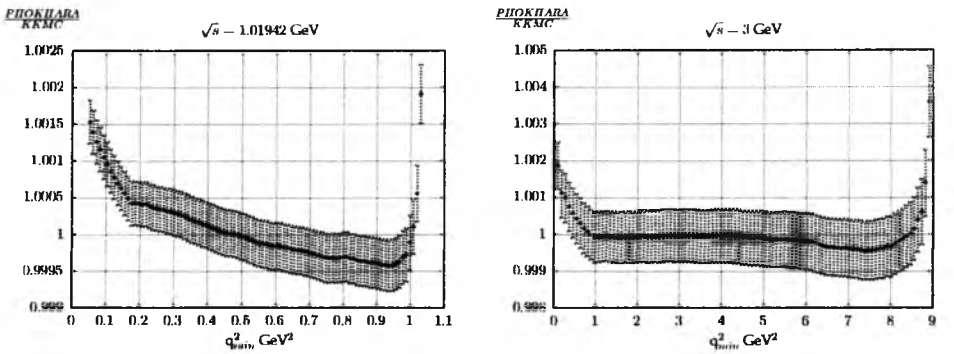

Figure 4.9: Comparison between integrated cross section obtained by KKMC4.13 and PHOKHARA8.0 MC generators as a function of q^2_{min}

show the difference between codes for the two energies. The smaller energy was also used in the test presented in [38] . In both cases the agreement is very good and is at per mile level. The differences that show for q^2_{min} close to s are caused by multiphoton emission that is not present in PHOKHARA8.0.

A similar test can be done for a missing transverse momentum. Defined as the difference between momenta of initial and final fermions, this magnitude shows the significance of the contribution of the multiphoton emission. This contribution is absent in the PHOKHARA8.0 generator. The example of the influence of this contribution is presented in Fig. 4.10. The left part shows the distribution of missing momentum and the right part the ratio between results obtained by KKMC4.13 and PHOKHARA8.0. The difference is not big but visible.

Another possible test between KKMC4.13 and PHOKHARA8.0 for the process $\sigma(e^+e^- \to \text{muons} + \text{photons})$ is a comparison of the angular distributions. The result of this test for energy 3 GeV is presented in Fig. 4.11. The average between the number of muons and antimuons as a function of angle was calculated with the generators. The relative difference was calculated and presented as a function of $\cos\theta$. The relative difference between the results is equal to a few per mile. The results obtained for other checked energies (2, 2.5, 3 GeV) show similar behaviour.

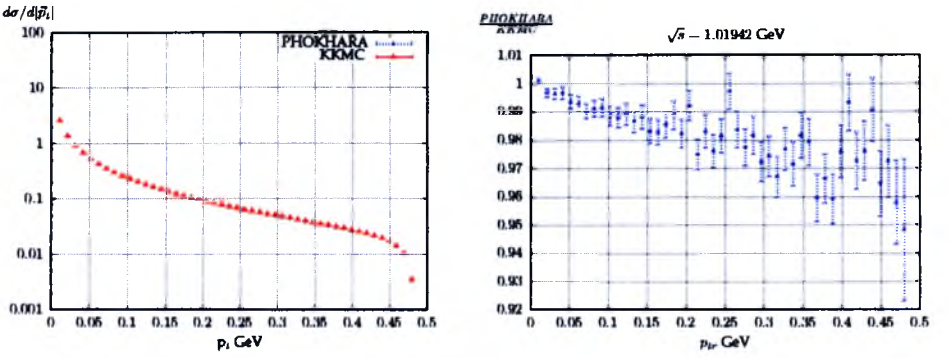

Figure 4.10: Comparison of the missing momentum distribution between results obtained by PHOKHARA9.0 and KKMC4.13 MC generators for the process with muons. $\sqrt{s} = 1.01942$ GeV

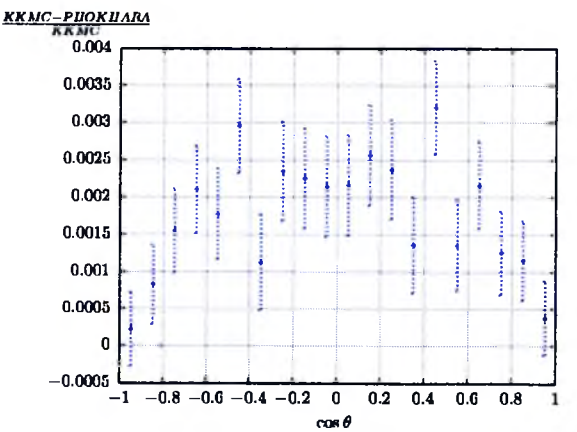

Figure 4.11: The relative difference between results obtained by KKMC4.13 and PHOKHARA8.0 for the angular distribution and for $\sqrt{s}$ =3GeV

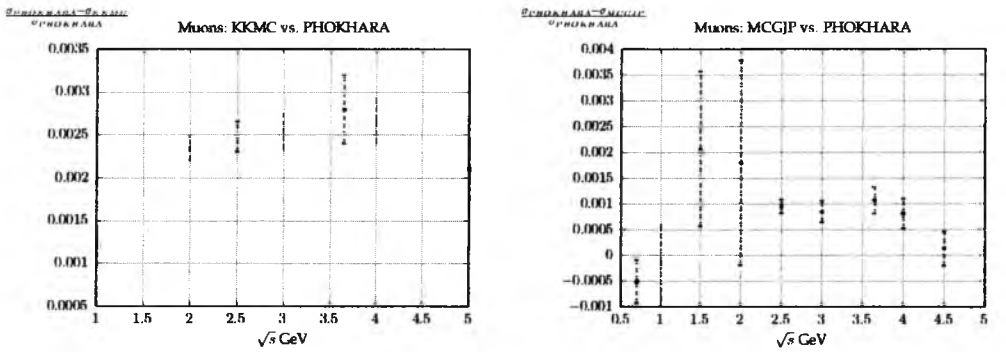

Figure 4.12: Comparison between results obtained for PHOKHARA8.0 and KKMC4.13 and MCGJP for different CM energies for the process of muon production in final state.

Energy scan for $\sigma(e^+e^- \to \text{muons} + \text{photons})$

Another possible test of the generator is the comparison between the results obtained for PHOKHARA9.0, KKMC4.13 and MCGJP for the process $\sigma(e^+e^- \to \text{muons} + \text{photons})$. It is possible to compare the total cross section produced by the listed generators for different values of energy. The results are presented in Fig. 4.12. The differences between PHOKHARA8.0 and the other two generators do not depend strongly on the center of mass energy. The differences are at per mile level. The bigger errors for smaller energies for the comparison with the MCGJP generator result from some numerical problems for this generator. The used version of the MCGJP generator was downloaded from the web page: Working Group on Rad. Corrections and MC Generators for Low Energies [39]. This version was not stable when trying to reach better accuracy for some energies. For some energies, the generator does not calculate the cross section when trying to increase the accuracy. Also, because of similar numerical instabilities caused by the used version of MCGJP generator, it was not possible to do this same type of test for pions and kaons. Both modes should, in principle, be available for MCGJP.

4.3 Conclusions

The new version of the generator PHOKHARA8.0 allows the user to calculate the full NNLO ISR corrections for various hadron final states and

muons. The generator is complementary to routines already used in experiments; KKMC4.13 and MCGJP. The differences between these routines and PHOKHARA8.0 generator for muon mode are at the per mile level. Moreover, all distributed PHOKHARA versions include exact kinematics in the one and two photon emissions.

Part III

Complete one loop corrections to $e^+e^- \to \mu^+\mu^-\gamma$ in the PHOKHARA generator

Chapter 5

One loop corrections to $e^+e^- \to \mu^+\mu^-\gamma$

The PHOKHARA Monte Carlo generator [14], [37] is a tool for simulation of the processes with photon radiation: $e^+e^- \to hadrons(muons)+\gamma$ (startig from PHOKHARA8.0 for ISR there is also mode $e^+e^- \to hadrons(muons)$). For this process, the generator contains the corrections up to the emissions of two real and hard photons. It allows the user to simulate a number of various final states: $\mu^+\mu^-$, $\pi^+\pi^-$, $2\pi_0\pi^+\pi^-$, $2\pi^+2\pi^-$, $\bar{p}p$, $\bar{n}n$, K^+K^-, $\bar{K}^0K^0$, $\pi^+\pi^-\pi^0$, $\Lambda(\to \pi^-p)\bar{\Lambda}(\to \pi^+\bar{p})$, $\eta\pi^+\pi^-$. The program has been already used in the low energy particle physics experiments like KLOE, BELLE, BES or BaBar. As noted in the Introduction, the mode with muons in the final state played a crucial role in the BaBar and KLOE analysis for the process: $e^+e^- \to \pi^+\pi^-$. The discrepancies between the results obtained for pion production by the KLOE and BaBar experiments called for the search of the source of these discrepancies.

The mode with the muon production and photon radiation ($e^+e^- \to \mu^+\mu^-\gamma$) contains the contribution up to one-loop. However the generator does not contain full one-loop corrections. The influence of these missing contributions was estimated; the estimated accuracy of the PHOKHARA8.0 code for this mode is 0.5%. The progress done on the numerical calculations has allowed the missing contributions to be included into the PHOKHARA8.0 generator [20]. Now, it is possible to check their size and influence on the error of analysis for the process with pion production.

PHOKHARA9.0, the new and extended version of the PHOKHARA8.0 Monte Carlo generator, was prepared and used to check the influence of the new contributions on the total cross section. The calculations were done with energies and cuts close to the experimental ones for KLOE and BaBar. In this chapter, the theoretical part of this work is presented.

5.1 Corrections to $e^+e^- \to \mu^+\mu^-\gamma$

The corrections for the process $e^+e^- \to \mu^+\mu^-\gamma$ can be presented as a sum of the contributions with emission of one and two real hard photons:

$$\begin{aligned} \sigma(e^+e^- \to \text{muons} + \text{photons}) &= \\ \sigma(e^+e^- \to \text{muons} + \text{one hard photon}) & \\ +\sigma(e^+e^- \to \text{muons} + \text{two hard photons}) & \end{aligned} \tag{5.1}$$

The contribution with the emission of one real hard photon:

$$\sigma_{1ph} = \sigma(e^+e^- \to \text{muons} + \text{one hard photon}) \tag{5.2}$$

consists of:

- σ_B Born contribution with emission of one real hard photon (Fig. 5.1);
- σ_s the soft part with emission of one hard and one soft photon (Fig. 5.2);
- σ_v - virtual corrections (Figs. 5.3, 5.4, 5.5). All these corrections interfere with the Born diagrams.

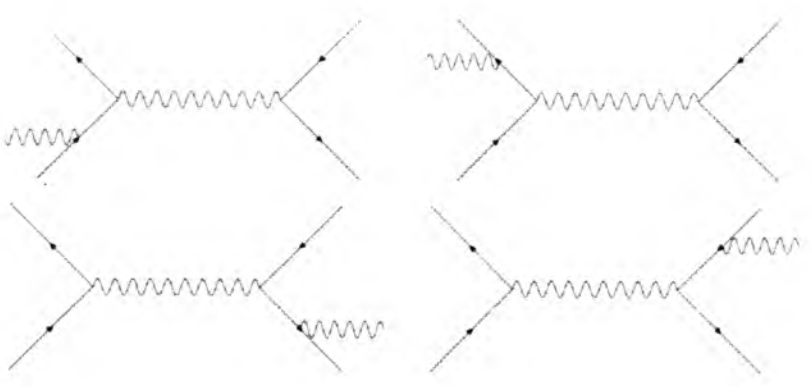

Figure 5.1: Born contribution to the process $e^+e^- \to \mu^+\mu^-\gamma$

The contributions with emission of two real, hard photons:

$$\sigma_{2ph} = \sigma(e^+e^- \to \text{muons} + \text{two hard photons}) \tag{5.3}$$

consists of the corrections presented in Fig. 5.6. The total cross section includes the square of the amplitude of the sum of all these corrections.

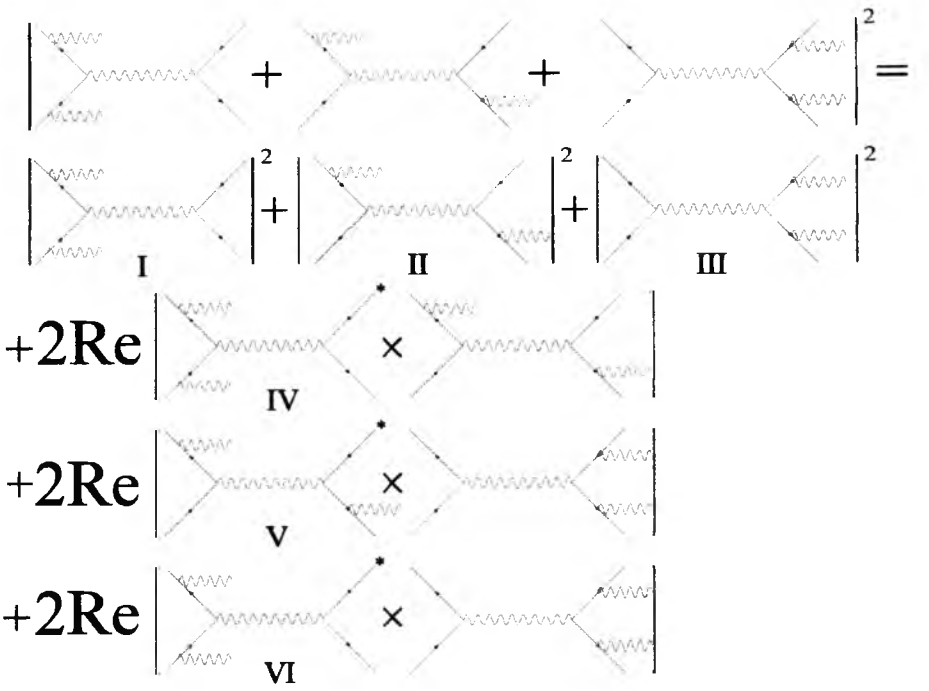

Figure 5.2: The soft contributions to the process $e^+e^- \to \mu^+\mu^-\gamma$

5.1.1 Missing corrections

Compared with the distributed version of the PHOKHARA Monte Carlo generator (PHOKHARA8.0), the new version includes the following missing corrections:

- the contributions with two hard photons emitted from muon line (FSR) Fig. 5.6c - the square of the amplitude and the interference with contributions: Figs. 5.6a and 5.6b;
- all interferences between corrections 5.6a and 5.6b. In PHOKHARA8.0 this was included only partly [37] ;
- full soft part σ_s when one photon is soft and one is hard (Fig. 5.2). In PHOKHARA8.0, only chosen fragments of this contribution were used;
- all so-called pentabox corrections presented in Fig. 5.5 that interfere with Born (Fig. 5.1);

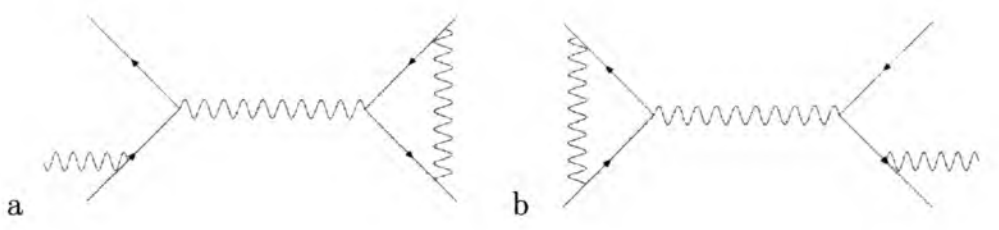

Figure 5.3: Samples of triangles for the process $e^+e^- \to \mu^+\mu^-\gamma$

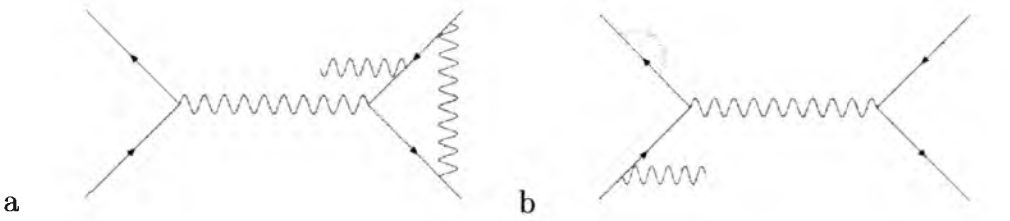

Figure 5.4: Samples of so-called boxes for the process $e^+e^- \to \mu^+\mu^-\gamma$

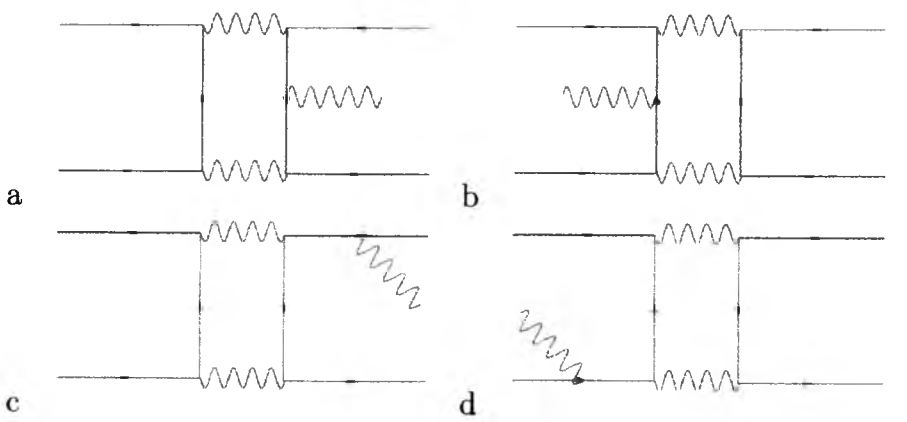

Figure 5.5: Samples of so-called pentaboxes for the process $e^+e^- \to \mu^+\mu^-\gamma$

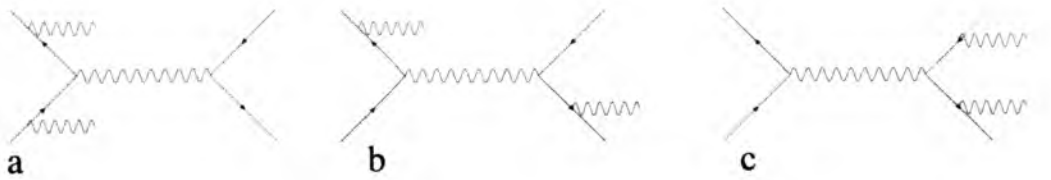

Figure 5.6: Samples of contributions with two real photon emissions for the process $e^+e^- \to \mu^+\mu^-\gamma$

- box diagrams with photon radiation from final state and all interferences between box diagrams (Fig. 5.4) and Born (Fig. 5.1);
- interference between triangle virtual correction (Fig. 5.3b) and Born part (Fig. 5.1) with radiation form ISR, and between triangle virtual correction (Fig. 5.3a) and Born part (Fig. 5.1) with radiation from FSR;

A study of the differences between the results obtained with PHOKHARA8.0 and the new one enables one to determine whether the missing parts of the corrections are responsible for the discrepancies between the experiments.

Before implementation to the generator, theoretical formulas were prepared and coded to the form useful in software. Wherever it was possible, a helicity method for construction of the amplitudes was used. The formula with the emission of two real photons was divided into two parts. The first part contains the process with emission of two hard photons $\sigma_{2ph}(\omega)$ (Fig. 5.6). For this part, the amplitude was prepared and the cross section was calculated numerically. The second part contains all diagrams with one hard and one soft photon $\sigma_s(\omega)$ (Fig. 5.2). Here the integration over the soft photon was done analytically. Both parts are separated by infrared cut-off ω. This cut is defined as:

$$\omega = \frac{E_{cut}}{\sqrt{s}} \tag{5.4}$$

where in the numerator there is a maximum energy of soft photon and in the denominator there is an energy of initial particles.

For virtual corrections, two versions of software were created with different calculation methods: [40] and [41]. This is very important due to the fact that it was possible to test this part of the calculations independently.

Coordinate system and momenta convention

In this part of the work, the following convention is used:

- p_1 - positron (e^+) four-momenta;
- p_2 - electron (e^-) four-momenta;
- q_1 - antimuon (μ^+) four-momenta;
- q_2 - muon (μ^-) four-momenta;
- k_1, k_2 - photons four-momenta.

All calculations are made in the centre of mass frame of the e^+e^-. Incoming positrons move along the z-axis. It means that: $p_1 = (E, 0, 0, \sqrt{E^2 - m_e^2})$ and $p_2 = (E, 0, 0, -\sqrt{E^2 - m_e^2})$.

5.2 Two hard photon emissions

For all hard photon emissions, the helicity method for calculations of the amplitudes was used. The convention introduced in [42] was adapted. The gamma matrices are defined in the following form:

$$\gamma^\mu = \begin{pmatrix} 0 & \sigma_+^\mu \\ \sigma_-^\mu & 0 \end{pmatrix}, \qquad \mu = 0, 1, 2, 3\,, \tag{5.5}$$

The following convention was used for the other matrices:

$$\not{a} = a_\mu \gamma^\mu = \begin{pmatrix} 0 & a^+ \\ a^- & 0 \end{pmatrix}, \tag{5.6}$$

$$a^\pm = a^\mu \sigma_\mu^\pm = \begin{pmatrix} a^0 \mp a^3 & \mp(a^1 - ia^2) \\ \mp(a^1 + ia^2) & a^0 \pm a^3 \end{pmatrix}. \tag{5.7}$$

The spinors u and v in helicity basis for a particle and an antiparticle are given by:

$$\begin{aligned} u(p,\lambda) &= \begin{pmatrix} \sqrt{E - \lambda|\mathbf{p}|}\,\chi(\mathbf{p},\lambda) \\ \sqrt{E + \lambda|\mathbf{p}|}\,\chi(\mathbf{p},\lambda) \end{pmatrix} \equiv \begin{pmatrix} u_I \\ u_{II} \end{pmatrix}, \\ v(p,\lambda) &= \begin{pmatrix} -\lambda\sqrt{E + \lambda|\mathbf{p}|}\,\chi(\mathbf{p},-\lambda) \\ \lambda\sqrt{E - \lambda|\mathbf{p}|}\,\chi(\mathbf{p},-\lambda) \end{pmatrix} \equiv \begin{pmatrix} v_I \\ v_{II} \end{pmatrix}. \end{aligned} \tag{5.8}$$

Where helicity $\lambda/2 = \pm 1/2$.

The helicity eigenstates $\chi(\mathbf{p}, \lambda)$ are expressed in terms of the polar and azimuthal angles of the momentum vector $\mathbf{p}$:

$$\chi(\mathbf{p}, +1) = \begin{pmatrix} \cos(\theta/2) \\ e^{i\phi}\sin(\theta/2) \end{pmatrix},$$
$$\chi(\mathbf{p}, -1) = \begin{pmatrix} -e^{-i\phi}\sin(\theta/2) \\ \cos(\theta/2) \end{pmatrix}. \tag{5.9}$$

They are presented in the general form for particles of four-momentum $p = (E, \mathbf{p})$. However, for the incoming particles in our coordinate system they can be presented in the following form:

$$\chi(\mathbf{p_1}, +1) = \begin{pmatrix} 1 \\ 0 \end{pmatrix},$$
$$\chi(\mathbf{p_1}, -1) = \begin{pmatrix} 0 \\ 1 \end{pmatrix}. \tag{5.10}$$

for positron and

$$\chi(\mathbf{p_2}, +1) = \begin{pmatrix} 0 \\ -1 \end{pmatrix},$$
$$\chi(\mathbf{p_2}, -1) = \begin{pmatrix} 1 \\ 0 \end{pmatrix}. \tag{5.11}$$

for electron.

For all our calculations, the complex polarisation vectors in the helicity basis are defined for the real photons:

$$\varepsilon^\mu(k_i, \lambda_i = \mp) = \frac{1}{\sqrt{2}}\big(0, \pm\cos\theta_i\cos\phi_i + i\sin\phi_i,$$
$$\pm\cos\theta_i\sin\phi_i - i\cos\phi_i, \mp\sin\theta_i\big), \tag{5.12}$$

with $i = 1, 2$.

5.2.1 Two photon emission FSR amplitude

One of the new NLO contributions in the PHOKHARA9.0 MC generator is the emission of two real hard photons from final states. Here the calculations of the amplitudes are presented.

FSR diagrams with two real photon emissions can be divided into three groups:

- diagrams with emission of both photons from antimuon line (Fig. 5.7a.);
- diagrams with emission of both photons form muon line (Fig. 5.7b.);
- diagrams with emission of one photon from muon and one from antimuon line (Fig. 5.7c.).

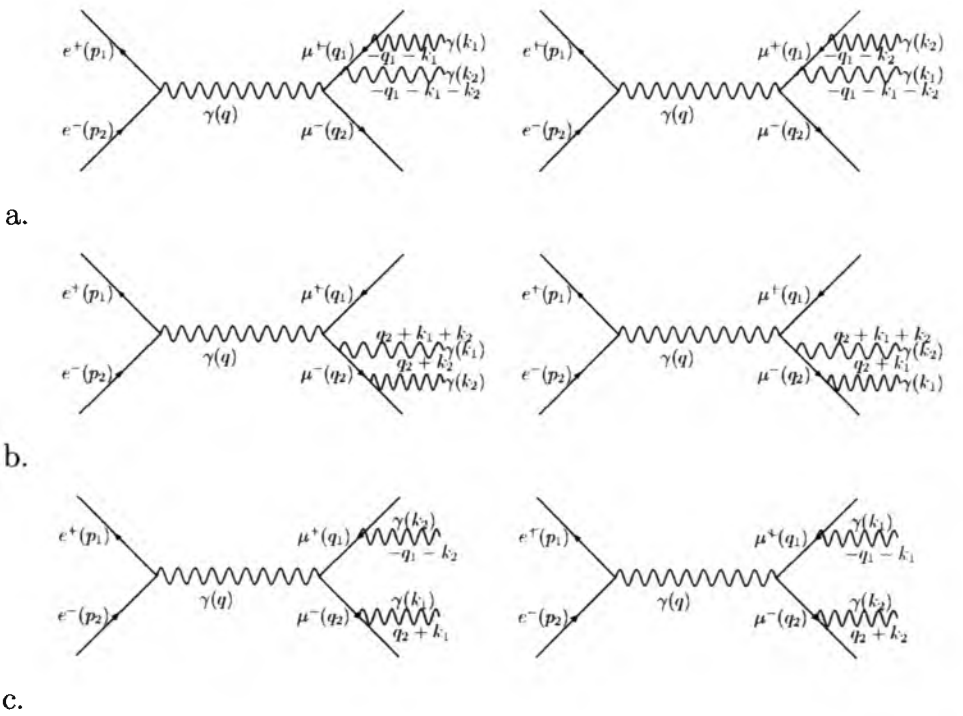

Figure 5.7: The FSR hard photon corrections to the process $e^+e^- \to \mu^+\mu^-\gamma$

An amplitude for the first diagram (emission of photons from μ^+ line) written with use of Feynman rules got the following form:

$$M_1 = \bar{u}(q_2) ie\gamma^\nu i \frac{-\not{k}_1 - \not{k}_2 - \not{q}_1 + m_\mu}{(-k_1 - k_2 - q_1)^2 - m_\mu^2} ie\not{\epsilon}_2^* \qquad (5.13)$$
$$i \frac{-\not{k}_1 - \not{q}_1 + m_\mu}{(-k_1 - q_1)^2 - m_\mu^2} ie\not{\epsilon}_1^* \nu(q_1) \frac{-ig_{\nu\delta}}{s} J^\delta_{e^+e^-}$$

$$M_1 = \frac{e^3}{s} \bar{u}(q_2) \frac{\gamma^\nu(-\not{k}_1 - \not{k}_2 - \not{q}_1 + m_\mu)\not{\epsilon}_2^*(-\not{k}_1 - \not{q}_1 + m_\mu)\not{\epsilon}_1^*}{2k_1 \cdot q_1 (2k_1 \cdot q_1 + 2k_2 \cdot q_1 + 2k_1 \cdot k_2)} \nu(q_1) J_{\nu e^+e^-} \qquad (5.14)$$

Here $J^{\delta}_{e^+e^-}$ denotes a current of the incoming particles.

$$J^{\delta}_{e^+e^-}(\lambda_1,\lambda_2) \equiv J^{\delta}_{e^+e^-} = -ie\bar{\nu}(p_1,\lambda_1)\gamma^{\delta}u(p_2,\lambda_2) \tag{5.15}$$

It is possible to write M_1 into a more useful form. In the next step, the Dirac equation is used. The expression with the spinor $\bar{u}$ can be expressed as follows:

$$\bar{u}(q_2)m_{\mu}\gamma^{\nu} = \bar{u}(q_2)\not{q}_2\gamma^{\nu} \tag{5.16}$$

Here anticommutation rules for the gamma matrices are used:

$$\bar{u}(q_2)\not{q}_2\gamma^{\nu} = \bar{u}(q_2)q_{2\alpha}(-\gamma^{\nu}\gamma^{\alpha} + 2g^{\nu\alpha}) \tag{5.17}$$

The same procedure works for the spinor v.

$$\not{\varepsilon}^*_1 m_{\mu}\nu(q_1) = -\not{\varepsilon}^*_1\not{q}_1\nu(q_1) \tag{5.18}$$

$$-\not{\varepsilon}^*_1\not{q}_1\nu(q_1) = -\varepsilon^*_{1\sigma}q_{1\beta}(-\gamma^{\beta}\gamma^{\sigma} + 2g^{\beta\sigma}) \tag{5.19}$$

Below the part of the outgoing current is written:

$$\begin{aligned} A^{\nu} = \bar{u}(q_2)\gamma^{\nu}(-\not{k}_1 - \not{k}_2 - \not{q}_1 + m_{\mu})\not{\varepsilon}^*_2(-\not{k}_1 - \not{q}_1 + m_{\mu})\not{\varepsilon}^*_1\nu(q_1) \\ = -\bar{u}(q_2)\gamma^{\nu}(-\not{k}_1 - \not{k}_2 - \not{q}_1 - \not{q}_2)\not{\varepsilon}^*_2\not{k}_1\not{\varepsilon}^*_1\nu(q_1) \\ -\bar{u}(q_2)\gamma^{\nu}(-\not{k}_1 - \not{k}_2 - \not{q}_1 - \not{q}_2)\not{\varepsilon}^*_2 2(\varepsilon^*_1\cdot q_1)\nu(q_1) \\ -\bar{u}(q_2)2q^{\nu}_2\not{\varepsilon}^*_2\not{k}_1\not{\varepsilon}^*_1\nu(q_1) \\ -\bar{u}(q_2)4q^{\nu}_2\not{\varepsilon}^*_2(\varepsilon^*_1\cdot q_1)\nu(q_1) \end{aligned} \tag{5.20}$$

It can be split into four parts.

$$A^{\nu} = A^{\nu}_1 + A^{\nu}_2 + A^{\nu}_3 + A^{\nu}_4 \tag{5.21}$$

For example the first part has the following form:

$$\begin{aligned} A^{\nu}_1 = \bar{u}(q_2)\gamma^{\nu}(-\not{k}_1 - \not{k}_2 - \not{q}_1 - \not{q}_2)\not{\varepsilon}^*_2\not{k}_1\not{\varepsilon}^*_1\nu(q_1) \\ = \bar{u}(q_2)\gamma^{\nu}(\not{k}_1 + \not{k}_2 + \not{Q})\not{\varepsilon}^*_2\not{k}_1\not{\varepsilon}^*_1\nu(q_1) \end{aligned} \tag{5.22}$$

with $\not{Q} = \not{q}_1 + \not{q}_2$.The matrices are multiplied:

$$\begin{aligned} A^{\nu}_1 = u^+_I(q_2)[\sigma^{\nu}_-(k^+_1 + k^+_2 + Q^+)\varepsilon^{*-}_2 k^+_1\varepsilon^{*-}_1]\nu_I(q_1) \\ +u^+_{II}(q_2)[\sigma^{\nu}_+(k^-_1 + k^-_2 + Q^-)\varepsilon^{*+}_2 k^-_1\varepsilon^{*+}_1]\nu_{II}(q_1) \end{aligned} \tag{5.23}$$

By doing the same for the other parts of A^ν and putting them into the amplitude, the following form is received:

$$M_1 = \frac{e^3}{4s}\{u_I^+(q_2)[\sigma_-^\nu(k_1^+ + k_2^+ + Q^+) - 2q_2^\nu]\varepsilon_2^{*-}[k_1^+\varepsilon_1^{*-} + 2(\varepsilon_1^*\cdot q_1)]\nu_I(q_1)$$
$$+u_{II}^+(q_2)[\sigma_+^\nu(k_1^- + k_2^- + Q^-) - 2q_2^\nu]\varepsilon_2^{*+}[k_1^-\varepsilon_1^{*+} + 2(\varepsilon_1^*\cdot q_1)]\nu_{II}(q_1)\}$$
$$\frac{J_{\nu e^+e^-}}{k_1\cdot q_1(k_1\cdot q_1 + k_2\cdot q_1 + k_1\cdot k_2)} \quad (5.24)$$

This same procedure used for the other five diagrams gives the following results:

$$M_2 = \frac{e^3}{4s}\{u_I^+(q_2)[\sigma_-^\nu(k_1^+ + k_2^+ + Q^+) - 2q_2^\nu]\varepsilon_1^{*-}[k_2^+\varepsilon_2^{*-} + 2(\varepsilon_2^*\cdot q_1)]\nu_I(q_1)$$
$$+u_{II}^+(q_2)[\sigma_+^\nu(k_1^- + k_2^- + Q^-) - 2q_2^\nu]\varepsilon_1^{*+}[k_2^-\varepsilon_2^{*+} + 2(\varepsilon_2^*\cdot q_1)]\nu_{II}(q_1)\}$$
$$\frac{J_{\nu e^+e^-}}{k_2\cdot q_1(k_1\cdot q_1 + k_2\cdot q_1 + k_1\cdot k_2)} \quad (5.25)$$

$$M_3 = \frac{e^3}{4s}\{u_I^+(q_2)[\varepsilon_2^{*-}k_2^+ + 2(\varepsilon_2^*\cdot q_2)]\varepsilon_1^{*-}[(k_1^+ + k_2^+ + Q^+)\sigma_-^\nu - 2q_1^\nu]\nu_I(q_1)$$
$$+u_{II}^+(q_2)[\varepsilon_2^{*+}k_2^- + 2(\varepsilon_2^*\cdot q_2)]\varepsilon_1^{*+}[(k_1^- + k_2^- + Q^-)\sigma_+^\nu - 2q_1^\nu]\nu_{II}(q_1)\}$$
$$\frac{J_{\nu e^+e^-}}{k_2\cdot q_2(k_1\cdot q_2 + k_2\cdot q_2 + k_1\cdot k_2)} \quad (5.26)$$

$$M_4 = \frac{e^3}{4s}\{u_I^+(q_2)[\varepsilon_1^{*-}k_1^+ + 2(\varepsilon_1^*\cdot q_2)]\varepsilon_2^{*-}[(k_1^+ + k_2^+ + Q^+)\sigma_-^\nu - 2q_1^\nu]\nu_I(q_1)$$
$$+u_{II}^+(q_2)[\varepsilon_1^{*+}k_1^- + 2(\varepsilon_1^*\cdot q_2)]\varepsilon_2^{*+}[(k_1^- + k_2^- + Q^-)\sigma_+^\nu - 2q_1^\nu]\nu_{II}(q_1)\}$$
$$\frac{J_{\nu e^+e^-}}{k_1\cdot q_2(k_1\cdot q_2 + k_2\cdot q_2 + k_1\cdot k_2)} \quad (5.27)$$

$$M_5 = \frac{-e^3}{4s}\{u_I^+(q_2)[\varepsilon_2^{*-}k_2^+ + 2(\varepsilon_2^*\cdot q_2)]\sigma_-^\nu[2(\varepsilon_1^*\cdot q_1) + k_1^+\varepsilon_1^{*-}]\nu_I(q_1)$$
$$+u_{II}^+(q_2)[\varepsilon_2^{*+}k_2^- + 2(\varepsilon_2^*\cdot q_2)]\sigma_+^\nu[2(\varepsilon_1^*\cdot q_1) + k_1^-\varepsilon_1^{*+}]\nu_{II}(q_1)\}\frac{J_{\nu e^+e^-}}{(k_1\cdot q_1)(k_2\cdot q_2)} \quad (5.28)$$

$$M_6 = \frac{-e^3}{4s}\{u_I^+(q_2)[\varepsilon_1^{*-}k_1^+ + 2(\varepsilon_1^*\cdot q_2)]\sigma_-^\nu[2(\varepsilon_2^*\cdot q_1) + k_2^+\varepsilon_2^{*-}]\nu_I(q_1)$$
$$+u_{II}^+(q_2)[\varepsilon_1^{*+}k_1^- + 2(\varepsilon_1^*\cdot q_2)]\sigma_+^\nu[2(\varepsilon_2^*\cdot q_1) + k_2^-\varepsilon_2^{*+}]\nu_{II}(q_1)\}\frac{J_{\nu e^+e^-}}{(k_2\cdot q_1)(k_1\cdot q_2)} \quad (5.29)$$

It is possible to present the complete amplitude for the process of emission of two final state real photons in a more consistent form:

$$\begin{aligned} M(\lambda_{\mu^+}, \lambda_{\mu^-}, \lambda_1, \lambda_2) = & \quad v_I^\dagger(\lambda_{\mu^+}) A(\lambda_1, \lambda_2)\, u_I(\lambda_{\mu^-}) \\ + & \quad v_{II}^\dagger(\lambda_{\mu^+}) B(\lambda_1, \lambda_2)\, u_{II}(\lambda_{\mu^-}) \,, \end{aligned} \tag{5.30}$$

The same convention was used for the PHOKHARA8.0 MC generator for the ISR hard part. The matrices A and B are defined as follows:

$$\begin{aligned} A(\lambda_1, \lambda_2) = \frac{-e^3}{4s}\Big(&\frac{a_1 \varepsilon_2^{*-} a_3}{(k_1\cdot q_1)N_1} + \frac{a_1 \varepsilon_1^{*-} a_5}{(k_2\cdot q_1)N_1} + \frac{a_7 \varepsilon_1^{*-} a_9}{(k_2\cdot q_2)N_2} \\ &+ \frac{a_{11}\varepsilon_2^{*-} a_9}{(k_1\cdot q_2)N_2} - \frac{a_7 J^-_{e^+e^-} a_3}{(k_1\cdot q_1)(k_2\cdot q_2)} - \frac{a_{11} J^-_{e^+e^-} a_5}{(k_2\cdot q_1)(k_1\cdot q_2)}\Big) \end{aligned} \tag{5.31}$$

$$\begin{aligned} B(\lambda_1, \lambda_2) = \frac{-e^3}{4s}\Big(&\frac{a_2 \varepsilon_2^{*+} a_4}{(k_1\cdot q_1)N_1} + \frac{a_2 \varepsilon_1^{*+} a_6}{(k_2\cdot q_1)N_1} + \frac{a_8 \varepsilon_1^{*+} a_{10}}{(k_2\cdot q_2)N_2} \\ &+ \frac{a_{12}\varepsilon_2^{*+} a_{10}}{(k_1\cdot q_2)N_2} - \frac{a_8 J^+_{e^+e^-} a_4}{(k_1\cdot q_1)(k_2\cdot q_2)} - \frac{a_{12} J^+_{e^+e^-} a_6}{(k_2\cdot q_1)(k_1\cdot q_2)}\Big) \end{aligned} \tag{5.32}$$

$$\begin{aligned} N_1 &= k_1\cdot q_1 + k_2\cdot q_1 + k_1\cdot k_2 \\ N_2 &= k_1\cdot q_2 + k_2\cdot q_2 + k_1\cdot k_2 \\ a_1 &= J^-_{e^+e^-}(p_1^+ + p_2^+) - 2q_2\cdot J_{e^+e^-} \\ a_2 &= J^+_{e^+e^-}(p_1^- + p_2^-) - 2q_2\cdot J_{e^+e^-} \\ a_3 &= k_1^+ \varepsilon_1^{*-} + 2(\varepsilon_1^*\cdot q_1) \\ a_4 &= k_1^- \varepsilon_1^{*+} + 2(\varepsilon_1^*\cdot q_1) \\ a_5 &= k_2^+ \varepsilon_2^{*-} + 2(\varepsilon_2^*\cdot q_1) \\ a_6 &= k_2^- \varepsilon_2^{*+} + 2(\varepsilon_2^*\cdot q_1) \\ a_7 &= \varepsilon_2^{*-} k_2^+ + 2(\varepsilon_2^*\cdot q_2) \\ a_8 &= \varepsilon_2^{*+} k_2^- + 2(\varepsilon_2^*\cdot q_2) \\ a_9 &= (p_1^+ + p_2^+) J^-_{e^+e^-} - 2q_1\cdot J_{e^+e^-} \\ a_{10} &= (p_1^- + p_2^-) J^+_{e^+e^-} - 2q_1\cdot J_{e^+e^-} \\ a_{11} &= \varepsilon_1^{*-} k_1^+ + 2(\varepsilon_1^*\cdot q_2) \\ a_{12} &= \varepsilon_1^{*+} k_1^- + 2(\varepsilon_1^*\cdot q_2) \end{aligned} \tag{5.33}$$

The presented structure of the FSR amplitude was used inside the PHOKHARA9.0 MC generator for calculations. Inside the PHOKHARA9.0 MC generator, the amplitude for the FSR two hard photon emissions was added to the part of the code that contains the emission of two hard photons from the initial line and mixing radiation: one hard photon ISR and one FSR. This combination allows the acquisition of all possible interferences between the diagrams with two real and hard photon radiations. In next section, the results of calculations and the analytical formulas for corresponding diagrams, with one soft and one hard photon, are presented.

Gauge invariance

The full set of the diagrams for FSR of two photons is gauge invariant. This property can be used as a primary test of the correctness of the obtained formula Eq. 5.30. In practice, it means that the amplitude M is equal to 0 in the following cases:

- in formula 5.30 both photon polarisations are replaced by corresponding photon momenta: $\varepsilon_1 = k_1$, $\varepsilon_2 = k_2$;
- in formula 5.30 exactly one of the photon polarisations are replaced by corresponding photon momenta: $\varepsilon_1 = k_1$ or $\varepsilon_2 = k_2$.

Both of these possibilities were checked for the analytical expression using the FORM [44] algebra system and gave expected results. The numerical test of the obtained formulas are presented in the next chapter.

5.3 Soft photon emission

As it was mentioned before, the phase space for the contribution with the emission of two photons was divided into two parts, soft and hard. Both parts depend on the infrared cut-off ω, but their sum is cut independent. The two real and hard photon's set of corrections requires the addition of the contributions with one hard and one soft photon. Only then are obtained results of calculations independent of the applied cut ω. Figure 5.2 presents a class of necessary corrections. One of the photons is hard and one is soft. The part that contains only ISR photons has been already presented in the PHOKHARA8.0 MC generator with some chosen interferences between two ISR photons and the contributions with one ISR and one FSR photon. The square of the amplitude for the full soft correction can be written as a product of the Born amplitude square and an integrand over the soft photon phase

space. It is possible to write the soft part of the cross section σ_s as a sum of six parts (Fig. 5.2):

$$\sigma_s = I + II + III + IV + V + VI \tag{5.34}$$

Where:

$$I = \frac{-\alpha}{4\pi}\int \frac{d^3k_1}{E_{k_1}}\left[\frac{p_1^\mu}{p_1\cdot k_1} - \frac{p_2^\mu}{k_1\cdot p_2}\right]\left[\frac{p_{1\mu}}{p_1\cdot k_1} - \frac{p_{2\mu}}{k_1\cdot p_2}\right]\cdot |M_{1ISR}|^2 \tag{5.35}$$

$$\begin{aligned} II = {} & \frac{-\alpha}{4\pi}\int \frac{d^3k_1}{E_{k_1}}\left[\frac{p_1^\mu}{p_1\cdot k_1} - \frac{p_2^\mu}{k_1\cdot p_2}\right]\left[\frac{p_{1\mu}}{p_1\cdot k_1} - \frac{p_{2\mu}}{k_1\cdot p_2}\right]\cdot |M_{1FSR}|^2 \\ & -\frac{\alpha}{2\pi}\mathrm{Re}\left(\int \frac{d^3k_1}{E_{k_1}}\left[\frac{p_1^\mu}{p_1\cdot k_1} - \frac{p_2^\mu}{k_1\cdot p_2}\right]\left[\frac{q_{2\mu}}{q_2\cdot k_1} - \frac{q_{1\mu}}{k_1\cdot q_1}\right]\cdot M_{1ISR}^* M_{1FSR}\right) \\ & -\frac{\alpha}{4\pi}\int \frac{d^3k_1}{E_{k_1}}\left[\frac{q_2^\mu}{q_2\cdot k_1} - \frac{q_1^\mu}{k_1\cdot q_1}\right]\left[\frac{q_{2\mu}}{q_2\cdot k_1} - \frac{q_{1\mu}}{k_1\cdot q_1}\right]\cdot |M_{1ISR}|^2 \end{aligned} \tag{5.36}$$

$$III = \frac{-\alpha}{4\pi}\int \frac{d^3k_1}{E_{k_1}}\left[\frac{q_2^\mu}{q_2\cdot k_1} - \frac{q_1^\mu}{k_1\cdot q_1}\right]\left[\frac{q_{2\mu}}{q_2\cdot k_1} - \frac{q_{1\mu}}{k_1\cdot q_1}\right]\cdot |M_{1FSR}|^2 \tag{5.37}$$

$$\begin{aligned} IV = {} & \frac{-\alpha}{2\pi}\mathrm{Re}\left(\int \frac{d^3k_1}{E_{k_1}}\left[\frac{p_1^\mu}{p_1\cdot k_1} - \frac{p_2^\mu}{k_1\cdot p_2}\right]\left[\frac{p_{1\mu}}{p_1\cdot k_1} - \frac{p_{2\mu}}{k_1\cdot p_2}\right]\cdot M_{1FSR}^* M_{1ISR}\right) \\ & -\frac{\alpha}{2\pi}\mathrm{Re}\left(\int \frac{d^3k_1}{E_{k_1}}\left[\frac{p_1^\mu}{p_1\cdot k_1} - \frac{p_2^\mu}{k_1\cdot p_2}\right]\left[\frac{q_{2\mu}}{q_2\cdot k_1} - \frac{q_{1\mu}}{k_1\cdot q_1}\right]\cdot |M_{1ISR}|^2\right) \end{aligned} \tag{5.38}$$

$$\begin{aligned} V = {} & \frac{-\alpha}{2\pi}\mathrm{Re}\left(\int \frac{d^3k_1}{E_{k_1}}\left[\frac{q_2^\mu}{q_2\cdot k_1} - \frac{q_1^\mu}{k_1\cdot q_1}\right]\left[\frac{p_{1\mu}}{p_1\cdot k_1} - \frac{p_{2\mu}}{k_1\cdot p_2}\right]\cdot |M_{1FSR}|^2\right) \\ & -\frac{\alpha}{2\pi}\mathrm{Re}\left(\int \frac{d^3k_1}{E_{k_1}}\left[\frac{p_1^\mu}{p_1\cdot k_1} - \frac{p_2^\mu}{k_1\cdot p_2}\right]\left[\frac{q_{2\mu}}{q_2\cdot k_1} - \frac{q_{1\mu}}{k_1\cdot q_1}\right]\cdot M_{1ISR}^* M_{1FSR}\right) \end{aligned} \tag{5.39}$$

$$VI = \frac{-\alpha}{2\pi}\mathrm{Re}\left(\int \frac{d^3k_1}{E_{k_1}}\left[\frac{p_1^\mu}{p_1\cdot k_1} - \frac{p_2^\mu}{k_1\cdot p_2}\right]\left[\frac{q_{2\mu}}{q_2\cdot k_1} - \frac{q_{1\mu}}{k_1\cdot q_1}\right]\cdot M_{1ISR}^* M_{1FSR}\right) \tag{5.40}$$

The sum of the presented parts of the soft contribution can be written in the following form (M_{1ISR}, M_{1FSR} - amplitudes with one hard photon from

initial and final state, σ_B - Born cross section):

$$\sigma_s = \frac{-\alpha}{4\pi}\int \frac{d^3k_1}{E_{k_1}}\left(\frac{p_1}{p_1\cdot k_1}-\frac{p_2}{k_1\cdot p_2}\right)^2 |M_{1ISR}+M_{1FSR}|^2 \quad (5.41)$$
$$\frac{-\alpha}{4\pi}\int \frac{d^3k_1}{E_{k_1}}\left(\frac{q_2}{q_2\cdot k_1}-\frac{q_1}{k_1\cdot q_1}\right)^2 |M_{1ISR}+M_{1FSR}|^2$$
$$\frac{-\alpha}{2\pi}\int \frac{d^3k_1}{E_{k_1}}\left(\frac{p_1^\mu}{p_1\cdot k_1}-\frac{p_2^\mu}{k_1\cdot p_2}\right)\left(\frac{q_{2\mu}}{q_2\cdot k_1}-\frac{q_{1\mu}}{k_1\cdot q_1}\right) |M_{1ISR}+M_{1FSR}|^2$$

$$\sigma_s = \frac{-\alpha}{4\pi}\int \frac{d^3k_1}{E_{k_1}}\left[\left(\frac{p_1}{p_1\cdot k_1}-\frac{p_2}{k_1\cdot p_2}\right)+\left(\frac{q_2}{q_2\cdot k_1}-\frac{q_1}{k_1\cdot q_1}\right)\right]^2 \sigma_B \quad (5.42)$$

$$\sigma_s = F(p_1,p_2,q_1,q_2,\omega)\sigma_B \quad (5.43)$$

Function $F(p_1,p_2,q_1,q_2,\omega)$ can be presented as a sum of three ingredients:

$$F(p_1,p_2,q_1,q_2,\omega) = F_{ISR}(p_1,p_2,\omega) + 2F_{INT}(p_1,p_2,q_1,q_2,\omega) + F_{FSR}(q_1,q_2,\omega) \quad (5.44)$$

$$F_{ISR}(p_1,p_2,\omega) = \frac{-\alpha}{4\pi}\int \frac{d^3k_1}{E_{k_1}}\left(\frac{p_1}{p_1\cdot k_1}-\frac{p_2}{k_1\cdot p_2}\right)^2 \quad (5.45)$$

$$F_{FSR}(q_1,q_2,\omega) = \frac{-\alpha}{4\pi}\int \frac{d^3k_1}{E_{k_1}}\left(\frac{q_2}{q_2\cdot k_1}-\frac{q_1}{k_1\cdot q_1}\right)^2 \quad (5.46)$$

$$F_{INT}(p_1,p_2,q_1,q_2,\omega) = \quad (5.47)$$
$$\frac{-\alpha}{4\pi}\int \frac{d^3k_1}{E_{k_1}}\left(\frac{p_1^\mu}{p_1\cdot k_1}-\frac{p_2^\mu}{k_1\cdot p_2}\right)\left(\frac{q_{2\mu}}{q_2\cdot k_1}-\frac{q_{1\mu}}{k_1\cdot q_1}\right)$$

Analytical integration

To solve the integrand $F(p_1,p_2,q_1,q_2,\omega)$, a change of variables to the spherical coordinate system is done.

$$d^3k_1 = |\overline{k_1}|^2 dk_1 d\varphi dcos\phi \quad (5.48)$$

The discussed soft contribution is infrared divergent. To resolve this, regularisation with a photon mass λ is used. The logarithmic part of the soft

contribution that contains the photon mass cancels with the appropriate contribution coming from the virtual part. This cancellation was done before the formulas were used in the PHOKHARA9.0 code. There remains only the ω cut dependence, which cancels with contribution by the two hard photons (Fig. 5.6). After the introduction of the photon mass λ, its energy can be written as:

$$E_{k_1}^2 = |\overrightarrow{k_1}|^2 + \lambda^2 \tag{5.49}$$

To merge two denominators into one, a substitution is used [43]. It is based on the relationship Eq. 7.8 (Appendix). In the presented case, $a = k_1 q_i$, $b = k_1 p_j$ i,j =1,2. It gives the:

$$\frac{1}{(k_1 \cdot p_j)(k_1 \cdot q_i)} = \int_0^1 \frac{dx}{(p_x \cdot k_1)^2} \tag{5.50}$$

The new four-momenta is defined as:

$$p_x = xq_i + (1-x)p_j \tag{5.51}$$

The function $F(p_1, p_2, q_1, q_2, \omega)$ can be written in a form of sum of a two components. The first one $F_\omega(p_1, p_2, q_1, q_2, \omega)$ depends on ω cut and the lepton four-momenta, while the second one $F_{fin}(p_1, p_2, q_1, q_2)$ depends only on the lepton four momenta. The part with $\log\omega$ is in the following form:

$$\begin{aligned} F_\omega(p_1, p_2, q_1, q_2, \omega) = F_{ISR\omega}(p_1, p_2, \omega) + 2F_{INT\omega}(p_1, p_2, q_1, q_2, \omega) \\ + F_{FSR\omega}(q_1, q_2, \omega) \end{aligned} \tag{5.52}$$

$$F_{ISR\omega}(p_1, p_2, \omega) = -\frac{2\alpha}{\pi}\left[1 - \frac{p_1 p_2 \log\left(\frac{(1+\beta_e)^4}{16m_e^4/s^2}\right)}{s\beta_e}\right]\log\left(\frac{2\omega\sqrt{s}}{\lambda}\right) \tag{5.53}$$

$$F_{FSR\omega}(q_1, q_2, \omega) = -\frac{2\alpha}{\pi}\left[1 - \frac{q_1 q_2 \log\left(\frac{(1+\beta_\mu)^4}{16m_\mu^4/q^4}\right)}{q^2\beta_\mu}\right]\log\left(\frac{2\omega\sqrt{s}}{\lambda}\right) \tag{5.54}$$

$$F_{INT\omega}(p_1, p_2, q_1, q_2, \omega) = -\frac{\alpha}{\pi}\sum_{i,j=1}^{2}\frac{(-1)^j p_i q_j \log\left(\frac{(1+\beta_{ij})^2 (p_i q_j)^2}{m_e^2 m_\mu^2}\right)}{2\sqrt{(p_i q_j)^2 - m_e^2 m_\mu^2}}\log\left(\frac{2\omega\sqrt{s}}{\lambda}\right) \tag{5.55}$$

$$\beta_e = \sqrt{1 - 4m_e^2/s}$$
$$\beta_\mu = \sqrt{1 - 4m_\mu^2/q^2}$$
$$\beta_{ij} = \sqrt{1 - m_e^2 m_\mu^2/(p_i q_j)^2} \tag{5.56}$$

The finite part of the soft contribution calculated in the e^+e^- center of mass frame contains a number of dilogarithm contributions and is presented in Appendix 7.0.6.

Approximation The analytical solution of the integral 5.44 is made with the use of the approximations for the limits of the calculated integrands. As was mentioned before, the photon mass λ is used for the regularisation. The solution of integral 5.44 depends on the ratio $\frac{\Delta}{\lambda}$, where Δ denotes the maximal value of the length of the soft photon vector $|\bar{k}|$ and is connected with energy of the soft cut $E_{cut} = \omega\sqrt{s}$ according to the following formula: $\Delta = \sqrt{E_{cut}^2 - \lambda^2}$. The following approximation is used in the solution of Eq. 5.44 ($\lambda/\Delta << 1$):

$$\sqrt{\left(\frac{\Delta}{\lambda}\right)^2 + 1} = \frac{\Delta}{\lambda}\sqrt{1 + \left(\frac{\lambda}{\Delta}\right)^2} \approx \frac{\Delta}{\lambda} + O\left(\frac{\lambda}{\Delta}\right) \tag{5.57}$$

It means that the hard soft cut independence is consistent to the level of the leading terms of the soft contribution, proportional to Δ. This approximation does not omit any terms that are divergent when the photon mass goes to 0.

5.4 Virtual corrections

The one-loop virtual corrections for the process of muon pair production, included in the PHOKHARA9.0 MC generator, are divided into three gauge invariant groups. The first one, presented in Fig. 5.5, contains pentagon diagrams (Fig. 5.5a, b) complete with box diagrams (Fig. 5.5c, d). Pentagons do not form a class of gauge independent diagrams. Together with box diagrams with emission of the real photon from the external line, they are gauge independent. The sum of these diagrams is multiplied by tree level diagrams (Born) presented in Fig. 5.1. This class of contributions is called the pentabox contribution.

The second gauge independent class of virtual corrections constitutes box (box-triangle) contributions. The samples of diagrams of this class are presented in Fig. 5.4. In this case both virtual and real photons are located in the same vertex, and are multiplied by the Born diagrams (Fig. 5.1).

Two different routines were used for numerical calculations of the pentabox and box contributions: written in the double precision routine, based on PJFry library [41], and the quad precision routine [40]. The first routine requires use of the CERNLIB library and uses the trace method. The second one is an independent software that does not use any external libraries and uses the helicity method for calculations. The existence of two independent routines enables their proper implementation in the PHOKHARA generator and correctness of the codes used for calculations to be check. It is especially important for the pentabox contribution, since this has not been used for calculations in physical regions. Both codes reproduced a result for one phase space point for the one loop virtual corrections presented in [45].

The third gauge invariant class of contributions, triangles, consists of diagrams presented in Fig. 5.3. The sum of these diagrams interferes with Born. The missing part of the triangle contributions can be written in the following form:

$$\sigma_{mis} = \frac{\alpha}{2\pi}\mathrm{Re}[(V_1 + V_2 + 2V_3)M_{ISR}M^*_{FSR}] \tag{5.58}$$

Here $M_{ISR}M^*_{FSR}$ is the interference between the ISR and FSR parts of Born amplitude. The coefficients V_i (i = 1,2,3) have the following form:

$$\begin{aligned} V_1 = {} & \frac{5q^2 - 12m_\mu^2}{q^2\beta_\mu}\log(p_3) - 4 - 2\log q^2/m_\mu^2 \\ & -2\frac{1+\beta_\mu^2}{\beta_\mu}\left(\log(p_3)\log(1+\beta_\mu/2) + 2Li_2(p_1) - \frac{\pi^2}{2}\right) \\ & +4\left[\frac{-\log(p_3)}{\beta_\mu} + \frac{1+\beta_\mu^2}{\beta_\mu}\left(\frac{\log(p_3)^2}{4} + Li_2(p_1)\right)\right] \\ & -2\left(2 - \frac{1+\beta_\mu^2}{\beta_\mu}\log(p_3)\right)\log(s/q^2) \end{aligned} \tag{5.59}$$

$$V_2 = \frac{m_\mu}{q^2\beta_\mu}C_1, C_1 = -p_3 + i\pi) \tag{5.60}$$

$$V_3 = \log(s/m_e^2)^2 + \log(s/m_e^2) - 4 + \frac{4\pi^2}{3} \tag{5.61}$$

Here:

$$\beta_\mu = \left(1 - \frac{4m_\mu^2}{q^2}\right)^{\frac{1}{2}} \tag{5.62}$$

$$p_1 = 2\frac{\beta_\mu}{1+\beta_\mu} \tag{5.63}$$

$$p_3 = \frac{q^2(1+\beta_\mu)^2}{4m_\mu^2} \tag{5.64}$$

The missing triangle corrections are coded inside the PHOKHARA9.0 generator with the use of existing routines. However, the package PJFry also contains the routine eemmgloopmix, which calculates the triangle corrections. So it is possible to test proper implementation of the missing contributions in the generator. Both routines are written in double precision.

Chapter 6

Numerical studies of $e^+e^- \to \mu^+\mu^-\gamma$ in PHOKHARA9.0

6.1 Tests in PHOKHARA9.0 for $e^+e^- \to \mu^+\mu^-\gamma$

In Chapter 5, information about the one loop corrections to the process $e^+e^- \to \mu^+\mu^-\gamma$ used for the development of the PHOKHARA Monte Carlo generator was presented. All prepared formulas were coded inside the generator. Various numerical tests were made to check the proper implementation of the prepared formulas:

- test of the agreement between the trace and helicity method for the amplitudes with the hard emission of two FSR photons;
- comparison for the soft contribution between the analytical formula and the numerical integral for the space phase points generated by PHOKHARA9.0;
- test of the agreement between quad and double precision for the soft analytical formula;
- test for the cut independence between the hard and soft contribution;
- test of the agreement between two independent subroutines for all virtual corrections.

For all general tests, two energies of the incoming particles were used: $\sqrt{s} = 1.02$ GeV and 10.56 GeV. The smaller energy characterises the KLOE

experiment and the bigger characterises the BaBar experiment. Additional cuts describing these experiments were not added.

The KLOE and BaBar cuts used in the calculations are presented in Appendix 7.0.7.

There are two types of the PHOKHARA generator accuracy. The first one, called the technical accuracy of the generator, results from used ω cuts, development of the formulas, etc. The second one is the physical accuracy of the generator related with the missing corrections. In case of PHOKHARA8.0, it is equal to 0.5% and is related to missing corrections like, for example ISR corrections with three real photons.

In the tests presented in this chapter, we are mostly focusing on technical accuracy. Only the results of the comparison between PHOKHARA8.0 and PHOKHARA9.0 for KLOE and BaBar cuts check the influence of the missing NLO corrections at the physical accuracy.

6.1.1 Hard photons emission

Gauge invariance

In paragraph 5.2.1, the gauge test for the formulas that describe the process of the emission of two real photons emitted from final particles line is presented. The gauge test was also done numerically. The tested formulas were coded inside the PHOKHARA9.0 MC generator.

Two energies were used for the gauge test: $\sqrt{s} = 1.02$ GeV and 10.56 GeV. In both cases the double precision code was used and three tests were made. In the first case both polarisation vectors of hard photons were replaced by the corresponding photon four momenta. In the other two cases, one of the photon polarisation vectors was replaced by the photon four-momenta. In all these cases and both energies, half a million space phase points generated by PHOKHARA9.0 were used. No values of the amplitude square bigger than 10^{-15} are noticed. For the double precision code it means numerical zero. As such, gauge independence of the new PHOKHARA9.0 code for the part that contains two hard photon emissions from the final state is confirmed.

Helicity vs. trace method

The amplitudes in the PHOKHARA9.0 MC generator are mostly calculated with the use of the helicity method. Furthermore, the part of the code containing the two real hard photon emissions is prepared that way. The formula for the emission of two hard FSR photons is presented in the form of Eq. 5.30. To check the correctness of its implementation inside the genera-

NO CUTS $\sqrt{s}$ = 1.02 [GeV]			
$\sigma_{2ph_{ISR}}$ = 6.791(5)[nb]			
$\sigma_{2ph_{PRES}}$ =8.28(2) [nb]			
σ_{2ph} =8.591(4) [nb]			
helicity: $\sigma_{2ph_{FSR}}$ =0.1016 [nb]			
trace: $\sigma_{2ph_{FSR}}$ =0.1016 [nb]			
	trace	helicity	
$\|\Delta\| >$	σ_Δ [nb]	σ_Δ [nb]	N_{event}
0.0001	$1(2)\cdot 10^{-13}$	$1(2)\cdot 10^{-13}$	1
0.00001	$1(8)\cdot 10^{-12}$	$1(8)\cdot 10^{-12}$	8
0.000001	$8(9)\cdot 10^{-12}$	$8(9)\cdot 10^{-12}$	66

Table 6.1: The comparison between helicity and trace method for the emission of two real and hard photons for the energy $\sqrt{s}$=1.02 GeV

tor, the trace method was used. The new FORTRAN routine with the trace amplitude was created with the use of the FORM [44] algebra system and coded inside the PHOKHARA9.0 generator. The results obtained with these two methods were compared for every set of four momenta generated by the generator. The comparison between results obtained with these two methods checks the correctness of the coded analytical formula. The calculations were done for two energies $\sqrt{s}$ =1.02 GeV and $\sqrt{s}$ =10.56 GeV without any additional event selection. The amplitude square for the trace method was compared with the amplitude square for the helicity method summed over all polarisations.

The relative difference was used to analyse the agreement of both methods of calculations according to formulas Eq. 7.1 and 7.2. The result obtained with the helicity method was taken as a reference in denominator.

The results obtained with the helicity and trace method were used to calculate the part of the total cross section with two real hard photons emitted from the muon-antimuon line (FSR) $\sigma_{2ph_{FSR}}$. In both cases the Monte Carlo integrand (Eq. 7.4, 7.5) was used. The results are presented in Tab. 6.1 and 6.2. Here σ_{2ph} is the complete cross section for the emission of two real hard photons obtained with PHOKHARA9.0. It contains all two hard photon contributions and their interferences. $\sigma_{2ph_{ISR}}$ denotes the part of the total cross section with the emission of two real photons from the electron-positron line. It was calculated with PHOKHARA9.0. $\sigma_{2ph_{PRES}}$ contains all contributions to the two real photon emissions available in PHOKHARA8.0.

Tab. 6.1 and 6.2 also contain the contributions to the complete two real

NO CUTS $\sqrt{s}$ = 10.56 [GeV]			
$\sigma_{2ph_{ISR}}$ = 0.223(2) [nb]			
$\sigma_{2ph_{PRES}}$ = 0.295(2) [nb]			
σ_{2ph} = 0.3042(7) [nb]			
helicity: $\sigma_{2ph_{FSR}}$ = 0.0059(3) [nb]			
trace: $\sigma_{2ph_{FSR}}$ = 0.0059(3)[nb]			
	trace	helicity	
$\|\Delta\| >$	σ_Δ [nb]	σ_Δ [nb]	N_{event}
0.0001	$3.9(8)\cdot 10^{-15}$	$3.9(8)\cdot 10^{-15}$	71
0.00001	$4(4)\cdot 10^{-14}$	$4(4)\cdot 10^{-14}$	679
0.000001	$4(5)\cdot 10^{-13}$	$4(5)\cdot 10^{-13}$	6961

Table 6.2: The comparison between helicity and trace method for the emission of two real and hard photons for the energy $\sqrt{s}$=10.56 GeV

hard photon cross section σ_{2ph} given by the results with the worst value of the relative difference $|\Delta|$ obtained during the calculations - σ_Δ. These contributions were calculated for the results obtained using the helicity and trace method. The comparison between these results and the value of $\sigma_{2ph_{FSR}}$ checks if the difference between used methods is big enough to affect the generator's accuracy. The accuracy of the generator needed for the KLOE and BaBar calculations is equal to 10^{-4}. In that case the relative difference $|\Delta|$ should be better than 10^{-4}. If there are some points with a worse value of the relative difference, then it is necessary to check the size of the contribution to the complete result given by these points. If the contribution is below the needed accuracy then the differences do not affect the complete result of calculations and the methods are in agreement.

The statistic for the test with energy $\sqrt{s}$ =1.02 GeV is equal to 9662172 checked configurations of particles generated by PHOKHARA9.0. Only for 66 of them the result of the relative difference is bigger than 10^{-6} and for 7329103 is better than 10^{-13}.

The contribution σ_Δ given by the 66 phase space configurations with $|\Delta| > 10^{-6}$ (configurations with the worst agreement between methods) is presented in Tab. 6.1. The size of the ratio of σ_Δ to $\sigma_{2ph_{FSR}}$ is below 10^{-10}, both for the helicity and trace method. Both methods are in agreement.

For energy $\sqrt{s}$ =10.56 GeV (Tab. 6.2), the results of the amplitude square for 9740543 phase space configurations are collected. 6018585 phase space configurations give results of the relative difference between the helicity and trace method better than 10^{-13}. For 6961 phase space configurations the

value of relative difference is bigger than 10^{-6}, but their contribution to the total cross section $\sigma_{2ph_{FSR}}$ is still at the level of 10^{-10}. Both methods are in agreement.

6.1.2 Soft photon contribution

Analytical vs. numerical version

In Section 5.3 the analytical solution of the soft photon emission is presented where the photon energy cut is given in an arbitrary reference frame. The result of that calculation was coded to PHOKHARA9.0. Results available in the existing literature are obtained in a selected reference frame, while in a Monte Caro generator a result in an arbitrary frame is needed. The test that checks the implementation of the soft formula was done numerically. The computer code that calculates numerically the results of the function $F(p_1, p_2, q_1, q_2, \omega)$ presented in Section 5.3 (Eq. 5.44) was prepared. The Monte Carlo method for the calculations of this integral was used. The calculations were done in the spherical coordinate system. The code has the following structure:

- a set of the four momenta for leptons e^+, e^-, μ^+, μ^- with the value of q^2 generated by the PHOKHARA9.0 MC generator is chosen;
- in loop, for the declared number of draws N, values of integrated variables: ϕ angle, $\cos\theta$ and $|k_1|$ are generated in the limits of integration;
- soft photon four momenta k_1 is calculated for the generated variables;
- value for the integrand function I_i is calculated with the k_1 four momenta;
- the value I of the integrand and its error is calculated according to the formulas for the MC integrand (Eq. 7.4, 7.5).

The computer code for the soft photon contribution was constructed to check separately an integrand with FSR and ISR photons and the integrands containing products: p_1q_1, p_1q_2, p_2q_1, p_2q_2.

The comparison was done for two energies $\sqrt{s}$ =1.02, 10.56 [GeV] to check the analytical formulas. Tables 6.3 and 6.4 present examples of the relative differences for two random space phase points.

Because of the approximation done during the calculations of the analytical formulas, the analytical and numerical results should be in agreement in the first order of approximation proportional to the ratio $\frac{\lambda}{\Delta}$. The results in Tab. 6.3, 6.4 show this behaviour.

$\sqrt{s}=$	1.02 [GeV]	10.56 [GeV]
$\frac{\lambda}{\Delta}$	$\frac{F_a-F_n}{F_a}$	
FSR:		
10^{-5}	0.00001(2)	0.00005(9)
10^{-4}	0.00001(1)	0.00001(4)
10^{-3}	0.00001(4)	0.00001(2)
ISR:		
10^{-5}	0.00018(9)	0.0003(3)
10^{-4}	0.00005(5)	0.0001(1)
10^{-3}	0.00112(1)	0.00107(4)

Table 6.3: The comparison for the soft formula between results obtained analytically F_a and with numerical calculations F_n for two energies and three values of the ratio $\frac{\lambda}{\Delta}$.

$\sqrt{s}=$	1.02 [GeV]	10.56 [GeV]
$\frac{\lambda}{\Delta}$	$\frac{F_a-F_n}{F_a}$	
INTERFERENCE:		
$p_1 \cdot q_2$		
10^{-5}	0.0001(2)	0.0001(4)
10^{-4}	0.00001(6)	0.0001(1)
10^{-3}	0.00527(2)	0.00407(6)
$p_1 \cdot q_1$		
10^{-5}	0.0001(2)	0.0001(4)
10^{-4}	0.00001(7)	0.0002(2)
10^{-3}	0.00564(2)	0.00559(8)
$p_2 \cdot q_2$		
10^{-5}	0.0002(2)	0.0002(3)
10^{-4}	0.00003(8)	0.0002(2)
10^{-3}	0.00614(3)	0.00404(6)
$p_2 \cdot q_1$		
10^{-5}	0.0002(2)	0.0001(4)
10^{-4}	0.00003(8)	0.0002(2)
10^{-3}	0.00669(3)	0.00498(7)

Table 6.4: The comparison for the soft formula between results obtained analytically F_a and with numerical calculations F_n for two energies and three values of the ratio $\frac{\lambda}{\Delta}$.

Berends formula for ISR

For the ISR part of the soft contribution, it is possible to compare the results from the PHOKHARA9.0 MC generator with the results for the formula published by Berends [46]. PHOKHARA9.0 works in the e^+e^- centre of mass frame. Positron and electron four-momenta are calculated at the beginning of the simulation and do not change during the computation. The ISR part of the soft contribution depends only on $\sqrt{s}$ and electron, positron initial four-momenta, so for a given ω cut and energy, it is constant.

In Table 6.5 the comparison between results obtained for the ISR soft formula included in PHOKHARA9.0 and for the Berends formula is presented for two values of energy. The results of the test for the logarithmic and the finite part of the correction are presented separately. The agreement between

$\sqrt{s}$ =	1.02 [GeV]	10.56 [GeV]
ISR correction		
ISR_{PH}	-0.802376749923983	-1.16687884577329
ISR_{BER}	-0.802376749956546	-1.16687885148792
$\frac{ISR_{BER}-ISR_{PH}}{ISR_{BER}}$	$-4*10^{-11}$	$-4*10^{-9}$
ISR correction - finite part		
ISR_{PH}	-0.240597402826786	-0.420138143711782
ISR_{BER}	-0.240597402859349	-0.420138149426412
$\frac{ISR_{BER}-ISR_{PH}}{ISR_{BER}}$	$-1*10^{-10}$	$-1*10^{-8}$
ISR correction - logarithmic part		
ISR_{PH}	-0.561779347097197	-0.746740702061512
ISR_{BER}	-0.561779347097197	-0.746740702061511
$\frac{ISR_{BER}-ISR_{PH}}{ISR_{BER}}$	$-2*10^{-16}$	$-7*10^{-16}$

Table 6.5: The comparison between Berends soft formula ISR_{BER} and the new ISR_{PH} for two energies $\sqrt{s}$ =1.02 and 10.56 GeV

formulas is very good. The fact that the agreement for finite part is worse for bigger energy indicates that for even higher energies some expansions of the soft formula may be needed.

Stability of the soft code

To check if the code containing the soft corrections was stable, a second version of the soft routine in quadrupole precision was prepared. This routine preserves the structure of the double precision version. Both subroutines

calculate values of the soft function $F(p_1, p_2, q_1, q_2, \omega)$ (Eq. 5.44). The results obtained by both versions were compared in the same phase space points.

SOFT				
	1.02 GeV	10.56 GeV	KLOE	BaBar
$\lvert\Delta_s\rvert$	number of events			
$< 10^{-14}$	6037	12	7936	3
$(10^{-14}, 10^{-13} >$	53332	83	71849	64
$(10^{-13}, 10^{-12} >$	530396	1045	718220	494
$(10^{-12}, 10^{-11} >$	4631194	10440	6059503	5075
$(10^{-11}, 10^{-10} >$	4338839	106648	3142492	50845
$(10^{-10}, 10^{-9} >$	407115	1354114	0	1038164
$(10^{-9}, 10^{-8} >$	32961	6468603	0	8905355
$(10^{-8}, 10^{-7} >$	126	1311198	0	0
$(10^{-7}, 10^{-6} >$	0	563875	0	0
$(10^{-6}, 10^{-5} >$	0	158423	0	0
$(10^{-5}, 10^{-4} >$	0	23507	0	0
$(10^{-4}, 0.001 >$	0	1953	0	0
$(0.001, 0.01 >$	0	99	0	0

Table 6.6: The comparison between results obtained for the soft formula written in quad precision and the results obtained for the double precision soft formula. The rows contain the number of checked values that give $|\Delta_s|$. For KLOE and BaBar the event selection with $q^2 \in < 0.34, 0.96 >$ GeV^2 was chosen.

Table 6.6 presents the results of the comparison between double and quad precision. 10^7 sets of the variables were used for this test. This test was made for energies 1.02 and 10.56[GeV] without additional angular and energetic cuts, and for cuts close to the ones used in the KLOE and BaBar experiments. The relative difference Δ_s was calculated as a difference between the quad and double result in the numerator and the quad value in the denominator. Table 6.6 contains the number of events corresponding to the given interval of $|\Delta_s|$.

The agreement between codes is very good. For $\sqrt{s} = 1.02$ GeV, the accuracy between codes described by the relative difference is better than 10^{-7}. Most of the examined cases (9500249 points) give results from interval $< 10^{-13}, 10^{-10} >$. For the KLOE experimental cuts, the accuracy is better than 10^{-10}. For BaBar the accuracy is better than 10^{-8}. The worst result of the comparison is for $\sqrt{s} = 10.56$ GeV without additional cuts. For 99 of

the checked points, the accuracy is between $< 10^{-3}, 10^{-2} >$. An additional test was done to check if there is any specific case of that result. The q^2 distribution for the points with $|\Delta_s| > 0.00001$ is presented in Fig. 6.1. For $q^2 < 2.5$ GeV^2, the percentage of points with $|\Delta_s| > 0.00001$ decreases. The calculations for both type of cuts (KLOE and BaBar) were made for low values of q^2. It is one of the reasons why the agreement between precisions improves a lot for them.

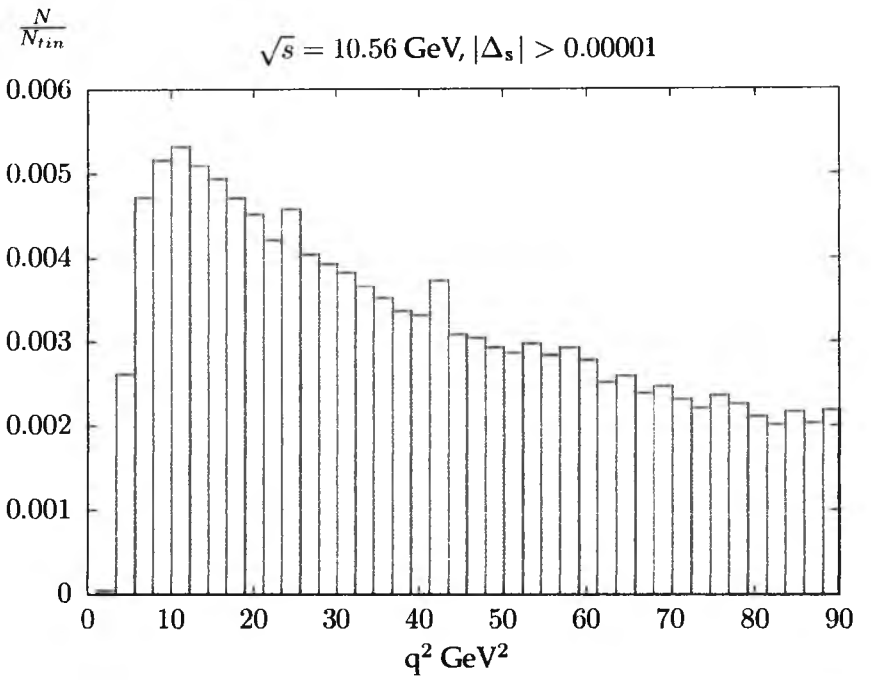

Figure 6.1: q^2 distribution for points with $|\Delta_s| > 0.00001$ and $\sqrt{s}$ =10.56 GeV. The Y -axis shows the ratio of the number of points N with $|\Delta_s| > 0.00001$ in the q^2 interval to the total number of points N_{tin} in this same range.

The check of the angular distribution for the θ angle between muon, antimuon or photon and direction of incoming positron was done. The points with the accuracy worse than 10^{-5} come for the values of $|\cos\theta_i| > 0.9$ for i=μ^+, μ^-, γ.

For $\sqrt{s}$ = 10.56 GeV, the value of the cross section, for the part with all corrections with one real photon emission σ_{1ph}, is equal to 0.07004(4) [nb]. The contributions $\sigma_{\Delta s}$ ($\sigma_{\Delta_{sq}}$ for quad precision) to the cross section for chosen values of $|\Delta_s|$ are presented in Tab. 6.7. Their contribution to the cross section is relatively small, and they give an error much smaller than

$\sigma_{1ph_q} = 0.07004(4)$ [nb]				
$\sigma_{1ph} = 0.07004(4)$ [nb]				
$\lvert\Delta_s\rvert >$	σ_{Δ_s} [nb]	$\sigma_{\Delta_{sq}}$	$\frac{\sigma_{\Delta_s}}{\sigma_{1ph}}$	N_{event}
0.01	0	0	0	0
0.001	$7.1(9)\cdot 10^{-9}$	$7.1(9)\cdot 10^{-9}$	$1.0(1)\cdot 10^{-7}$	99
0.0001	$1.9(8)\cdot 10^{-7}$	$1.9(8)\cdot 10^{-7}$	$2.7(1)\cdot 10^{-6}$	2052
0.00001	$5.2(1)\cdot 10^{-6}$	$5.2(1)\cdot 10^{-6}$	$7.4(1)\cdot 10^{-6}$	25559

Table 6.7: The contribution σ_{Δ_s} to the cross section σ_{1ph} for chosen $|\Delta_s|$ and $\sqrt{s}$ =10.56 GeV. q - index sign quad precision.

10^{-4}. The difference between quad and double precision results does not affect the 10^{-4} accuracy of the generator. The soft part of the code in double precision is sufficient for our calculations.

Cut independence

In Sections 5.2 and 5.3 the hard contribution σ_{2ph} and the soft contribution σ_s for the two photon emissions are presented. These parts are separated by the cut (Eq. 5.4). The sum of these contributions has to be ω cut independent. For the full NLO contribution that involves the hard photon emission, the virtual and soft corrections, the logarithmic part that depends on the photon mass λ, is cancelled between virtual and soft corrections. The remaining part of soft corrections σ_s with ω is cancelled with the hard contribution σ_{2ph}. The comparison between the values of the cross sections for different ω al-

ω	σ [nb]
NO CUTS $\sqrt{s} = 1.02$ [GeV]	
10^{-4}	14.925(1)
10^{-5}	14.928(2)
relative difference $\frac{10^{-4}-10^{-5}}{10^{-4}}$	0.0002(2)
NO CUTS $\sqrt{s} = 10.56$ [GeV]	
10^{-4}	0.3740(1)
10^{-5}	0.3740(2)
relative difference $\frac{10^{-4}-10^{-5}}{10^{-4}}$	0.0002(8)

Table 6.8: The cut independence test for $\sqrt{s}$ =1.02 and 10.56 GeV.

lows us to verify the correctness of the part of the PHOKHARA9.0 code that contains hard photons radiation and the part that contains the soft photon emission with $\log(\omega)$. For the hard contribution with two FSR photons, the correctness of the formulas and the code is confirmed by comparison with trace method. The cut's independence test also checks if all interferences between the amplitudes with two hard photons are implemented inside the code in the correct way.

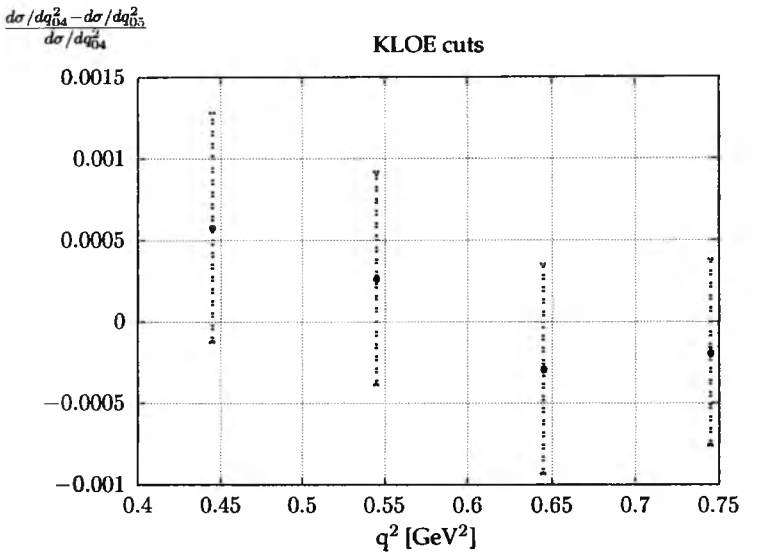

Figure 6.2: The cut independence test for KLOE event selection

In Tab. 6.8 the values of the total cross section for the simulations with two different energies are presented: $\sqrt{s} = 1.02$ and 10.56 GeV. Two values of the ω cut were used for this test: $\omega = 10^{-5}$ and $\omega = 10^{-4}$. The results were obtained using the Monte Carlo integral implemented inside the PHOKHARA9.0 MC generator. For both values of ω, results of the total cross section should be in agreement with the accuracy proportional to the bigger of them.

For $\sqrt{s} = 1.02$ GeV, the results are in agreement with the accuracy $2(2) \cdot 10^{-4}$ and for the second energy $\sqrt{s} = 10.56$ GeV with $2(8) \cdot 10^{-4}$. The cut independence of the results is confirmed.

As an additional check of the ω cut independence, the calculations for the KLOE experimental cuts were prepared for the same choice of ω and for four intervals of q^2: (0.44;0.45), (0.54;0.55), (0.64;0.65), (0.74;0.75) [GeV^2].

The results come from the simulation with use of the final PHOKHARA9.0 version and are presented in Fig. 6.2. Also for the KLOE cuts, the obtained results are cut independent.

6.1.3 Virtual corrections

Two independent versions of the codes for the pentagons and box corrections were used for tests:

- quad precision version;
- double precision version: PJFry.

Similarly, two independent versions of the codes for the triangle contributions were checked:

- extended version of PHOKHARA subroutine for the triangle corrections (double precision);
- double precision version: PJFry.

Both routines were coded inside PHOKHARA9.0. The comparison between routines was done for four cases: for energies $\sqrt{s}$=1.02 GeV, $\sqrt{s}$=10.56 GeV without additional cuts, and for KLOE and BaBar event selections. A set of 10^7 four-momenta was generated in each case. Then, the comparison between the obtained results was done. The relative difference $|\Delta_v|$ was calculated.

The values of $|\Delta_v|$ were divided into intervals and the number of events for every interval was calculated. The value of $|\Delta_v|$ is a test of compatibility between codes. It cannot show which code gives the right result, but points the level of confidence of calculations. No matter which routine is selected, it is necessary to take into account the difference $|\Delta_v|$ and treat it as an additional source of uncertainty.

PENTABOX

The results for pentaboxes are presented in Tab. 6.9. The agreement between codes for most points is better than 10^{-7}.

The worst agreement is observed for calculations with energy $\sqrt{s}$=10.56 GeV, without additional cuts. To check the influence of the points with worst agreement, their contribution σ_{Δ_v} (index q denotes quad precision version) to the total cross section σ_{1ph} were calculated. The results for the chosen values of $|\Delta_v|$ are presented in Tab. 6.10, 6.11, 6.12 and 6.13. In all presented cases, the size of the contributions given by these results (σ_{Δ_v}) is not big enough to threaten the 10^{-4} accuracy of the generator.

PENTABOX				
	1.02 GeV	10.56 GeV	KLOE	BaBar
$\lvert\Delta_v\rvert$	number of events			
$< 10^{-14}$	28133	2610	2379	285
$(10^{-14}, 10^{-13} >$	247670	23545	21313	2681
$(10^{-13}, 10^{-12} >$	1641790	203777	213400	27818
$(10^{-12}, 10^{-11} >$	3643821	894750	1988801	274498
$(10^{-11}, 10^{-10} >$	3061231	2099847	5190105	2247191
$(10^{-10}, 10^{-9} >$	1038470	2963868	2062030	5496138
$(10^{-9}, 10^{-8} >$	291463	2468760	434531	1710963
$(10^{-8}, 10^{-7} >$	42368	918297	74717	211811
$(10^{-7}, 10^{-6} >$	4432	293543	10088	25316
$(10^{-6}, 10^{-5} >$	555	107209	2339	2893
$(10^{-5}, 10^{-4} >$	62	21009	272	347
$(10^{-4}, 0.001 >$	4	2625	25	48
$(0.001, 0.01 >$	1	147	0	10
$(0.01, 0.1 >$	0	10	0	1
$(0.1, 1 >$	0	3	0	0

Table 6.9: The comparison between results obtained for the pentabox contributions with PJFry and the results obtained with the quad precision code. The rows contain the number of checked values that give $|\Delta_v|$. For KLOE and BaBar the event selection with $q^2 \in < 0.34, 0.96 >$ GeV^2 was chosen.

It is also possible to check how the agreement depends on the angular distribution for the θ angle for muons and antimuons and real hard photons. Fig. 6.3 is prepared for $|\Delta_v| > 0.00001$ and $\sqrt{s} = 10.56$ GeV. The results for $\cos\theta_i$ (i $= \mu^+, \mu^-, \gamma$) for muons, antimuons and photons were calculated. On the Y-axis there is the ratio of the number N of events that give the relative difference $|\Delta_v| > 0.00001$ in chosen intervals of $\cos\theta$ to the total number of events accepted for this interval N_{tin}. The number of events that give $|\Delta_v| > 0.00001$ for final leptons is between 1.5 and 4 ‰ of the total number of registered events in the interval. Photon angles give the worst result for $\cos\theta_\gamma > 0.92$, which is 6 ‰.

In the same way, the q^2 distribution is constructed. Fig. 6.4 presents obtained results. The largest percentage of cases that gives $|\Delta_v| > 0.00001$ was registered for the big values of q^2. For these intervals about 1% of the investigated points give $|\Delta_v| > 0.00001$.

$\sqrt{s}$=1.02 GeV				
σ_{1ph_q} = 6.332(1) [nb]				
σ_{1ph} = 6.332(1) [nb]				
$\|\Delta_v\| >$	σ_{Δ_v} [nb]	$\sigma_{\Delta_v^q}$	$\frac{\sigma_{\Delta_v}}{\sigma_{1ph}}$	N_{event}
0.01	0	0	0	0
0.001	$7.(7)\cdot 10^{-8}$	$7.(7)\cdot 10^{-8}$	$1(1)\cdot 10^{-8}$	1
0.0001	$1.(2)\cdot 10^{-6}$	$1.(2)\cdot 10^{-6}$	$1(1)\cdot 10^{-7}$	5
0.00001	$4.5(2)\cdot 10^{-5}$	$4.5(2)\cdot 10^{-5}$	$7(1)\cdot 10^{-6}$	67

Table 6.10: Pentabox - The contribution σ_{Δ_v} to the cross section σ_{1ph} for chosen $|\Delta_v|$ and $\sqrt{s}$ =1.02 GeV.

$\sqrt{s}$=10.56 GeV				
σ_{1ph_q} = 0.07004(4) [nb]				
σ_{1ph} = 0.07004(4) [nb]				
$\|\Delta_v\| >$	σ_{Δ_v} [nb]	$\sigma_{\Delta_v^q}$	$\frac{\sigma_{\Delta_v}}{\sigma_{1ph}}$	N_{event}
0.1	$-3(3)\cdot 10^{-9}$	$-1(1)\cdot 10^{-9}$	$-4(4)\cdot 10^{-8}$	3
0.01	$8(9)\cdot 10^{-9}$	$9(9)\cdot 10^{-9}$	$1(1)\cdot 10^{-7}$	13
0.001	$3.9(9)\cdot 10^{-7}$	$3.8(9)\cdot 10^{-7}$	$6(1)\cdot 10^{-6}$	160
0.0001	$5.0(3)\cdot 10^{-6}$	$5.0(3)\cdot 10^{-6}$	$7.1(5)\cdot 10^{-5}$	2785
0.00001	$5.0(1)\cdot 10^{-5}$	$5.0(1)\cdot 10^{-5}$	$7.2(2)\cdot 10^{-4}$	23794

Table 6.11: Pentabox - The contribution σ_{Δ_v} to the cross section σ_{1ph} for chosen $|\Delta_v|$ and $\sqrt{s}$ =10.56 GeV.

KLOE				
σ_{1ph_q} =1.575(2) [nb]				
σ_{1ph} = 1.575(2) [nb]				
$\|\Delta_v\| >$	σ_{Δ_v} [nb]	$\sigma_{\Delta_v^q}$	$\frac{\sigma_{\Delta_v}}{\sigma_{1ph}}$	N_{event}
0.001	0	0	0	0
0.0001	$4(2)\cdot 10^{-7}$	$4(2)\cdot 10^{-7}$	$2(1)\cdot 10^{-7}$	25
0.00001	$4.8(7)\cdot 10^{-6}$	$4.8(7)\cdot 10^{-6}$	$3.0(5)\cdot 10^{-6}$	297

Table 6.12: Pentabox - The contribution $\sigma_{\Delta v}$ to the cross section σ_{1ph} for chosen $|\Delta_v|$ and KLOE event selection. q - index sign quad precision. $q^2 \in <0.34, 0.96>$ GeV^2

BaBar				
$\sigma_{1ph_q} = 0.0005655(7)$[nb]				
$\sigma_{1ph} = 0.0005655(7)$[nb]				
$\|\Delta_v\| >$	σ_{Δ_v} [nb]	$\sigma_{\Delta_v^q}$	$\frac{\sigma_{\Delta_v}}{\sigma_{1ph}}$	N_{event}
0.1	0	0	0	0
0.01	$4(4)\cdot 10^{-11}$	$4(4)\cdot 10^{-11}$	$7(7)\cdot 10^{-8}$	1
0.001	$5(2)\cdot 10^{-10}$	$5(2)\cdot 10^{-10}$	$9(3)\cdot 10^{-7}$	11
0.0001	$2.5(3)\cdot 10^{-11}$	$2.5(3)\cdot 10^{-9}$	$4.5(6)\cdot 10^{-6}$	59
0.00001	$1.84(2)\cdot 10^{-8}$	$1.84(2)\cdot 10^{-8}$	$3.3(2)\cdot 10^{-5}$	406

Table 6.13: Pentabox - The contribution $\sigma_{\Delta v}$ to the cross section σ_{1ph} for chosen $|\Delta_v|$ and BaBar event selection. q - index sign quad precision. $q^2 \in < 0.34, 0.96 >$ GeV^2

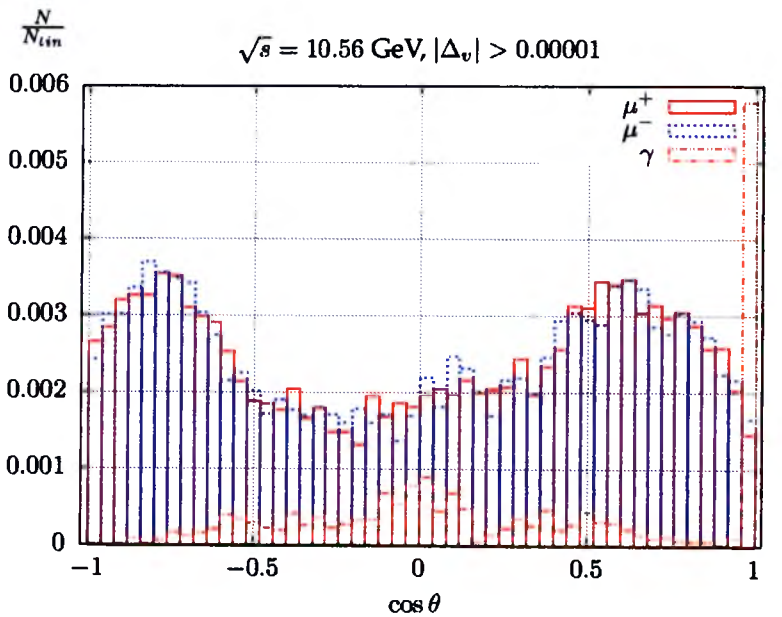

Figure 6.3: Pentabox - angular distribution for points with $|\Delta_v| > 0.00001$ and $\sqrt{s}$ =10.56 GeV. The Y -axis shows the ratio of the number of points N with $|\Delta_v| > 0.00001$ in the $\cos\theta$ interval to the total number of points N_{tin} in this same range.

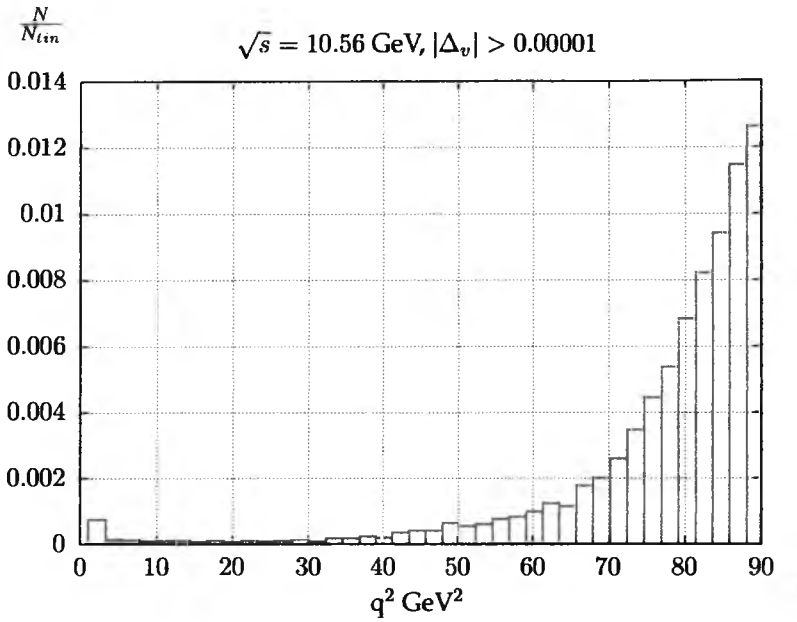

Figure 6.4: Pentabox - q^2 distribution for points with $|\Delta_v| > 0.00001$ and $\sqrt{s}$ =10.56 GeV. The Y - axis shows the ratio of the number of points with $|\Delta_v| > 0.00001$ N in the q^2 interval to the total number of points N_{tin} in this same range.

BOX

The same tests as the pentabox contributions are presented for the box contributions. The results of the relative difference are presented in Tab. 6.14.

The agreement between the codes is better than 10^{-7} for the majority of the investigated configurations of involved particles. However, the results are much more sensitive for the BaBar cuts; the agreement for all cases is better than 10^{-11}. For $\sqrt{s}$ = 10.56 GeV there are observed phase space configurations, where both codes give completely different results of the box contribution. Once again for the chosen intervals of $|\Delta_v|$, the contributions to the total cross section were calculated to see if the phase space configurations with worst agreement of the results could be crucial in determining the accuracy of the program. The results are presented in Tables 6.15, 6.16 and 6.17 (for the BaBar event selection the agreement between the codes is better than 10^{-10}).

BOX				
	1.02 GeV	10.56 GeV	KLOE	BaBar
$\lvert\Delta_v\rvert$	number of events			
$< 10^{-14}$	155611	9205	434925	3
$(10^{-14}, 10^{-13} >$	1250269	81729	388229	26
$(10^{-13}, 10^{-12} >$	4483493	628182	3298857	2342
$(10^{-12}, 10^{-11} >$	2616497	2021274	3381569	3979099
$(10^{-11}, 10^{-10} >$	1296978	4193131	2089532	6018530
$(10^{-10}, 10^{-9} >$	153076	1695962	634325	0
$(10^{-9}, 10^{-8} >$	34097	1053833	123443	0
$(10^{-8}, 10^{-7} >$	6300	215521	26779	0
$(10^{-7}, 10^{-6} >$	2173	49128	8180	0
$(10^{-6}, 10^{-5} >$	672	12207	3551	0
$(10^{-5}, 10^{-4} >$	267	8123	1222	0
$(10^{-4}, 0.001 >$	546	31515	819	0
$(0.001, 0.01 >$	13	134	2	0
$(0.01, 0.1 >$	7	39	0	0
$(0.1, 1 >$	1	10	0	0
> 1	0	7	0	0

Table 6.14: The comparison between results obtained for the box contributions with PJFry and the results obtained with the quad precision code. The rows contain the number of checked values that give $|\Delta_v|$. For KLOE and BaBar the event selection with $q^2 \in < 0.34, 0.96 >$ GeV^2 was chosen.

In all investigated cases, the contributions σ_{Δ_v} do not affect the accuracy of the generator.

The angular distribution of points with $|\Delta_v| > 0.00001$ for $\sqrt{s} = 10.56$ GeV is presented in Fig. 6.5. The number of the points with the worst agreement oscillates between 4 and 5 ‰ of the total number of the points in the given interval of $\cos\theta$ for all values of $\cos\theta_i$ (i $= \mu^+, \mu^-, \gamma$).

For the q^2 distribution, the ratio of the number of events that give $|\Delta_v| > 0.00001$ to the total number of events is the smallest for $q^2 < 2.5$ GeV^2. Figure 6.6 is made for $\sqrt{s} = 10.56$ GeV and illustrates this test.

$\sqrt{s}$=1.02 GeV				
σ_{1ph_q} = 6.332(1) [nb]				
σ_{1ph} = 6.332(1) [nb]				
$\|\Delta_v\| >$	σ_{Δ_v} [nb]	$\sigma_{\Delta_v^q}$	$\frac{\sigma_{\Delta_v}}{\sigma_{1ph}}$	N_{event}
0.1	$4(4)\cdot 10^{-8}$	$4(4)\cdot 10^{-8}$	$6(6)\cdot 10^{-9}$	1
0.01	$4(1)\cdot 10^{-7}$	$4(1)\cdot 10^{-7}$	$6(2)\cdot 10^{-8}$	8
0.001	$1.0(2)\cdot 10^{-8}$	$1.0(2)\cdot 10^{-8}$	$1.5(3)\cdot 10^{-5}$	21
0.0001	$2.4(1)\cdot 10^{-4}$	$2.4(1)\cdot 10^{-4}$	$3.8(2)\cdot 10^{-5}$	567
0.00001	$2.7(1)\cdot 10^{-4}$	$2.7(1)\cdot 10^{-4}$	$4.2(2)\cdot 10^{-5}$	834

Table 6.15: Box - The contribution σ_{Δ_v} to the cross section σ_{1ph} for chosen $|\Delta_v|$ and $\sqrt{s}$ =1.02 GeV. q - index sign quad precision.

$\sqrt{s}$=10.56 GeV				
σ_{1ph_q} = 0.07004(4) [nb]				
σ_{1ph} = 0.07004(4) [nb]				
$\|\Delta_v\| >$	σ_{Δ_v} [nb]	$\sigma_{\Delta_v^q}$	$\frac{\sigma_{\Delta_v}}{\sigma_{1ph}}$	N_{event}
0.1	$6(6)\cdot 10^{-7}$	$1.2(7)\cdot 10^{-8}$	$8(8)\cdot 10^{-6}$	17
0.01	$7(6)\cdot 10^{-7}$	$1.3(3)\cdot 10^{-7}$	$1(1)\cdot 10^{-5}$	56
0.001	$9(6)\cdot 10^{-7}$	$3.6(6)\cdot 10^{-7}$	$1(1)\cdot 10^{-5}$	190
0.0001	$6.3(1)\cdot 10^{-5}$	$6.2(1)\cdot 10^{-5}$	$8.9(1)\cdot 10^{-4}$	31705
0.00001	$2.02(2)\cdot 10^{-4}$	$2.02(2)\cdot 10^{-4}$	$2.89(4)\cdot 10^{-3}$	39828

Table 6.16: Box - The contribution σ_{Δ_v} to the cross section σ_{1ph} for chosen $|\Delta_v|$ and $\sqrt{s}$ =10.56 GeV. q - index sign quad precision.

KLOE				
σ_{1ph_q} = 1.575(2) [nb]				
σ_{1ph} = 1.575(2) [nb]				
$\|\Delta_v\| >$	σ_{Δ_v} [nb]	$\sigma_{\Delta_v^q}$	$\frac{\sigma_{\Delta_v}}{\sigma_{1ph}}$	N_{event}
0.001	0	0	0	0
0.001	$2(2)\cdot 10^{-9}$	$2(2)\cdot 10^{-9}$	$2(1)\cdot 10^{-9}$	2
0.0001	$8.8(4)\cdot 10^{-5}$	$8.8(4)\cdot 10^{-5}$	$6.0(2)\cdot 10^{-5}$	821
0.00001	$1.03(4)\cdot 10^{-4}$	$1.03(4)\cdot 10^{-4}$	$6.6(2)\cdot 10^{-5}$	2043

Table 6.17: Box - The contribution σ_{Δ_v} to the cross section σ_{1ph} for chosen $|\Delta_v|$ and KLOE event selection. q - index sign quad precision. $q^2 \in < 0.34, 0.96 > \text{GeV}^2$

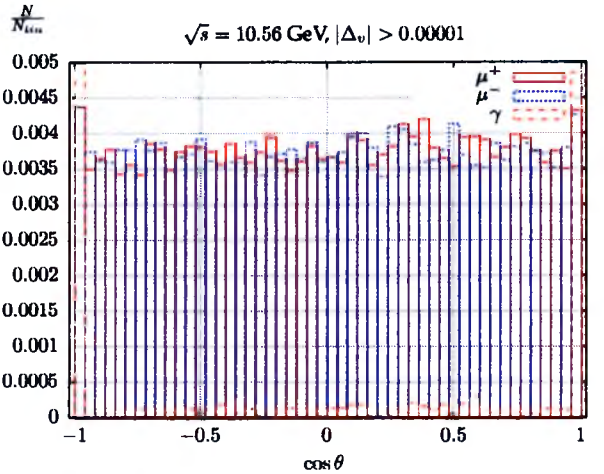

Figure 6.5: Box - angular distribution for points with $|\Delta_v| > 0.00001$ and $\sqrt{s}$ =10.56 GeV. The Y -axis shows the ratio of the number of points N with $|\Delta_v| > 0.00001$ in the $\cos\theta$ interval to the total number of points N_{tin} in this same range.

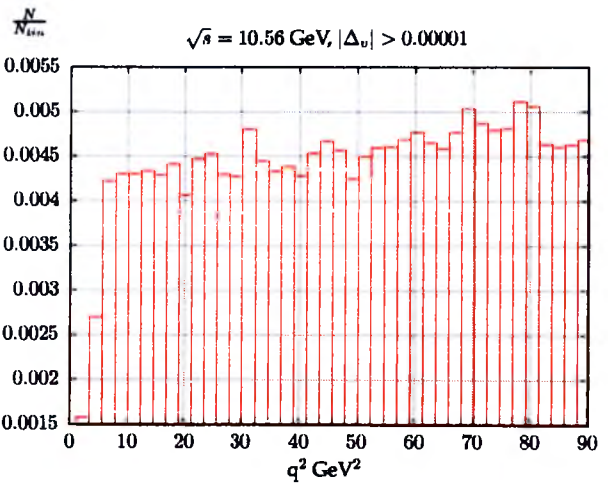

Figure 6.6: Box - q^2 distribution for points with $|\Delta_v| > 0.00001$ and $\sqrt{s}$ =10.56 GeV. The Y -axis shows the ratio of the number of points N with $|\Delta_v| > 0.00001$ in the q^2 interval to the total number of points N_{tin} in this same range.

TRIANGLE

Tab. 6.18 presents the results of the relative difference for the triangle contributions obtained with two codes. For most of the space phase configurations, the agreement between the codes is better than 10^{-8}. BaBar cuts

TRIANGLE				
	1.02 GeV	10.56 GeV	KLOE	BaBar
$\lvert\Delta_v\rvert$	number of events			
$< 10^{-14}$	3886803	3303915	1802537	9821489
$(10^{-14}, 10^{-13} >$	1646589	1363947	21588202	115824
$(10^{-13}, 10^{-12} >$	1547670	1257213	2088408	62687
$(10^{-12}, 10^{-11} >$	1518114	1019606	2082657	0
$(10^{-11}, 10^{-10} >$	1138462	991373	1536909	0
$(10^{-10}, 10^{-9} >$	235439	1004498	283949	0
$(10^{-9}, 10^{-8} >$	23962	824913	43017	0
$(10^{-8}, 10^{-7} >$	2627	205203	3263	0
$(10^{-7}, 10^{-6} >$	300	26440	385	0
$(10^{-6}, 10^{-5} >$	30	2596	51	0
$(10^{-5}, 10^{-4} >$	2	266	4	0
$(10^{-4}, 0.001 >$	2	27	2	0
$(0.001, 0.01 >$	0	3	0	0

Table 6.18: The comparison between results obtained for the triangle contributions with PJFry and the results obtained with PHOKHARA extended mode. The rows contain the number of checked values that give $|\Delta_v|$. For KLOE and BaBar the event selection with $q^2 \in < 0.34, 0.96 >$ GeV^2 was chosen.

cause all the problematic configurations to be rejected and the agreement to be better than 10^{-12}. Even for $\sqrt{s} = 10.56$ GeV the agreement is always better than 10^{-2}. The contribution of σ_{v_Δ} to the total cross section σ_{1ph} is smaller than 0.00005, even in the worst case for $\sqrt{s} = 10.56$ GeV.

6.1.4 One real photon emission cross section test

The same tests as the soft and virtual contributions are prepared for the differential cross section $d\sigma_{1ph}$. The examined differential cross section contains all contributions that include one real photon emission i.e. all tested virtual and soft corrections and Born.

CROSS SECTION				
	1.02 GeV	10.56 GeV	KLOE	BaBar
$\lvert\Delta\rvert$	number of events			
$< 10^{-14}$	2586	0	2800	0
$(10^{-14}, 10^{-13} >$	23179	18	25046	10
$(10^{-13}, 10^{-12} >$	231973	172	250425	93
$(10^{-12}, 10^{-11} >$	2245557	1732	2431217	923
$(10^{-11}, 10^{-10} >$	6280800	17514	6556884	9245
$(10^{-10}, 10^{-9} >$	1014394	176716	579530	94883
$(10^{-9}, 10^{-8} >$	175617	2194903	117201	3841242
$(10^{-8}, 10^{-7} >$	22226	5545970	24261	6053416
$(10^{-7}, 10^{-6} >$	2253	1564665	7568	162
$(10^{-6}, 10^{-5} >$	628	383219	3216	20
$(10^{-5}, 10^{-4} >$	266	72470	1139	6
$(10^{-4}, 0.001 >$	489	33022	711	0
$(0.001, 0.01 >$	31	8555	2	0
$(0.01, 0.1 >$	1	919	0	0
> 0.1	0	125	0	0

Table 6.19: The comparison between the results of the differential cross section $d\sigma_{1ph}$ obtained with quad and double precision versions of the PHOKHARA MC generator. The rows contain the number of checked values that give $|\Delta|$. For KLOE and BaBar the event selection with $q^2 \in < 0.34, 0.96 >$ GeV^2 was chosen.

The tests were done for 10^7 phase space points. Two versions of the PHOKHARA generator were used. The first one, prepared as a double precision code, contains the PJFry routine, and the second one, prepared as a quad precision code, contains the quad precision routine used for the previous tests and the expanded triangle mode. The relative difference between results obtained by the two versions of the generator should be treated as a source of possible uncertainty. For both versions of the generator, only the soft part is based on this same subroutine, which was already tested. Here:

$$\Delta = \frac{quad - double}{quad} \tag{6.1}$$

where "double" refers to the double precision version of PHOKHARA and "quad" refers to the quad precision version of PHOKHARA.

$\sqrt{s} = 1.02$ GeV and $\sqrt{s} = 10.56$ GeV

Table 6.19 shows the results obtained for $\sqrt{s} = 1.02$ GeV, when no additional energy and angular cuts are used. The comparison between codes shows that they are consistent at the level between 10^{-13} and 10^{-7} for the majority of points. It means that the obtained numbers agree at least with seven significant digits and shows that both codes can be found reliable. However, to declare if they are consistent, it is necessary to check the contribution to the cross section from the points with the worst agreement. This is because there is the possibility that they could produce a significant contribution to the total cross section.

The value of the total cross section σ_{1ph} was calculated using the differential cross sections from previous analysis. The Monte Carlo integral was used according to Eq. 7.4 and 7.5. The values of σ_Δ for the points with the worst agreement between codes were calculated. The ratio of σ_Δ to the total cross section σ_{1ph} was calculated. All the calculations are presented in Tab. 6.20. σ_{1phq}, σ_{Δ_q} denotes the cross sections calculated by the quad precision generator.

$\sigma_{1ph_q} = 6.332(1)$ [nb]				
$\sigma_{1ph} = 6.332(1)$ [nb]				
$\Delta >$	σ_Δ [nb]	σ_{Δ_q} [nb]	$\frac{\sigma_\Delta}{\sigma_{1ph}}$	N_{event}
0.1	0	0	0	0
0.01	$4(4)\cdot 10^{-8}$	$4(4)\cdot 10^{-8}$	$6(6)\cdot 10^{-9}$	1
0.001	$1.4(3)\cdot 10^{-6}$	$1.4(3)\cdot 10^{-6}$	$2.2(4)\cdot 10^{-7}$	32
0.0001	$2.1(1)\cdot 10^{-4}$	$2.1(1)\cdot 10^{-4}$	$3.4(2)\cdot 10^{-5}$	521
0.00001	$2.7(1)\cdot 10^{-4}$	$2.7(1)\cdot 10^{-4}$	$4.2(2)\cdot 10^{-5}$	787
0.000001	$3.0(1)\cdot 10^{-4}$	$3.0(1)\cdot 10^{-4}$	$4.8(2)\cdot 10^{-5}$	1415

Table 6.20: The contribution σ_Δ to the cross section σ_{1ph} for chosen $|\Delta|$ and $\sqrt{s}$ =1.02 GeV. q - index sign quad precision.

σ_{Δ_q} and σ_Δ give the same results for all checked ranges of $|\Delta|$. The ratios of the values of σ_Δ to the total cross section σ_{1ph} are the same for double and quadrupole precision.

For all checked values of $|\Delta|$, the contribution of σ_Δ is smaller than the value of used cut $\omega = 10^{-4}$. This means that the difference between two codes does not affect the value of declared accuracy.

The results for $\sqrt{s} = 10.56$ GeV without additional cuts are presented in Tab. 6.19. In this case there are 20 points, where all digits of the examined values are different. Table 6.21 shows that for $\Delta > 0.001$ the contribution

$\sigma_{1ph_q} = 0.07004(4)$ [nb]				
$\sigma_{1ph} = 0.07004(4)$ [nb]				
$\Delta >$	σ_Δ [nb]	σ_{Δ_q} [nb]	$\frac{\sigma_\Delta}{\sigma_{1ph}}$	N_{event}
0.1	$6(6)\cdot 10^{-7}$	$2(1)\cdot 10^{-8}$	$9(9)\cdot 10^{-6}$	125
0.01	$7(5)\cdot 10^{-7}$	$1.4(4)\cdot 10^{-7}$	$1.1(9)\cdot 10^{-5}$	1044
0.001	$7.7(6)\cdot 10^{-6}$	$7.1(2)\cdot 10^{-6}$	$1.10(9)\cdot 10^{-4}$	9599
0.0001	$8.3(1)\cdot 10^{-5}$	$8.3(1)\cdot 10^{-5}$	$1.18(2)\cdot 10^{-3}$	42621
0.00001	$2.24(2)\cdot 10^{-4}$	$2.24(2)\cdot 10^{-4}$	$3.21(4)\cdot 10^{-3}$	115091

Table 6.21: The contribution σ_Δ to the cross section σ_{1ph} for chosen $|\Delta|$ and $\sqrt{s}$ =10.56 GeV. q - index sign quad precision.

from these phase space points into the total cross section is already at the level of 10^{-4}. The ratio $\frac{\sigma_\Delta}{\sigma}$ grows up to 10^{-3} for a wider interval of Δ . If the difference between two independent codes is treated as an additional source of the uncertainty, then for the case when cut $\omega = 10^{-4}$ was used, it could disturb the assumed precision of calculations.

In this case also, the differences between σ_{Δ_q} and σ_Δ are visible for some intervals of Δ. Yet they do not differ significantly.

The angular and q^2 distributions for $|\Delta| > 0.00001$ and for both energies show that the structure of one photon contribution is complicated. Figure 6.7 illustrates the angular distribution for $|\Delta| > 0.00001$ and $\sqrt{s} = 10.56$ GeV. The number of the points that give $|\Delta| > 0.00001$ can reach almost 2.5% of the total number of points present in the examined interval of $|\cos\theta_i|$ (i $= \mu^+, \mu^-, \gamma$).

For the q^2 distribution, the smallest value of the ratio of the events with $|\Delta| > 0.00001$ to the total number of the events in the interval exists for q^2 <2.5 GeV^2 (Fig. 6.8).

For KLOE and BaBar simulations are made for small values of q^2, and also the angles with $|\cos\theta_i| < 0.92$ (i $= \mu^+, \mu^-, \gamma$) are cut off. As such, for both type of cuts the agreement between codes is much better than for $\sqrt{s} = 10.56$ GeV.

KLOE and BaBar

In Tab. 6.19 results of the relative differences for the cross section are presented. For the KLOE cuts the vast majority of the checked points give the results from interval $|\Delta|$ between 10^{-12} and 10^{-10}, while for BaBar between 10^{-9} and 10^{-7}. For the second experiment, the worst results give the agreement below the value of 10^{-4}. For KLOE cuts there are 713 registered

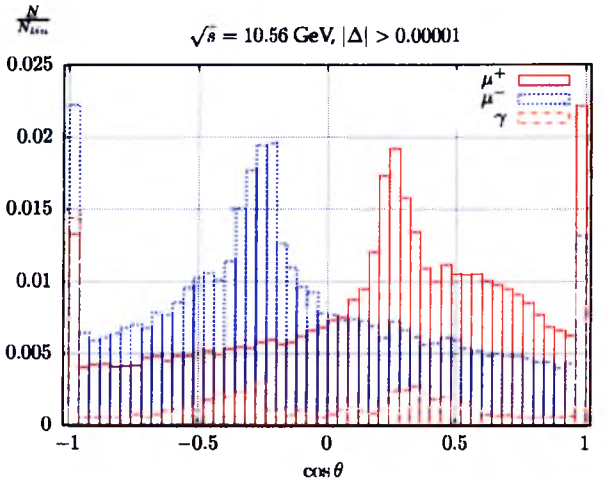

Figure 6.7: Angular distribution for points with $|\Delta_v| > 0.00001$ and $\sqrt{s}$ =10.56 GeV. The Y - axis shows the ratio of the number of points N with $|\Delta_v| > 0.00001$ in the $\cos\theta$ interval to the total number of points N_{tin} in this same range.

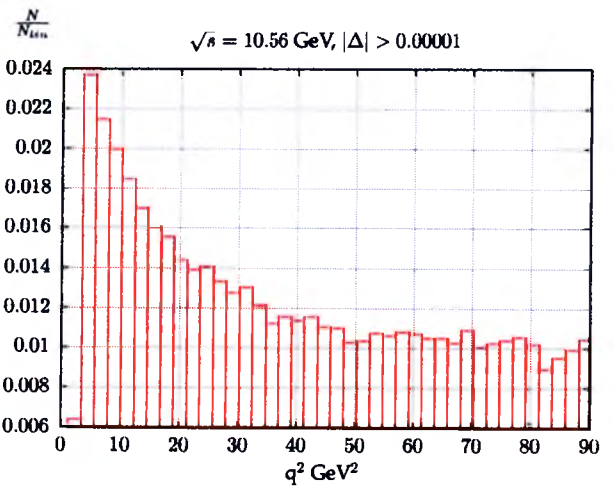

Figure 6.8: q^2 distribution for points with $|\Delta_v| > 0.00001$ and $\sqrt{s}$ =10.56 GeV. The Y - axis shows the ratio of the number of points N with $|\Delta_v| > 0.00001$ in the q^2 interval to the total number of points N_{tin} in this same range.

$\sigma_{1ph_q} = 1.575(2)$ [nb]				
$\sigma_{1ph} = 1.575(2)$ [nb]				
$\Delta >$	σ_Δ [nb]	σ_{Δ_q} [nb]	$\frac{\sigma_\Delta}{\sigma_{1ph}}$	N_{event}
0.01	0	0	0	0
0.001	$2(2)\cdot 10^{-9}$	$2(2)\cdot 10^{-9}$	$2(1)\cdot 10^{-9}$	2
0.0001	$7.7(3)\cdot 10^{-5}$	$7.7(3)\cdot 10^{-5}$	$4.9(2)\cdot 10^{-5}$	713
0.00001	$1.02(4)\cdot 10^{-4}$	$1.02(4)\cdot 10^{-4}$	$6.5(2)\cdot 10^{-5}$	1852
0.000001	$1.17(4)\cdot 10^{-4}$	$1.17(4)\cdot 10^{-4}$	$7.4(2)\cdot 10^{-5}$	5068

Table 6.22: The contribution σ_Δ to the cross section σ_{1ph} for chosen $|\Delta|$ and KLOE event selection. q - index sign quad precision. $q^2 \in < 0.34, 0.96 >$ GeV^2

$\sigma_{1ph_q} = 0.0005655(7)$ [nb]				
$\sigma_{1ph} = 0.0005655(7)$ [nb]				
$\Delta >$	σ_Δ [nb]	σ_{Δ_q} [nb]	$\frac{\sigma_\Delta}{\sigma_{1ph}}$	N_{event}
0.0001	0	0	0	0
0.00001	$3(1)\cdot 10^{-10}$	$3(1)\cdot 10^{-10}$	$5(2)\cdot 10^{-7}$	6
0.000001	$1.2(2)\cdot 10^{-9}$	$1.2(2)\cdot 10^{-9}$	$2.1(4)\cdot 10^{-6}$	26

Table 6.23: The contribution σ_Δ to the cross section σ_{1ph} for chosen $|\Delta|$ and BaBar event selection. q - index sign quad precision. $q^2 \in < 0.34, 0.96 >$ GeV^2

cases where the relative difference is from interval $< 10^{-4}, 10^{-2})$. The contribution to the total cross section given by the values with the worst agreement between the codes is presented in Tab. 6.22 and 6.23. All calculations were done with $\omega = 10^{-4}$.

The results obtained for the KLOE and BaBar cuts, for the chosen conditions of the relative difference, show that the losses of accuracy caused by points with the worst agreement between both codes are smaller than the uncertainty resulting from the used values of ω cut.

From the presented analysis of the differential cross sections, it can be seen that the uncertainty of the new PHOKHARA9.0 code is sensitive to the choice of energy and event selection. However, all tests prove that the PHOKHARA9.0 generator is a proper tool for calculations done for the KLOE and BaBar event selection.

6.1.5 Negative weights

The main Monte Carlo method used in the PHOKHARA9.0 generator to obtain cross sections and distributions is of a generation with unweighted events [47]. In this method the maximum of the investigated function is determined first. Then the acceptance and rejection method is used. This operation is made inside PHOKHARA9.0 separately for parts with contributions of one real hard photon emission and of two hard photons. This method requires the values of the investigated function to be positive. The cases when the weights are negative should be treated as an additional source of the error added to the error of the Monte Carlo method.

The second method used during tests and calculations was Monte Carlo integrand (Eq. 7.4, 7.5). In this case, the sign of the values of the investigated function can be arbitrary. The calculations for both methods should give the same results.

The calculations and tests for $\sqrt{s} = 1.02$ GeV (without cuts), KLOE, and BaBar cuts for the value of $\omega = 10^{-4}$ do not show any negative weights. For $\sqrt{s} = 1.02$ GeV without cuts, the negative weights are present for $\omega = 10^{-5}$.

Unfortunately, for $\sqrt{s} = 10.56$ GeV the negative weights are present for both used values of ω. The negative weights appear in the routine for the one real hard photon emission correction. This part contains the Born contribution, the virtual, and soft corrections.

Both new versions of PHOKHARA, double precision and quad precision, were tested for the presence of negative weights. The same set of 10^7 phase space points for $\sqrt{s} = 10.56$ GeV was used. The value of the total cross section obtained for one real hard photon emission is equal to $\sigma_{1ph} = 0.07004(2)$ [nb]. For the double precision version of PHOKHARA and $\omega = 10^{-4}$, the number of the negative weights is equal to 2770598 and gives the contribution $\sigma_- =$ -0.006092(2) [nb]. This is almost 9% of σ_{1ph}. For the quad precision PHOKHARA there are 2770597 negative weights. They give the contribution $\sigma_{-quad} =$ -0.006092(7)[nb]. This is also almost 9% of σ_{1ph_q}. 2770594 negative values of the examined cases are the same for double and quad precision. The values of the contribution from the few cases when only the quad or double precision codes give the negative weights are in both cases below 10^{-10}. This means that the presence of the negative weights is not generally connected with the used version of the routine. In the final version of the generator, the routine that calculates the Monte Carlo integrand was also added, so if the negative weights are observed it is possible to confront the results obtained with both methods and to check, if for a given event selection, the unweighted events can be used.

6.1.6 Runtime and acceptance

All tests show that there are no contraindications to use both developed versions of the PHOKHARA Monte Carlo generator for calculations. However, one important criterion is to use runtime. The following processor was used for this test:

```
vendor_id : GenuineIntel
cpu family : 6
model : 26
model name : Intel(R) Xeon(R) CPU           X5560  @ 2.80GHz
cpu MHz : 2792.805
cache size : 8192 KB
cpu cores : 4
```

For all calculations, 1000 events were generated inside the proper PHOKHARA version. Table 6.24 shows the results of the comparison of the time of calculations between both tested versions of PHOKHARA for the four cases. From this data it is obvious that the difference is considerable. Because of this, the double precision version of PHOKHARA (PHOKHARA9.0) was used to analyse the influence of the missing corrections on results obtained for the KLOE and BaBar cuts.

	double [s]	quad [s]	$\frac{quad}{double}$
$\sqrt{s} = 1.02$ GeV	7.76	170	22
$\sqrt{s} = 10.56$ GeV	7.92	171	22
KLOE	1.53	57.29	38
BaBar	2.30	135	59

Table 6.24: Time of calculations for two tested versions of PHOKHARA generator.

The PHOKHARA9.0 MC generator is constructed in such a way that, in an input file, the user declares the number of events to determine the maximum of the investigated function and declares the number of generated events. During calculations, the part of generated points is rejected because of simulation conditions. For the new, extended version of PHOKHARA9.0, for the investigated process for $\sqrt{s} = 1.02$ GeV the acceptance is equal to about 2% of the total number of generated events. However, the acceptance for the part of calculations with one real photon emission is about 34% of one photon generated events. The two photon emissions give the acceptance

equal to about 1%. The simulation for energy $\sqrt{s} = 10.56$ GeV gives the total acceptance at the level of 0.008%. Two other values are equal to: 10% for one photon part and 0.006% for two photon emissions. The acceptance of generated events for BaBar cuts is better than for $\sqrt{s} = 10.56$ GeV without additional cuts and it is equal to about 0.02%. In this case, the acceptance for one photon emission increases to 30% and for two photon emission is equal to about 0.02%. The total acceptance for KLOE is similar to the one for $\sqrt{s} = 1.02$ GeV, yet the acceptance of one photon events decreases to 13%.

6.2 Numerical studies

All presented tests and analyses allowed the creation of the new version of the generator, PHOKHARA9.0. All new parts of the program were checked separately. Agreement between two versions of the generator is confirmed. The double precision version with routine PJFry for virtual corrections has been chosen. Because of the large differences in runtime between both codes, the double precision version is the better choice. The new version of the generator was used for the analysis of the results of calculations for the KLOE and BaBar cuts. This analysis should be done with proper precision of calculations. Tests show that for calculations with KLOE and BaBar cuts it is possible to use new PHOKHARA9.0 with accuracy below per mile.

The measurements of KLOE and BaBar were done for q^2 in interval $< 0.09, 0.96 >$ GeV^2 (this interval was the same for both experiments). The comparison done by the experimental groups showed that for values of $q^2 >$ 0.34 GeV^2 the obtained results were incoherent. The results were higher by 2-3% for BaBar.

The values of the differential cross section $\frac{d\sigma}{dq^2}$ for q^2 in interval $< 0.34, 0.96 >$ [GeV^2] were calculated with PHOKHARA9.0. The energies and event selections for KLOE and BaBar experiments were used. The same calculations were done for the distributed version of the generator, PHOKHARA8.0. The results obtained by the two generators were compared to check the influence of the missing corrections. Also, the angular distributions for $\cos\theta$ were prepared and compared. The relative difference was used as a measure of the changes between the examined quantities.

6.2.1 KLOE

For the calculations done with the KLOE cuts, the interval of $q^2 \in <$ $0.34, 0.96 >$ [GeV^2] was divided into 62 equal parts. Figure 6.9 presents the

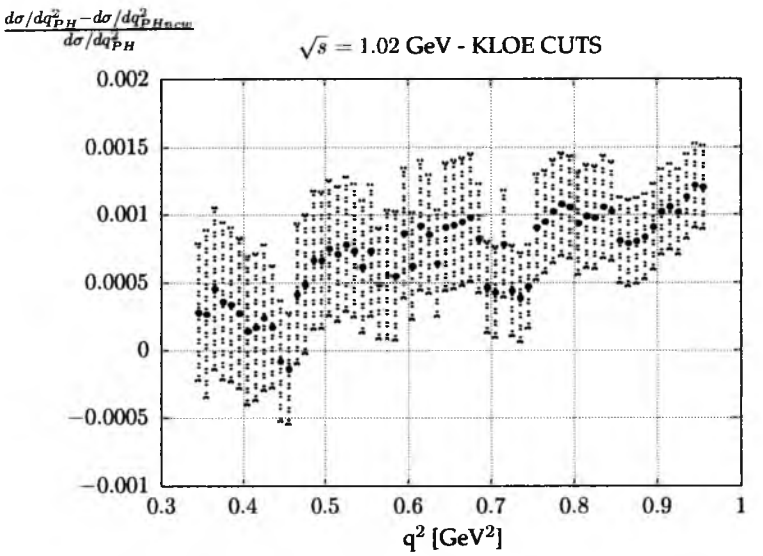

Figure 6.9: The relative difference between differential cross sections $\frac{d\sigma}{dq^2_{PH}}$ for PHOKHARA8.0 and $\frac{d\sigma}{dq^2_{PHnew}}$ for PHOKHARA9.0 as a function of q^2.

relative difference between the differential cross sections $\frac{d\sigma}{dq^2_{PH}}$ for PHOKHARA8.0 and $\frac{d\sigma}{dq^2_{PHnew}}$ for the new PHOKHARA9.0 as a function of q^2.

This figure shows that the difference between results is very small. For all points the results of the relative difference are at per mile level. The total cross sections were calculated for the results obtained with both versions of the generator. The comparison between the obtained cross sections is

	[nb]
σ_{PHncw}	3.1144(2)
σ_{PH}	3.11710(3)
$\frac{\sigma_{PH}-\sigma_{PHnew}}{\sigma_{PH}}$	0.086(5)%

Table 6.25: Comparison of the total cross section obtained for KLOE cuts between the PHOKHARA8.0 MC generator (σ_{PH}) and the new one PHOKHARA9.0 (σ_{PHnew}) containing full NLO contributions to the muon mode.

presented in table 6.25. The relative difference between the values of the total cross sections obtained by two versions of the PHOKHARA generator is equal

to 0.086(5)% of the result for the PHOKHARA8.0 generator. So, for the KLOE cuts, this contribution is too small to explain the discrepancy between KLOE and BaBar for the analysis of the experiment for the $e^+e^- \to \pi^+\pi^-$.

The charge averaged angular distribution for chosen q^2 for PHOKHARA8.0 and PHOKHARA9.0 is presented in Fig. 6.10. The figure presents the values of the differential cross section $\frac{d}{d\cos\theta}(\frac{\mu^+ + \mu^-}{2})$ as a function of $\cos\theta$. The shape of the distribution is caused by the KLOE cuts. The relative difference for the charge averaged angular distribution is at the per mile level. The bigger errors for some points are caused by the fact that the values are close to 0.

The relative difference for the asymmetry is at percent level (Fig. 6.11). The reason for this big difference is that in PHOKHARA8.0 the contributions for the asymmetry sensitive for the charge (ISR-FSR interference) are only at LO. Also, the KLOE event selection is crucial for the asymmetry size. The experimental cuts were chosen in such a way that they reduced the influence of the FSR radiative corrections. That suppressed the asymmetry coming from the one photon emission.

6.2.2 BaBar

For the BaBar cuts, calculations were done for five points from q^2 interval: $< 0.34, 0.96 >$ GeV^2. Figure 6.12 presents the relative difference between the results obtained with PHOKHARA8.0 and PHOKHARA9.0. Similarly to the case of the KLOE cuts, the difference for the cross sections $\frac{d\sigma}{dq^2}$ between two versions of the generators are at the level of 1-2 per mile.

For interval $q^2 \in < 0.34, 0.96 >$ GeV^2 the value of σ was calculated using these points (Tab. 6.26). The relative difference is once again small. The

	[nb]
σ_{PH}	0.002662(7)
σ_{PHnew}	0.002658(6)
$\frac{\sigma_{PH}-\sigma_{PHnew}}{\sigma_{PH}}$	0.17(3)%

Table 6.26: Comparison of the estimated total cross section obtained for BaBar cuts between the PHOKHARA8.0 MC generator (σ_{PH}) and the new one PHOKHARA9.0 (σ_{PHnew}) containing full NLO contributions to the muon mode.

loss of the accuracy caused by missing NLO corrections is at per mile level. The charge averaged angular distribution presented in Fig. 6.13 gives the difference between versions of PHOKHARA at the level of few per mile. So, for BaBar cuts also the influence of missing NLO corrections should not

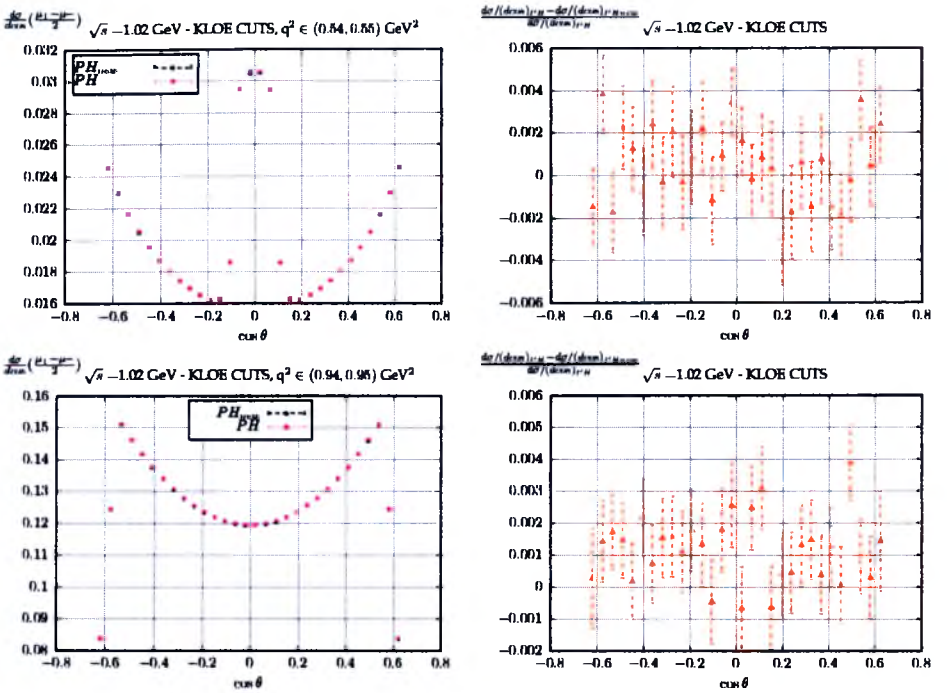

Figure 6.10: The charge averaged angular distribution for KLOE event selection and chosen values of q^2 for PHOKHARA8.0 and PHOKHARA9.0 (left) and relative difference between results (right). PH - PHOKHARA8.0, PH_{new} - PHOKHARA9.0.

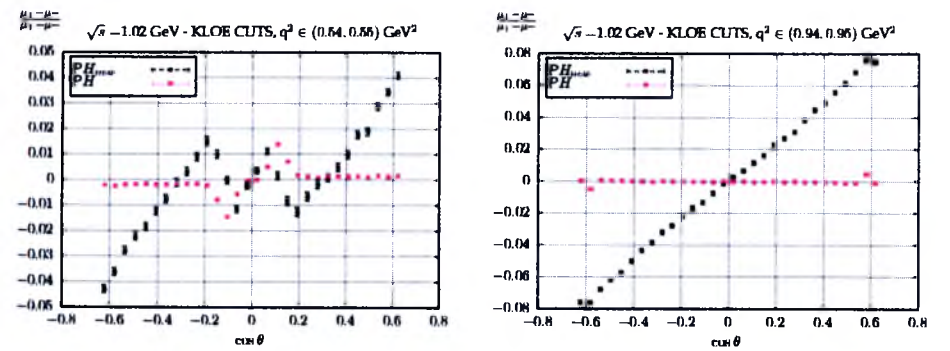

Figure 6.11: The asymmetry as a function of $\cos\theta$ for KLOE event selection and chosen values of q^2; PH (LO) - PHOKHARA8.0 and PH_{new} (NLO) - PHOKHARA9.0.

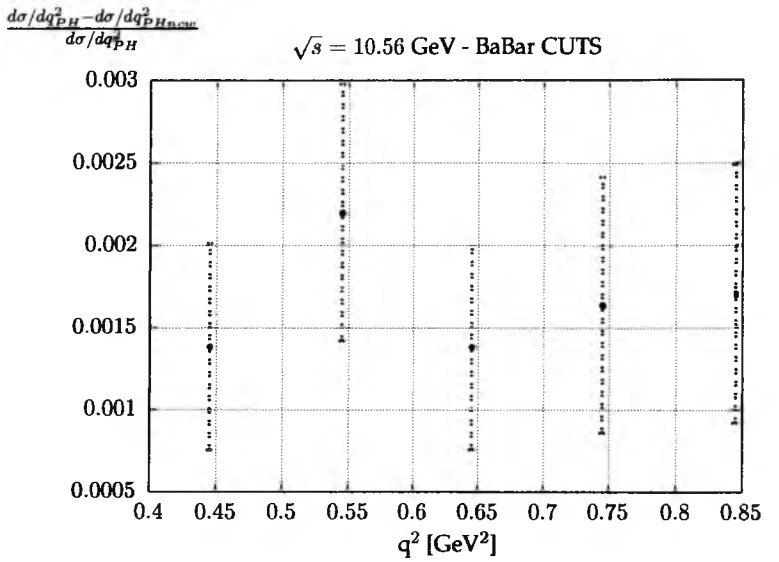

Figure 6.12: The relative difference between differential cross sections $\frac{d\sigma}{dq^2_{PH}}$ for PHOKHARA8.0 and $\frac{d\sigma}{dq^2_{PHnew}}$ for PHOKHARA9.0 as a function of q^2

been crucial to explaining the discrepancies between the KLOE and BaBar experiments.

For the BaBar cuts, asymmetry is dominated by the LO part of contributions. The experimental cuts and energy suppress additional influence of NLO corrections (Fig. 6.14).

6.3 Conclusions

The new version of the PHOKHARA Monte Carlo generator that includes the full one-loop corrections to the process $e^+e^- \to \mu^+\mu^-\gamma$ was prepared. The new version was marked as PHOKHARA9.0, and various tests were performed to check its stability and the accuracy.

The new version of the generator was used for the analysis of the results of calculations for the KLOE and BaBar event selections. The comparison between results obtained for PHOKHARA8.0 and the new PHOKHARA9.0 for KLOE and BaBar event selection shows that the influence of the missing NLO corrections is too small to explain the difference between experiments for process with pion pair production.

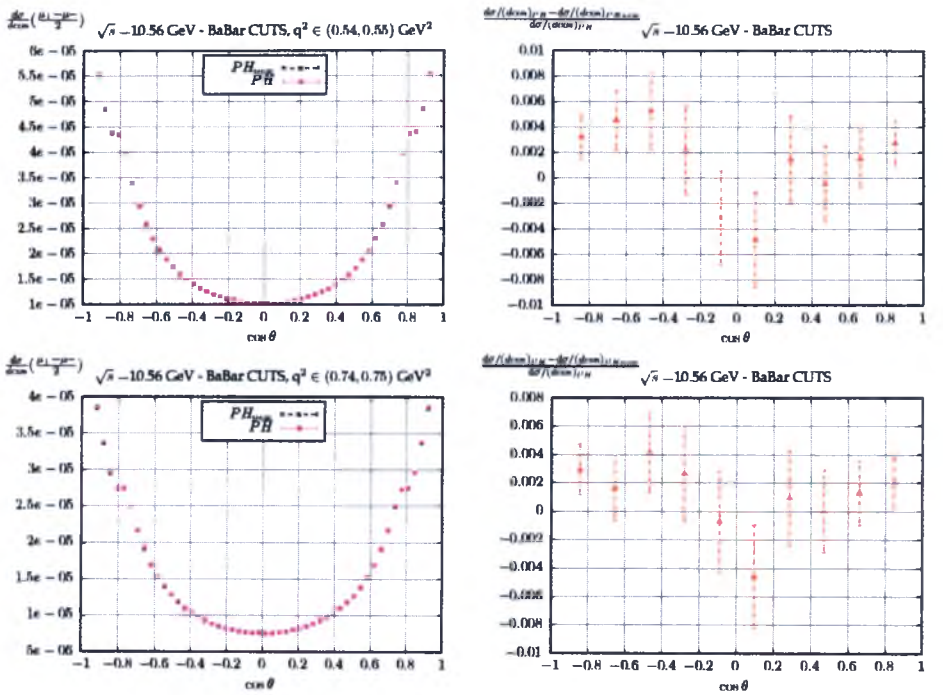

Figure 6.13: The charge averaged angular distribution for BaBar event selection and chosen values of q^2 for PHOKHARA8.0 and PHOKHARA9.0 (left) and relative difference between results (right). PH - PHOKHARA8.0, PH_{new} - PHOKHARA9.0.

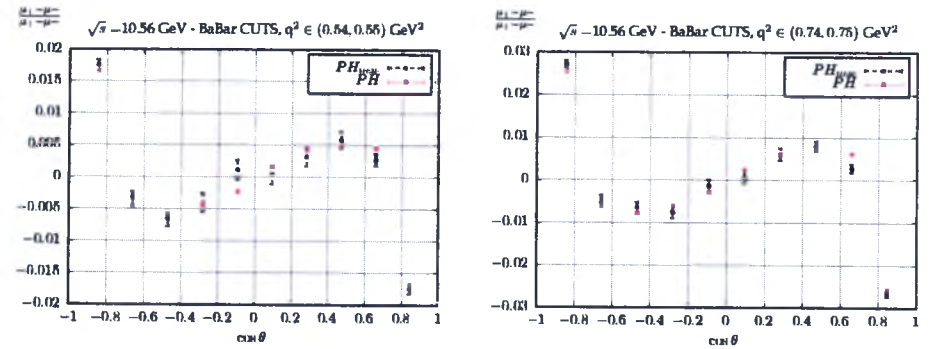

Figure 6.14: The asymmetry as a function of $\cos\theta$ for BaBar event selection and chosen values of q^2; PH (LO) - PHOKHARA8.0 and PH_{new} (NLO) - PHOKHARA9.0.

Chapter 7

Appendix

7.0.1 Relative difference

In all the tests presented in this work, where comparison between the corresponding results were obtained with two different methods, relative difference or its modulus was used. Equation 7.1 presented this method for two values: a and b. The error of relative difference was calculated as a differential Eq. 7.2 (δa, δb - errors). In the case when the compared values were independent, the formula described by equation 7.3 was used.

$$\Delta = \frac{a-b}{a} \tag{7.1}$$

$$\delta\Delta = \frac{|\delta b|}{|a|} + \frac{|b|}{|a|^2}|\delta b| \tag{7.2}$$

$$\delta\Delta = \sqrt{(\frac{\delta b}{a})^2 + (\frac{b}{a^2}\delta b)^2} \tag{7.3}$$

7.0.2 Monte Carlo integration

Some of the presented in this work tests and calculations required the calculations of some integrands. In most cases the Monte Carlo integration method was used [47], [48]. The estimate for calculated integral of the function f(x) for finite number of arguments x_i (i = 1,N) is based on the formula:

$$I = \frac{\sum_{i=1}^{N} f(x_i)}{N} \tag{7.4}$$

The error for this method is given by:

$$\Delta I = \sqrt{\frac{\sum_{i=1}^{N} f(x_i)^2}{N^2} - \frac{I^2}{N}} \tag{7.5}$$

7.0.3 Experimental cuts and event selection for luminosity measurement

Φ factories KLOE/DAΦNE (Frascati)

(a) $\sqrt{s}$ = 1.02 GeV
(b) E_{min} = 0.4 GeV
(c) For $\theta\pm$ two selections have to be checked
i. tighter selection 55° < $\theta\pm$ < 125 °
ii. wider selection 20° < $\theta\pm$ < 160 °
(d) ζ_{max}=4,5,6,7,8,...,14°, with reference value ζ_{max}=9°

B-factories BABAR/PEP-II (SLAC) & BELLE/KEKB (KEK)

(a) $\sqrt{s}$ = 10.56 GeV
(b) $|\vec{p}_+|/E_{beam} > 0.75$ and $|\vec{p}_-|/E_{beam} > 0.50$
or $|\vec{p}_-|/E_{beam} > 0.75$ and $|\vec{p}_+|/E_{beam} > 0.50$
(c) For $|cos(\theta\pm)|$ the following selections have to be checked
i. $|cos(\theta\pm)| < 0.65$ and $|cos(\theta+)| < 0.60$ or $|cos(\theta-)| < 0.60$
ii. $|cos(\theta\pm)| < 0.70$ and $|cos(\theta+)| < 0.65$ or $|cos(\theta-)| < 0.65$
iii. $|cos(\theta\pm)| < 0.60$ and $|cos(\theta+)| < 0.55$ or $|cos(\theta-)| < 0.55$
(d) ζ^{3d}_{max}= 20,22,24,...,40°, with reference value ζ^{3d}_{max}=30 °

BES-III experiment at BEPCII (Beijing)

(a) $\sqrt{s}$ = 3.686 GeV, 3.65 GeV and 3.097 GeV

(b) $|\cos\theta| < 0.8$, where θ is the polar angle of the electron or positron in the lab system, this corresponds to the barrel region of BES-III detector. Since in BEPC, e^+ and e^- beams are colliding with equal energy but at a 22mrad crossing angle, the lab system is slightly different from the CM system.

(c) $E_{e^+} > 1.0$ GeV and $E_{e^-} > 1.0$ GeV, where E is the energy deposited in the electromagnetic calorimeter (EMC).

(d) E/p for one track greater than 0.5 and the other track greater than 0.8, here E is the energy deposited in the electromagnetic calorimeter (EMC), and p is the track momentum measured in the Main Drift Chamber.

To see how the NNLO corrections depend on the event selection we obtained results also for $|\cos\theta| < 0.7,\ 0.75,\ 0.85$ and 0.9

B-factory Belle (KEK)- the reference event selection

Belle runs at an asymmetric e^+e^- collider, but all criteria are expressed in the CoM fram (a) $\sqrt{s}$ =10.58 GeV

(b) For $\theta\pm$ two selections have to be checked

i. $50.5° < \theta_\pm < (180 - 50.5)°$

ii. $45.5° < \theta_\pm < (180 - 45.5)°$

iii. $55.5° < \theta_\pm < (180 - 55.5)°$

(c) Two charged tracks have momentum > 2.645 GeV

(d) The track with maximum deposited energy in the EMC greater than 2 GeV,

(e) The sum of the deposited energies of all tracks in the electromagnetic calorimeter (EMC) is greater than 4 GeV (both charged and neutral particles can deposit energy in the EMC and it is not checked if the particle is charged or neutral)

(f) Acollinearity angle (2d) ζ_{max}=5,6,7,8,...,15°, with reference value ζ_{max}=10°

(g) Transverse momentum of any observed charged particle greater than 0.1 GeV

7.0.4 Acollinearity

The 2d acolinearity is defined as follows:

$$\zeta = |\theta_+ + \theta_- - 180| \tag{7.6}$$

Here θ_+ (θ_-) denotes an angle between outgoing positron (electron) and z-axis in Centre of Mass System.

The 3d acolinearity is defined as follows:

$$\zeta^{3d} = |\arccos s(\vec{p}_+\vec{p}_-/|\vec{p}_+|/|\vec{p}_-|)180/\pi - 180| \tag{7.7}$$

$\vec{p}_+$ and $\vec{p}_-$ denotes positron and electron momenta.

7.0.5 Berends substitution

The so called Berends substitution is based on the following relationship [43]:

$$\frac{1}{ab} = \int_0^1 \frac{dx}{[ax + (1-x)b]^2} \tag{7.8}$$

The right side of the formula can be written in the form:

$$\int_0^1 \frac{dx}{[ax+(1-x)b]^2} = \int_0^1 \frac{dx}{[b+(a-b)x]^2} = \left[-\frac{1}{(b+(a-b)x)(a-b)}\right]_0^1 \quad (7.9)$$

After integration it gives:

$$\left[-\frac{1}{(b+(a-b)x)(a-b)}\right]_0^1 = -\frac{1}{(a-b)}\left(\frac{1}{a}-\frac{1}{b}\right) = \frac{1}{ab} \quad (7.10)$$

7.0.6 Soft contribution σ_s - finite part

The finite part of the soft formula presented in Section 5.3 has the following form:

$$F_{ISRfin}(p_1,p_2) = -\frac{\alpha}{2\pi^2}(I_1(p_1) - I_2(p_1,p_2)) \quad (7.11)$$

$$F_{FSRfin}(q_1,q_2) = -\frac{\alpha}{4\pi^2}(I_1(q_1) + I_1(q_2) - 2I_3(q_1,q_2)) \quad (7.12)$$

$$F_{INTfin}(p_1,p_2,q_1,q_2) = -\frac{4\alpha}{\pi^2}\sum_{i,j=1}^{2}(-1)^j I_3(p_i,q_j)) \quad (7.13)$$

The $I_1(x)$, $I_2(p_1,p_2)$, $I_3(x_1,x_2)$ have the form (x_1, x_2, x - four momenta):

$$I_1(x) = \frac{2\pi x(0) log(x(0) - |\bar{x}|)}{|\bar{x}|(x(0)+|\bar{x}|)} \quad (7.14)$$

$$I_2(p_1,p_2) = \frac{\pi p_1 \cdot p_2 C_1}{\sqrt{s(s/4-m_e^2)}} \quad (7.15)$$

$$I_3(x_1,x_2)) = f_1(C_{3a}I_{3a} + C_{3b}I_{3b} + C_{3c}I_{3c} + C_{3d}I_{3d}) \quad (7.16)$$

$$\begin{aligned} C_1 = &-\log^2(C_a-1) + \log^2(C_a) \\ &+2\log(2C_a-1)\log\left(\frac{C_a-1}{C_a}\right) \\ &-2\mathrm{Li}_2\left(\frac{C_a-1}{2C_a-1}\right) + 2\mathrm{Li}_2\left(\frac{C_a}{2C_a-1}\right) \\ &+4\mathrm{Li}_2\left(\frac{1}{1-2C_a}\right) - 4\mathrm{Li}_2\left(\frac{-1}{1-2C_a}\right) \end{aligned} \quad (7.17)$$

$$C_a = \frac{\sqrt{s}}{4\sqrt{s/4 - m_e^2}} + \frac{1}{2} \tag{7.18}$$

$$C_2 = \frac{(x_2 - x_1)^2}{(x_2(0) - x_1(0) + |\bar{x}_2 - \bar{x}_1|)^2} \tag{7.19}$$

$$f_1(x_1, x_2) \equiv f_1 = \frac{8\pi x_1 x_2 (|\bar{x}_2 - \bar{x}_1|)^{3/2}}{|\bar{x}_1|^2 \bar{x}_2|^2 - (\bar{x}_1 \bar{x}_2)(x_2 - x_1)^2} \tag{7.20}$$

The I_{3a} function depends on the sign of f_1. If $f_1 < 0$ then:

$$\begin{aligned} I_{3a}(x_1, x_2) \equiv I_{3a} = \log\left(\frac{t_y t_3 - 1}{t_x t_3 - 1}\right) \log\left(\frac{C_2(t_4 - t_3)t_3}{(1 + t_3 t_4)(1 + t_3^2)}\right) \\ + \frac{1}{2}\log^2\left(\frac{t_y t_3 - 1}{t_3}\right) - \frac{1}{2}\log^2\left(\frac{t_x t_3 - 1}{t_3}\right) - \mathrm{Li}_2\left(\frac{(t_y t_3 - 1)t_4}{t_3 - t_4}\right) \\ + \mathrm{Li}_2\left(\frac{(t_x t_3 - 1)t_4}{t_3 - t_4}\right) + \mathrm{Li}_2\left(\frac{1 - t_3 t_y}{1 + t_3^2}\right) - \mathrm{Li}_2\left(\frac{1 - t_3 t_x}{1 + t_3^2}\right) \\ + \mathrm{Li}_2\left(\frac{1 - t_3 t_y}{1 + t_3 t_4}\right) - \mathrm{Li}_2\left(\frac{1 - t_3 t_x}{1 + t_3 t_4}\right) \end{aligned} \tag{7.21}$$

If $f_1 > 0$ then:

$$\begin{aligned} I_{3a}(x_1, x_2) \equiv I_{3a} = \log\left(\frac{t_y t_3 - 1}{t_x t_3 - 1}\right) \log\left(\frac{C_2(t_4 - t_3)t_3}{(1 + t_3^2)}\right) \\ + \frac{1}{2}\log^2\left(\frac{1 - t_y t_3}{t_3}\right) - \frac{1}{2}\log^2\left(\frac{1 - t_x t_3}{t_3}\right) - \mathrm{Li}_2\left(\frac{(t_y t_3 - 1)t_4}{t_3 - t_4}\right) \\ + \log\left(\frac{1 + t_3 t_4 - 1}{t_3}\right) \log\left(\frac{t_y + t_4}{t_x + t_4}\right) - \log\left(\frac{1 - t_y t_3}{t_3}\right) \log(-t_y - t_4) \\ + \log\left(\frac{1 - t_x t_3}{t_3}\right) \log(-t_x - t_4) + \mathrm{Li}_2\left(\frac{(t_x t_3 - 1)t_4}{t_3 - t_4}\right) \\ + \mathrm{Li}_2\left(\frac{1 - t_3 t_y}{1 + t_3^2}\right) - \mathrm{Li}_2\left(\frac{1 - t_3 t_x}{1 + t_3^2}\right) - \mathrm{Li}_2\left(\frac{(t_y - t_4)t_3}{1 + t_3 t_4}\right) \\ + \mathrm{Li}_2\left(\frac{(t_x - t_4)t_3}{1 + t_3 t_4}\right) \end{aligned} \tag{7.22}$$

$$I_{3b}(x_1,x_2)\equiv I_{3b}=\log\left(\frac{t_yt_4-1}{t_xt_4-1}\right)\log\left(\frac{C_2(t_3-t_4)}{(1+t_4^2)t_3}\right)+\frac{1}{2}\log^2\left(\frac{t_yt_4-1}{t_4}\right)$$
$$-\frac{1}{2}\log^2\left(\frac{t_xt_4-1}{t_4}\right)-\log\left(\frac{t_yt_4-1}{t_4}\right)\log(t_y-t_3)$$
$$+\log\left(\frac{t_xt_4-1}{t_4}\right)\log(t_x-t_3)+\log\left(\frac{-t_3t_4-1}{t_4}\right)\log\left(\frac{t_y+t_3}{t_x+t_3}\right)$$
$$-\mathrm{Li}_2\left(\frac{(1-t_yt_4)t_4}{t_3-t_4}\right)+\mathrm{Li}_2\left(\frac{(1-t_xt_4)t_4}{t_3-t_4}\right)-\mathrm{Li}_2\left(\frac{(t_y+t_3)t_4}{1+t_3t_4}\right)$$
$$+\mathrm{Li}_2\left(\frac{(t_x+t_3)t_4}{1+t_3t_4}\right)+\mathrm{Li}_2\left(\frac{1-t_yt_4}{1+t_4^2}\right)-\mathrm{Li}_2\left(\frac{1-t_xt_4}{1+t_4^2}\right) \quad (7.23)$$

$$I_{3c}(x_1,x_2)\equiv I_{3c}=\log\left(\frac{t_y+t_3}{t_x+t_3}\right)\log\left(\frac{C_2(1+t_3^2)(1+t_3t_4}{t_3t_4(t_4-t_3)}\right)$$
$$-\frac{1}{2}\log^2(t_y+t_3)+\frac{1}{2}\log^2(t_x+t_3)-\mathrm{Li}_2\left(\frac{(t_y+t_3)t_3}{1+t_3^2}\right)$$
$$+\mathrm{Li}_2\left(\frac{(t_x+t_3)t_3}{1+t_3^2}\right)-\mathrm{Li}_2\left(\frac{(t_y+t_3)t_4}{1+t_3t_4}\right)+\mathrm{Li}_2\left(\frac{(t_x+t_3)t_4}{1+t_3t_4}\right)$$
$$+\mathrm{Li}_2\left(\frac{(t_y+t_3)t_4}{t_3-t_4}\right)-\mathrm{Li}_2\left(\frac{(t_x+t_3)t_4}{t_3-t_4}\right) \quad (7.24)$$

$$I_{3d}(x_1,x_2)\equiv I_{3d}(=-\log\left(\frac{t_y+t_4}{t_x+t_4}\right)\log\left(\frac{C_2(1+t_4^2)(1+t_3t_4}{t_3t_4(t_4-t_3)}\right)$$
$$+\frac{1}{2}\log^2(-t_y-t_4)-\frac{1}{2}\log^2(-t_x-t_4)+\mathrm{Li}_2\left(\frac{(t_y+t_4)t_3}{1+t_3t_4}\right)$$
$$-\mathrm{Li}_2\left(\frac{(t_x+t_4)t_3}{1+t_3t_4}\right)+\mathrm{Li}_2\left(\frac{(t_y+t_4)t_4}{1+t_4^2}\right)-\mathrm{Li}_2\left(\frac{(t_x+t_4)t_4}{1+t_4^2}\right)$$
$$-\mathrm{Li}_2\left(\frac{t_y+t_4}{t_4-t_3}\right)+\mathrm{Li}_2\left(\frac{t_x+t_4}{t_4-t_3}\right) \quad (7.25)$$

$$C_{3a}(x_1,x_2)\equiv C_{3a}=\frac{2(x_2(0)-x_1(0))\sqrt{|\bar{x}_1|^2|\bar{x}_2|^2-\bar{x}_1\bar{x}_2}(t_3^2-1)}{(|\bar{x}_1|^2+|\bar{x}_2|^2-2\bar{x}_1\bar{x}_2)t_3^2(t_3+\frac{1}{t_3})(t_4+\frac{1}{t_3})(\frac{1}{t_3}-\frac{1}{t_4})}$$
$$+\frac{4(x_2(0)-x_1(0))(|\bar{x}_1|^2-\bar{x}_1\bar{x}_2)t_3}{(|\bar{x}_1|^2+|\bar{x}_2|^2-2\bar{x}_1\bar{x}_2)t_3^2(t_3+\frac{1}{t_3})(t_4+\frac{1}{t_3})(\frac{1}{t_3}-\frac{1}{t_4})}$$
$$+\frac{4x_1(0)}{t_3(t_3+\frac{1}{t_3})(t_4+\frac{1}{t_3})(\frac{1}{t_3}-\frac{1}{t_4})} \quad (7.26)$$

$$C_{3b}(x_1,x_2) \equiv C_{3b} = -\frac{2(x_2(0)-x_1(0))\sqrt{|\bar{x}_1|^2|\bar{x}_2|^2-\bar{x}_1\bar{x}_2}(t_4^2-1)}{(|\bar{x}_1|^2+|\bar{x}_2|^2-2\bar{x}_1\bar{x}_2)t_4^2(\frac{1}{t_3}-\frac{1}{t_4})(t_3+\frac{1}{t_4})(t_4+\frac{1}{t_4})}$$
$$-\frac{4(x_2(0)-x_1(0))(|\bar{x}_1|^2-\bar{x}_1\bar{x}_2)t_3}{(|\bar{x}_1|^2+|\bar{x}_2|^2-2\bar{x}_1\bar{x}_2)t_4^2(\frac{1}{t_3}-\frac{1}{t_4})(t_3+\frac{1}{t_4})(t_4+\frac{1}{t_4})}$$
$$-\frac{4x_1(0)}{t_4(\frac{1}{t_3}-\frac{1}{t_4})(t_3+\frac{1}{t_4})(t_4+\frac{1}{t_4})} \quad (7.27)$$

$$C_{3c}(x_1,x_2) \equiv C_{3c} = \frac{2(x_2(0)-x_1(0))\sqrt{|\bar{x}_1|^2|\bar{x}_2|^2-\bar{x}_1\bar{x}_2}(t_3^2-1)}{(|\bar{x}_1|^2+|\bar{x}_2|^2-2\bar{x}_1\bar{x}_2)(t_3+\frac{1}{t_3})(t_3+\frac{1}{t_4})(t_3-t_4)}$$
$$+\frac{4(x_2(0)-x_1(0))(|\bar{x}_1|^2-\bar{x}_1\bar{x}_2)t_3}{(|\bar{x}_1|^2+|\bar{x}_2|^2-2\bar{x}_1\bar{x}_2)(t_3+\frac{1}{t_3})(t_3+\frac{1}{t_4})(t_3-t_4)}$$
$$+\frac{4x_1(0)t_3}{(t_3+\frac{1}{t_3})(t_3+\frac{1}{t_4})(t_3-t_4)} \quad (7.28)$$

$$C_{3d}(x_1,x_2) \equiv C_{3d} = \frac{2(x_2(0)-x_1(0))\sqrt{|\bar{x}_1|^2|\bar{x}_2|^2-\bar{x}_1\bar{x}_2}(1-t_4^2)}{(|\bar{x}_1|^2+|\bar{x}_2|^2-2\bar{x}_1\bar{x}_2)(t_4+\frac{1}{t_3})(t_4+\frac{1}{t_4})(t_3-t_4)}$$
$$-\frac{4(x_2(0)-x_1(0))(|\bar{x}_1|^2-\bar{x}_1\bar{x}_2)t_4}{(|\bar{x}_1|^2+|\bar{x}_2|^2-2\bar{x}_1\bar{x}_2)(t_4+\frac{1}{t_3})(t_4+\frac{1}{t_4})(t_3-t_4)}$$
$$-\frac{4x_1(0)t_4}{(t_4+\frac{1}{t_3})(t_4+\frac{1}{t_4})(t_3-t_4)} \quad (7.29)$$

$$t_x(x_1,x_2) \equiv t_x = \frac{|\bar{x}_1|^2-\bar{x}_1\bar{x}_2+|\bar{x}_1||\bar{x}_1-\bar{x}_2|}{\sqrt{|\bar{x}_1|^2|\bar{x}_1|^2-(\bar{x}_1\bar{x}_2)^2}} \quad (7.30)$$

$$t_y(x_1,x_2) \equiv t_y = \frac{2\bar{x}_1\bar{x}_2-|\bar{x}_1|^2-|\bar{x}_2|^2+|\bar{x}_2||\bar{x}_1+\bar{x}_2|}{\sqrt{|\bar{x}_1|^2|\bar{x}_1|^2-(\bar{x}_1\bar{x}_2)^2}} \quad (7.31)$$

$$t_{3,4}(x_1,x_2) \equiv t_{3,4} = \frac{x_1(0)(|\bar{x}_2|^2-\bar{x}_1\bar{x}_2)+x_2(0)(|\bar{x}_1|^2-\bar{x}_1\bar{x}_2)\mp\sqrt{\Delta}}{\sqrt{|\bar{x}_1|^2|\bar{x}_2|^2-(\bar{x}_1\bar{x}_2)^2}((x_2(0)-x_1(0))+|\bar{x}_2-\bar{x}_1|)} \quad (7.32)$$

$$\Delta = (x_1(0)(|\bar{x}_2|^2-\bar{x}_1\bar{x}_2)+x_2(0)(|\bar{x}_1|^2-\bar{x}_1\bar{x}_2))^2$$
$$+(|\bar{x}_1|^2|\bar{x}_2|^2-(\bar{x}_1\bar{x}_2)^2)(x_2-x_1)^2 \quad (7.33)$$

7.0.7 Experimental cuts and event selection used in PART III

KLOE

- $\sqrt{s} = 1.02$GeV
- tracks between 50° and 130°
- missing photon angle< 15°(> 165°)
- 80< m_{trk} <115 MeV
- $q^2 \in < 0.34, 0.96 >$

BaBar

- $\sqrt{s} = 10.56$GeV
- tracks between 20° and 160°
- 3 GeV minimal photon energy/missing energy
- $|q_1| > 1$GeV (antimuon) and $|q_2| > 1$GeV (muon)
- $q^2 \in < 0.34, 0.96 >$

Bibliography

[1] M. Peskin, D. Schroeder, *An Introduction to Quantum Field Theory*, Addison-Wesley Publishing Company, 1995

[2] S. Actis et al.: *Quest for precision in hadronic cross sections at low energy: Monte Carlo tools vs. experimental data*, Working Group on Radiative Corrections and Monte Carlo Generators for Low Energies Collaboration , Eur.Phys.J. C66, (2010)585-686

[3] M.Gourdin, E.De Rafael, Nucl. Phys. B10,(1969)667

[4] K. Hagiwaraa, R. Liaob, A. D. Martinc, D. Nomurad, T. Teubner. $(g-2)_\mu$ *and* $\alpha(M_z^2)$ *re-evaluated using new precise data* ,J. Phys. G 38 (2011) 085003

[5] N. Cabibbo, R. Gatto, *Electron-Positron Colliding Beam Experiments*, Phys. Rev. 124, (1961)1577

[6] C. Carloni Calame, H. Czyz, J. Gluza, M. Gunia, G. Montagna, O. Nicrosini, F. Piccinini, T. Riemann, M.Worek, *NNLO leptonic and hadronic corrections to Bhabha scattering and luminosity monitoring at meson factories*, JHEP 1107 (2011) 126

[7] M. Gunia, *A theoretical progress on the calculation of NNLO leptonic and hadronic corrections to Bhabha scattering and their implementation into BabaYaga Monte Carlo generator*, Acta Phys.Polon. B42 (2011) 2469-2476

[8] C. Carloni Calame, H. Czyz, J. Gluza, M. Gunia, G. Montagna, O. Nicrosini, F. Piccinini, T. Riemann, M.Worek*NNLO massive corrections to Bhabha scattering and theoretical precision of BabaYaga@NLO*, Nucl.Phys.Proc.Suppl. 225-227 (2012) 293-297

[9] F. Ambrosino et al. (KLOE),*Measurement of the DAϕNE luminosity with the KLOE detector using large angle Bhabha scattering* Eur. Phys. J. C47, 589(2006)

[10] C. M. Carloni Calame, G. Montagna, O. Nicrosini and F. Piccinini, *The BABAYAGA event generator*, Nucl. Phys. Proc. Suppl. 131 (2004) 4855

[11] F. Ambrosino et al. (KLOE), *Measurement of sigma(e+e− → pi+pi−) from threshold to 0.85 GeV^2 using Initial State Radiation with the KLOE detector*, Phys.Lett.B700:102-110,2011

[12] Graziano Venanzoni, *KLOE measurement of $\sigma(e+e- \to \pi+\pi-(\gamma))$ with Initial State Radiation and the* ΠΠ *contribution to the muon anomaly*, EPS HEP 2011, Grenoble, 23 July 2011

[13] H. Czyz, M. Gunia, J.H Kuhn, *Simulation of electron-positron annihilation into hadrons with the event generator PHOKHARA*, JHEP 1308 (2013) 110

[14] H. Czyz, A. Grzelinska, and J. H. Kuhn, *Narrow resonances studies with the radiative return method*, Phys.Rev.D81 (2010) 094014

[15] S. Jadach, B. Ward, and Z. Was, *The Precision Monte Carlo event generator K K for two fermion final states in e+e- collisions*, Comput.Phys.Commun. 130 (2000) 260325

[16] A. Arbuzov, V. Astakhov, A. Fedorov, G. Fedotovich, E. Kuraev, et al., *Radiative corrections for pion and kaon production at e+ e- colliders of energies below 2-GeV*, JHEP 9710 (1997) 006

[17] A. Arbuzov, G. Fedotovich, E. Kuraev, N. Merenkov, V. Rushai, et al., *Large angle QED processes at e+ ecolliders at energies below 3-Ge*V, JHEP 9710 (1997) 001

[18] G. Venanzoni, *KLOE measurement of $\sigma(e + e- \to \pi + \pi - (\gamma))$ with Initial State Radiation and the* ΠΠ *contribution to the muon anomaly*, RMCLWG Meeting, Mainz 27 Sep 2012

[19] J. P. Lees, others, *Precise Measurement of the e+ e- → pi+ pi- (gamma) Cross Section with the Initial-State Radiation Method at BABAR*, the BABAR Collaboration, BABAR-PUB-12/003

[20] F. Campanario, H. Czyz, J. Gluza, M. Gunia, T. Riemannc, G. Rodrigo, V. Yundin, *Complete QED NLO contributions to the reaction $e^+e^- \to \mu^+\mu^-\gamma$ and their implementation in the event generator PHOKHARA.* - work in preparation

[21] A. A. Penin, Two-loop corrections to Bhabha scattering, Phys. Rev. Lett. 95 (2005) 010408

[22] S. Actis, M. Czakon, J. Gluza and T. Riemann, *Virtual Hadronic and Leptonic Contributions to Bhabha Scattering*, Phys. Rev. Lett. 100 (2008) 131602

[23] S. Actis, M. Czakon, J. Gluza and T. Riemann, *Virtual hadronic and heavy-fermion O(a2) corrections to Bhabha scattering*, Phys. Rev. D78 (2008)

[24] J. H. Kuhn and S. Uccirati, *Two-loop QED hadronic corrections to Bhabha scattering*, Nucl. Phys. B806 (2009) 300326

[25] S. Actis, M. Czakon, J. Gluza, T. Riemann, Fortran package bha_nnlo_hf, obtainable on request from the authors

[26] H. Czyz and S. Ivashyn, *EKHARA: A Monte Carlo generator for* $e^+e^- \to e^+e^-\pi^0$ *and* $e^+e^- \to e^+e^-\pi^+\pi^-$ *processes*, Comput.Phys.Commun. 182 (2011) 13381349

[27] H. Czyz and M. Gunia, Fortran package BHAGEN-1PH-VAC, obtainable on request from the authors.

[28] M. Caffo and H. Czyz, *BHAGEN-1PH: A Monte Carlo event generator for radiative Bhabha scattering*, Comput. Phys. Commun. 100 (1997) 99118

[29] A. Cafarella, C. G. Papadopoulos and M. Worek, *Helac-Phegas: A generator for all parton level processes*, Comput. Phys. Commun. 180 (2009) 19411955

[30] T. Teubner et al., Fortran program VP_HLMNT_v2_0 (15 July 2010).The routine is available upon request from the authors.

[31] A. Arbuzov, E. A. Kuraev, N. P. Merenkov and L. Trentadue, *Virtual and soft real pair production in large angle Bhabha scattering*, Phys. Atom. Nucl. 60 (1997) 591600

[32] C. G. Papadopoulos, PHEGAS: *A phase space generator for automatic cross- section computation*, Comput. Phys. Commun. 137 (2001) 247254

[33] C. Bruch, A. Khodjamirian and J. H. Khn, *Modeling the pion and kaon form factors in the timelike region*, Eur. Phys. J. C39 (2005) 4154

[34] G. P. Lepage, *A new algorithm for adaptive multidimensional integration*, Journal of Computational Physics 27 (1978) 192

[35] F. A. Berends, W. van Neerven and G. Burgers, *Higher Order Radiative Corrections at LEP Energies*, Nucl.Phys. B297 (1988) 429

[36] F. A. Berends, G.J. Komen, *Soft and Hard Photon Corrections for mu Pair Production and Bhabha Scattering in Presence of a Resonance*, Nucl.Phys. B115 (1976) 114

[37] G. Rodrigo, H. Czyz, J. H. Kuhn, and M. Szopa, *Radiative return at NLO and the measurement of the hadronic cross-section in electron positron annihilation*, Eur.Phys.J. C24 (2002) 7182

[38] S. Jadach, *Studies of mu-pair and pi-pair production at the electron-positron low energy colliders*, Acta Phys.Polon.B36 (2005) 2387

[39] Working Group on Rad. Corrections and MC Generators for Low Energies, http://www.lnf.infn.it/wg/sighad/ (active 16.X.2013)

[40] Francisco Campanario, Theory Division, IFIC, University of Valencia-CSIC - the code available upon request

[41] Valery Yundin, *Massive Loop Corrections for Collider Physics*, PhD thesis, Mathematisch-Naturwissenschaftliche Fakultät I,Humboldt-Universität zu Berlin, 2012

[42] F. Jegerlehner and K. Kolodziej, *The hard bremsstrahlung correction to* $e^+e^- \to 4f$ *with finite fermion masses: results for* $e^+e^- \to ud\mu^-\upsilon_\mu$, Eur. Phys. J. C 12 (2000)77

[43] F. Berends, R. Kleiss, *Distributions in the process* $e + e- \to e + e - \gamma$, Nucl. Phys. B228 (1983)537

[44] J. A. Vermaseren:*Symbolic Manipulation with FORM*, Computer Algebra Nederland, Amsterdam, 1991

[45] S. Actis, P. Mastrolia, G. Ossola, *NLO QED Corrections to Hard-Bremsthalung Emission in Bhabha Scattering*,Phys.Lett.B682:419-427,2010

[46] F.A. Berends, K.Gaemers, R. Gastmans, *Hard photonic corrections for process* $e^+e^- \to \mu^+\mu^-$,Nucl. Phys. B 57 (1973) 381-400

[47] S. Weinzierl, *Introduction to Monte Carlo methods*,NIKHEF-00-012

[48] C. Morningstar, *The Monte Carlo method in quantum field theory*, arXiv:hep-lat/0702020